Editorial Manager(tm) for International Journal of Earth Sciences
Manuscript Draft

Manuscript Number: IJES-D-09-00202R2

Title: THE WITPUTS DIAMICTITE IN SOUTHERN NAMIBIA AND ASSOCIATED ROCKS - CONSTRAINTS FOR A GLOBAL GLACIATION?

Article Type: Original Paper

Keywords: Snowball earth, correlation, detrital zircon ages, Numees, Holgat Formation, Namibia

Corresponding Author: Dr. Udo Zimmermann, Dr.

Corresponding Author's Institution: University of Stavanger

First Author: Udo Zimmermann, Dr.

Order of Authors: Udo Zimmermann, Dr.; Jennifer Tait, Dr. habil.; Quentin G Crowley, Dr.; Vanessa Pashley, Dr.; Gijs Straathof, MSc

Abstract: The Witputs section of the Gariep Belt (S Namibia) comprises a sequence of clastic and chemical sediments, which have been interpreted as representative of a Late Neoproterozoic global or near-global ice age event, and recent biostratigraphic work in the upper rocks of the Witputs suggest a late Ediacaran age. To further characterise this sequence, and provide additional age constraints a detailed sedimentological and detrital zircon study has been carried out. The petrographic, sedimentological and geochemical characteristics of the Witputs diamictite determined in this study are homogenous and indicative of debris flow or palaeo-valley infill sediments, deposited in an oxic environment with no glaciogenic evidence. This homogeneity is also reflected in the detrital zircon age spectra with most ages falling between 1.0 and 1.3 Ga, representing the local geology, with the youngest grain at 1030.2 +/-10.9 (2σ) (n= 92 < 10% discordance), despite the fact that mid and Late Neoproterozoic volcanic activity is known in the local region.
The overlying carbonate rocks, often considered to be 'cap carbonates', show high Mn (up to 60% MnO), with base metal precipitation (Zn, V, Co), and are recrystallised. Their δ13CVPDB isotope ratios are homogeneous at around -3. Major and trace element ratios reach values which indicate that C-O isotopes may be disturbed and might not reflect primary global seawater composition, thus questioning their use for global correlation and comparison with composite chemostratigraphic curves. The contact to the overlying late Ediacaran Sanddrif Member is not exposed and the rocks dip in a different direction than the underlying carbonate rocks. The c. 40 m thick section is characterised by rapid lithology changes including shales, calcareous sandstones and wackes, fine-grained conglomerates and rare clean quartz-rich sandstones, all of which have strikingly similar detrital zircon populations and the youngest zircon is dated at 1082.8 +/- 10 Ma (2σ errors, from 72 grains with <10% discordance). Acritarchs earlier found in the Sanddrif Member, however, indicate a post-570 Ma depositional age.
If the diamictites are glacio-marine deposits, then an interesting conclusion is that the clastic sediments can display a very immature geochemical signature, indicating a localised provenance, with derivation purely from the local basement rocks, which is also reflected in the detrital zircon populations. However, we would hesitate to assign a glacial origin to the deposits as no glacial indicators, other than a diamictitic texture, were observed. Clearly far more work on the detailed mapping and sedimentology of the Neoproterozoic Gariep Belt deposits are required, particularly as many are currently used for global correlation. Age constraints derived from extensive detrital zircon

work can only constrain the deposits as being post 1.03 Ma with the detritus being purely locally derived.

THE WITPUTS DIAMICTITE IN SOUTHERN NAMIBIA AND ASSOCIATED ROCKS - CONSTRAINTS FOR A GLOBAL GLACIATION?

Udo Zimmermann[1*], Jennifer Tait[2], Quentin G. Crowley[3,4], Vanessa Pashley[3] and Gijs Straathof[2]

[1]University of Stavanger, Faculty of Science and Technology, Department of Petroleum Engineering, 4036 Stavanger, Norway; udo.zimmermann@uis.no
[2]School of Geosciences, Grant Institute, The King's Buildings, West Mains Road, Edinburgh EH9
[3]NERC Isotope Geosciences Laboratory, Keyworth, Nottingham NG12 5GG, UK
[4]Department of Geology, School of Natural Sciences, Trinity College, Dublin 2, Ireland
***corresponding author**

ABSTRACT

The Witputs section of the Gariep Belt (S Namibia) comprises a sequence of clastic and chemical sediments, which have been interpreted as representative of a Late Neoproterozoic global or near-global ice age event, and recent biostratigraphic work in the upper rocks of the Witputs suggest a late Ediacaran age. To further characterise this sequence, and provide additional age constraints a detailed sedimentological and detrital zircon study has been carried out. The petrographic, sedimentological and geochemical characteristics of the Witputs diamictite determined in this study are homogenous and indicative of debris flow or palaeo-valley infill sediments, deposited in an oxic environment with no glaciogenic evidence. This homogeneity is also reflected in the detrital zircon age spectra with most ages falling between 1.0 and 1.3 Ga, representing the local geology, with the youngest grain at 1030.2 +/-10.9 (2σ) (n= 92 < 10% discordance), despite the fact that mid and Late Neoproterozoic volcanic activity is known in the local region.

The overlying carbonate rocks, often considered to be ‘cap carbonates’, show high Mn (up to 60% MnO), with base metal precipitation (Zn, V, Co), and are recrystallised. Their $\delta^{13}C_{VPDB}$ isotope ratios are homogeneous at around -3. Major and trace element ratios reach values which indicate that C-O isotopes may be disturbed and might not reflect primary global seawater composition, thus questioning their use for global correlation and comparison with composite chemostratigraphic curves.

The contact to the overlying late Ediacaran Sanddrif Member is not exposed and the rocks dip in a different direction than the underlying carbonate rocks. The c. 40 m thick section is characterised by rapid lithology changes including shales, calcareous sandstones and wackes, fine-grained conglomerates and rare clean quartz-rich sandstones, all of which have strikingly similar detrital zircon populations and the youngest zircon is dated at 1082.8 +/- 10 Ma (2σ errors, from 72 grains with <10% discordance). Acritarchs earlier found in the Sanddrif Member, however, indicate a post-570 Ma depositional age.

If the diamictites are glacio-marine deposits, then an interesting conclusion is that the clastic sediments can display a very immature geochemical signature, indicating a localised provenance, with derivation purely from the local basement rocks, which is also reflected in the detrital zircon populations. However, we would hesitate to assign a glacial origin to the deposits as no glacial indicators, other than a diamictitic texture, were observed. Clearly far more work on the detailed mapping and sedimentology of the Neoproterozoic Gariep Belt deposits are required, particularly as many are currently used for global correlation. Age constraints derived from extensive detrital zircon work can only constrain the deposits as being post 1.03 Ma with the detritus being purely locally derived.

INTRODUCTION

The Neoproterozoic era remains one of the most interesting and controversial periods of Earth history. It marks the disintegration of the supercontinent Rodinia, at least two global glaciation events are thought to have occurred, and major reorganisation of the cratons resulted in formation of Gondwana. Palaeogeography and interaction of the cratons is critical to our understanding of the Neoproterozoic. The Kalahari craton plays a key role, yet interpretation of the collision belts, which bound three of its margins, remains controversial. The Gariep Belt of western South Africa (Fig. 1) is thought to result from the Late Neoproterozoic to Lower Palaeozoic collision of the Kalahari and the Río de la Plata cratons and/or peri-cratonic fragments (Stanistreet et al. 1991; Gray et al. 2006; Basei et al. 2008).

In the Gariep Belt the Neoproterozoic is characterised by carbonate as well as clastic sequences and at least four separate diamictite[1] horizons have been mapped (McMillan 1968). It has been suggested that there were numerous Neoproterozoic sub-basins within the Gariep belt, making correlation both within the Gariep Belt and externally to other South African and Namibian profiles problematic, if not impossible (Martin 1965, p 79). In his seminal work of 1965, Martin identified a number of sequences in the Gariep Belt with diamictite horizons, few of which were expressly described as being either glacial or non-glacial in origin. Kröner and Rankama (1972) then reassessed the sequences identified by Martin to determine whether or not there was substantial evidence for glaciation. The final verdict about a

[1] Diamictite refers to any deposit with a texture resembling a matrix-supported conglomeratic rock, with no implications regarding genesis. Tillites are only those rocks, which have a glacial origin beyond doubt (Schermerhorn and Stanton 1963).

glacial nature of the different diamictites still awaits final approbation and will discussed later in the text.

Nevertheless, in more recent years, and despite the inherent problems of correlation within the Gariep Belt, the diamicts of the Gariep Belt are generally classed and correlated into two distinct horizons, termed the Kaigas and the Numees Formations (Martin 1965; McMillan 1968 *nota bene* current classifications may differ from the original mapping and interpretation of these authors). The Kaigas Formation is generally considered to represent the Cryogenian glaciation, while the Numees is thought to be younger and related to the Marinoan (c. 630 Ma; e.g. Fölling and Frimmel 2002; Hoffman and Li 2009), Gaskiers (c. 580 Ma; e.g. Frimmel 2008, 2009) or Moëlv (< 570 Ma according to Gaucher et al. 2005) events.

Given that the younger ages are based on biostratigraphic evidence from the younger sediments exposed at the Witputs section in the Gariep Belt of southern Namibia, these sequences have been subjected to a detailed sedimentological, petrographic and provenance study, including geochemical analysis of the diamictite bed (Numees Formation), and the overlying carbonate rocks (Bloeddrif Member).

Our study opted as well for the use of detrital zircon age dating, motivated by three arguments (i) diamictites related to major glacial events often carry a much broader range of provenance information, reflecting the overall geological evolution of the craton in the detrital zircon spectra, in contrast to stratigraphically adjacent non-glaciogenic rocks (see for example McLennan et al. 2003, Van Staden et al. 2010b); (ii) Frimmel (2000, p201) reports exotic dropstones and extrabasinal lonestones in fine-laminated siltstones interpreted to be varves and Frimmel (2008, p466) correlates the Numees Formation with diamictites elsewhere on the Kalahari craton (iii) the overlying Nama Group records magmatic activity in form of detrital zircons with ages between 680 and 550 Ma derived from the interior of the Kalahari craton (Fig. 1a; Germs 1983; Zimmermann et al. 2008). If the Numees diamictite at Witputs was deposited in this time period, then the detrital zircon populations could provide vital age constraints. Such an input might be reworked from older parts of the Nama Group (Kuibis Subgroup) or other pre-Nama sedimentary successions like the Holgat Formation.

GEOLOGY

The Gariep Belt forms part of an extensive network of Neoproterozoic to Cambrian orogenic belts in western Gondwana (Fig. 1a). It stretches along the coast from Lüderitz in Namibia to Kleinzee in South Africa, continues offshore as far as Vredendal (Germs and Gresse 1991), and extends into the Dom Feliciano Belt in southern Brazil and Uruguay (Basei et al. 2005). In southern Namibia, the Namaqua metamorphic basement rocks are overlain by the Port Nolloth Group (Fig. 2) with basal volcano-sedimentary sequences of the Stinkfontein Subgroup of Cryogenian age (771+/-6 Ma Frimmel et al., 2001). Possible rift-related magmatism continued up to 741-754 Ma (the Rosh Pinah volcanic rocks, Frimmel et al. 1996; Borg et al., 2003), prior to collision related deformation and tectonism in the late Ediacaran to Early Palaeozoic formation of Gondwana (Gray et al. 2006; Gresse et al. 2006).

The Gariep Belt is subdivided into the continental, external, para-autochthonous Port Nolloth Zone in the east, and the oceanic, possibly allochthonous Marmora Terrane to the northwest. However, the palaeogeographic evolution and tectonic interpretation of the Gariep Belt remains unclear. Originally it was thought that the lower volcano-sedimentary sequences of the Port Nolloth Group were related to rifting of the Río de la Plata from the Kalahari during opening of the Adamaster

Ocean and that the mafic rocks of the Marmora Terrane are remnants of this ocean (Frimmel et al. 1996; Basei et al. 2000). The Gariep Belt has been recently reinterpreted as a retro-arc basin (Basei et al. 2005, 2008) related to a subduction zone scenario with the volcanic arc located in eastern Uruguay. In this model, eastern Uruguay (Dom Feliciano Belt; Basei et al., 2000) had been a part of the Kalahari Craton with rifting and suturing occurring during the Neoproterozoic further to the west in central Uruguay (Basei et al. 2005, 2008). In a reconnaissance provenance study from the Gariep and Dom Feliciano Belts, Basei et al. (2005) identify arc-like geochemical signatures in few metasedimentary samples, but the age and source of this specific detritus is not clear (palaeocurrents are absent), as the arc debris can be reworked and inherited from pre-depositional rocks. The few detrital zircon ages younger than 1.0 Ga published by Basei et al. (2005) are reported with undocumented concordance values and therefore the ages cannot be reliably used as a maximum age constraint for the time of deposition.

The Port Nolloth Group in the eastern Gariep Belt is subdivided into various subgroups and formations (see Fig 2 and Frimmel, 2000). According to Gaucher et al. (2005) the maximum true thickness of the Port Nolloth Group is approximately 3.2 km for the entire depositional cycle, which lasted for approximately 200 Ma and includes rifting, drift, and development of a passive margin, which would account for a period of c. 200 Ma. The ocean in between the rifted cratons or cratonic fragments is called the Adamastor Ocean interpreted as an Atlantic-like oceanic basin (Stanistreet et al. 1991; compiled by Gray et al. 2006; Gresse et al. 2006). Of particular interest here, are the Upper Port Nolloth Group successions, which overlie the Hilda Subgroup and contain diamictite deposits (Fig. 2).

At the Witputs locality in southern Namibia (S27°35'18.6'' E16°41'09.8''; Fig. 1b), the rock succession is considered to represent the upper part of the Neoproterozoic Port Nolloth Group comprising the Numees Formation, carbonate beds (Bloeddrif Member) and clastic rocks (Sanddrif Member) of the Holgat Formation, overlain by quartz-arenites of the Nama Group (Kanies Member of the Kuibis Subgroup) (Fig. 2). Several authors argue that the Nama Group rocks erode into the top of the Holgat Formation (Germs 1974).

Age Constraints for the Numees Formation

Of particular importance is the interpreted age of deposition for the Numees Formation, the diamictite here in question, while the age of the Kaigas Formation is now well accepted on the basis of U-Pb SHRIMP ages from the immediately overlying Rosh Pinah volcanic rocks (751 Ma, Borg and Armstrong 2002; U-Pb conventional method 741 Ma; Frimmel et al. 1996; Fig. 2). The age of the Numees is more controversial as no direct age constraints are so far available and during the last 40 years a number of different diamictites have been mapped and differentiated (Martin 1965; McMillan 1968). Kröner and Rankama (1972) and Kröner (1976) re-examined the deposits and could not prove a glacial origin beyond doubt for any of the deposits and refrained to designate the deposits as tillites. In the upper part of the Numees Formation they also identified dolostones interbedded with the diamictites and time-equivalent stromatolite reefs, which would make a (near-)global ice age rather improbable and highlight the problems of using the diamictites as marker horizons (Kröner and Rankama, 1972).

More recently, detailed inter- and intrabasinal correlations of Neoproterozoic sequences of the Gariep Belt and S Africa have been made, placing them within the context of global glacial events and using them for global correlation with the Numees being glaciogenic and the Bloeddrif Member the associated ‘cap carbonate’ (Fölling and Frimmel 2002, Hoffman 1998 Hoffman and Li 2009). Accurate age constraints for the Numees and Bloeddrif are still lacking. However, on the basis of C, O and Sr isotopic correlations, Fölling and Frimmel (2002) suggest an Ediacaran age the rocks correlation with the Marinoan (Fölling and Frimmel, 2002; Hoffman and Li, 2009) or Gaskiers (Frimmel et al. 2002; Frimmel 2000, 2008, 2009) glacial events have been made.

More recently, at the Witputs locality, Gaucher et al. (2005) identified a low diversity fauna of acritarchs in the overlying Sanddrif Member (Upper Holgat Formation), which is correlated to the Kotlin-Rovno assemblage of microfossils (after Vidal and Moczydlowska 1997) and inferred to be younger than the ECAP (Ediacaran complex acritarch palynoflora; Grey et al. 2003, Gaucher and Sprechmann 2009). Combining the acritarch assemblage with the Sr isotope data of the Bloeddrif Member it was argued that the Holgat Formation could be younger than 570 Ma, and an age of 555 Ma was proposed (Gaucher et al. 2005), thus suggesting correlation of the Numees Formation with the poorly dated Moëlv or Egan glacial events (Gaucher et al. 2005; Blanco et al. 2009). If the Numees Formation is correlated with the Gaskiers (Frimmel 2009) ice age event at 580 Ma, this in turn implies a sedimentary hiatus between the Numees Formation and the Sanddrif Member.

FIELD GEOLOGY AND PETROGRAPHY

Diamictite

The Witputs diamictite is exposed in a few isolated outcrops at Witputs, which is strictly spoken Witputs North (Figs. 1b, 2a and foreground in Fig. 2b). Basement rocks of the Mesoproterozoic Namaqua Metamorphic belt are exposed in close vicinity (Figs. 1a and 3a) and lava flows of the Rosh Pinah Formation, marking the proposed Neoproterozoic rift event, can be found in less than 15 km to the southeast. The deposit at Witputs was classified by McMillan (1968) as the 'lower tillite' of the Numees Formation named Kaigas Member by Martin (1965). According to them the rocks should be associated with phyllites, limestones, limestones, quartz-arenites and conglomerates, while the upper diamictite is interbedded with dolostones, siltstones, shales and coarse-grained sandstones (Kröner and Rankama 1972, p 15).

The Witputs diamictite is c. 12-15 m thick and matrix supported (Fig. 2c) with predominantly granitic clasts to few blocks, and occasional metamorphic pebbles (relation 9:1), while sedimentary and carbonate clasts are virtually absent. The rocks have been strongly deformed with a major trend from SW-NE and foliation as steep as 35°. The deposit is massive and shows no internal structure or any facies change. The very few larger boulders (c. 30 cm) are scattered and occur occasionally, larger clasts (>5 cm) are rounded. Facetted grains and striated surfaces on pebbles and boulders could not be observed either macroscopically in the field, using a hand lens, or microscopically using electron microscope analysis of separated grains. Similarly, during fieldwork none of the criteria used for classifying a glaciogenic deposit such as striated underlying rocks, dropstones, varve deposits, chimney-like sand veins (Murton and Bateman 2007), thermal contraction cracks (Vandenberghe et al. 2004) or permafrost wedges (Van Vliet-Lanoe 1989) or any other typical criteria other than a diamictitic texture could be observed. The diamictite matrix is poorly sorted, conglomeratic to silty with angular grains (Fig. 3a). None of the microstructural criteria proposed by Menzies et al. (2006) to identify glaciogenic facies such as rotational structures, grain stacking, contorted laminations or clay translocations cvould be observed. The majority of the smaller grains (in the matrix) are quartz and feldspar (often microcline) and relatively unsorted. Lithoclasts have a metasedimentary origin and are rounded and unsorted. The rocks suffered deformation and in a number of samples small white mica grew. Few biotite grains could be seen and chlorite occurs in one sample in clusters. Other samples displayed a number of pyrite overgrowing matrix and clasts. Volcanic and unmetamorphosed sedimentary debris is absent, and quartz grains are always undulose or polycrystalline. We observed a few quartz grains with resorbation bays but could not determine if these are of magmatic origin or result of dissolution (Schneider, 1993). The matrix accounts for c. 80% of the rock and the deposit is therefore matrix supported. In summary, the structures, fabrics and sedimentological characteristics observed are typical for debris flow or mass flow deposits with rounded clasts.

Bloeddrif Member Carbonates (Holgat Fm)

Carbonate rocks of the Holgat Formation, Bloeddrif Member (Fig. 2) lie on top of the diamictite with an undulating, highly weathered contact. At this locality, it is not possible to assess the conformity of the Holgat Formation. The carbonate rocks change in colour, composition and texture from bottom to top (max. 15-20 m), and show folding (possibly slumps; Fig. 3d), lamination and trough-like surfaces. The thickness is significantly reduced in comparison to other exposures of the Bloeddrif Member where it can be up to 100 m thick (Frimmel 2000) possibly controlled by facies changes and basin morphologies. The colour at the base is pink, grading into dark blueish grey carbonate rocks. The rocks are strongly affected by large patches (5-30 m wide) of Mn and base metal mineralization (Table 1; Fig. 4b). MnO concentration is between 1 to 3 % in the pink carbonate rocks at the base of the section (see Table 1). Interestingly, Mn-rich breccias are reported at contact of carbonate rocks and volcanic rocks by Frimmel (2009, p 345) in the Rosh Pinah Formation (Fig. 2). The contorted lamination has been interpreted as reflecting crystal growth directly on the sea floor (Knoll 2003, elsewhere in the Bloeddrif Member), and the large trough-like structures have been interpreted as wave ripples induced by wind in a water depth of more than 100 m at Namuskluft, c. 20 km further southeast in a similar proximal setting (Hoffman and Li 2009). We observed these features as c. 2 m wide, with a trough-like form but with relatively sharp trough borders which is not common for ripples. We could exclude a tepee-structure, as typical feature for such structures are lacking. A final sedimentological interpretation for these structures is still absent. Stromatolites are reported from proximal section elsewhere in the Bloeddrif Member (pers. com. A. Prave).

The carbonate rocks are recrystallised and affected by a number of cracks and veins (Fig. 3d) filled with a fine layer of calcite crystals followed by syntaxial quartz-cement and a centre filled with muscovite and Mn-oxides as well as fine dolomitic calcite. In the lower layers the cracks and veins are mainly parallel to the fine bedding, but c. 4 m from the bottom the carbonate rocks are partly brecciated and the veins are randomly orientated. The Mn influx is associated with high concentrations of Zn, Co, Ni, U and Ba. The Mn mineralisation reaches up to 60 % of the rocks in the upper part of the carbonate rock and is associated with chert which totally replaces the carbonate. In the carbonate rocks we found as detrital grains mainly biotite or phlogopite, apatite, zircon and quartz. Possibly precipitates are smaller (< 20 micron) apatite crystals, anhydrate as well as Fe-oxide and ilmenite. The Mn-rich facies is massive and penetrates the carbonate rocks widening cracks and veins. According to our observation the filled veins argues for a silica-rich fluid, which transported the base metals into the rock under relatively high temperatures, which allowed mica and quartz to crystallize, as these are hydrothermal phases.

The carbonate rocks exposed at Witputs are different to the Bloeddrif Member carbonates exposed at other localities in a proximal setting (see Frimmel 2000; Gaucher et al. 2005) in that (i) no sandstones are intercalated, (ii) they have undergone significant Mn and base metal emplacement, which led to massive Mn breccias, and (iii) they do not release a typical smell of high S concentrations (Fölling and Frimmel 2002) as their TOS content is 0.01 % (Table 1). The Mn and base metal mineralization have affected the entire carbonate rock, with the development of large patches of Mn breccias (5-10 x 30 m) at the upper part of the succession. Fluid flow and mineralization did not affect either the underlying or overlying clastics. Systematic microfacies studies in these carbonates are hampered by strong recrystallisation; veining and fluid flow along veins. The carbonate beds dip between 15° and 28° to the NE and, therefore, differently from the overlying Sanddrif Member and the base of the Nama Group (Fig. 1b, 2).

Sanddrif Member (Upper Holgat Formation)

The stratigraphic contact above the Bloeddrif Member is obscured by sand and regolith for about 5-10 m. The overlying Sanddrif Member (max. 40 m) and the entire Holgat Formation are condensed in this exposure (max. 60 m). This differs significantly from the general thickness given in the literature with reported several hundreds of meter elsewhere (e.g. Frimmel 2000). This can be explained by a different depositional environment and by the possible erosive activity of the Nama Group. An unconformable lower contact can be inferred as dip angle and dip direction change from the Bloeddrif to the Sanddrif Members (Fig. 2). The exposed lower part of the Sanddrif Member is dominated by small folds and slumped beds of feldspar-rich arenites and shales. Further up in the stratigraphy quartz-rich arenites are interbedded with soft clay and carbonate-rich wackes (Fig. 4c) and conglomeratic beds. A possible volcanic ash layer was observed in the middle of the stratigraphy (see below). Throughout the entire package carbonate cements are observed in all coarser grained rocks. Flute marks in quartz-rich arenites indicate a transport orientation NW-SE although the direction could not be determined. Turbidite sedimentation could not be observed. The lithological changes are rapid and rarely one lithology holds out more than some meters. Thin shale layers (0.5 to 3 cm) occur in between the different clastic sedimentary rocks.

The mineralogy and textures of the rocks are homogeneous with quartz and feldspar clasts dominating. Few metasedimentary lithoclasts occur and are nearly always well rounded. Roundness and sorting is relatively poor at the bottom and is getting better in rocks in the middle part of the section. Often larger white mica flakes are deposited, rarely carbonate fragments can be observed. However, the entire section is affected by fine-grained calcite cementation, which overprints the matrix and covers grain borders. Only in few sample we could observe matrix composed of quartz and feldspar and few illite. Volcanic or unmetamorphosed sedimentary lithoclasts could not be identified in the various lithotypes. However, one layer showed two different deformation direction marked by large elongated mica crystals. The rock is slightly graded and in the finer-grained part large angular crystals of quartz and feldspar could be observed. However, clear volcanic textures beyond doubt could not be observed and no zircons could be identified. The rocks are visibly deformed, but only beds at the bottom and the top show cleavage and new growth of mica in thin section.

Nama Group

The contact to the base of the Nama Group (Fig. 3f) is thought to be unconformable (Germs 1974), but the bedding of the Nama sandstones is similar to that of the underlying Sanddrif Member at Witputs (Fig. 2). The lowermost Kanies Member of the Nama Group is represented by a very mature quartz-arenite (Fig. 4d), and overlies a quartz conglomerate with grain sizes between 1 and 3 cm. The quartz-arenites at the base of the Nama are moderately sorted and composed of quartz and metasedimentary lithoclasts and can be found basin wide (Germs 1995). The rocks were sampled for detrital zircon dating but the grains were always smaller than 30 microns and not useful for dating purposes.

GEOCHEMISTRY

Major element geochemistry

The matrix of the Witputs diamictite is geochemically similar to typical upper continental crust (Table 1 and Table 1 data repository; UCC after McLennan et al. 2006). The samples do not show any influence of carbonate material with CaO concentrations below 0.55%. Four clasts were sampled (three granitic pebbles (DMP2, DMP3, DMP4) and one metamorphic clast, DMP1) and indicate comparable composition to the matrix of the diamictite with only slightly higher MgO and CaO concentrations (Table 1). The carbonates have up to 5% SiO_2, 10-21% MgO and 3% - 62 % MnO and can be classified as dolomitic limestones (Table 1 data repository). The relatively high amount of silica in the Bloeddrif Member carbonate rocks is due to silica-rich cements, quartz grains and relatively abundant silicates observed. The influence of Mn-rich fluids can be observed from bottom to the top of the Bloeddrif carbonate package but is absent in the underlying diamictite and the overlying Sanddrif Member. The alteration patches of Mn contain up to 62% MnO, high values

(0.5 – 2 %) for Zn, Co and Ni, with a chert matrix and depleted in CaO and MgO (Table 1). The rocks of the overlying Sanddrif Member are variable in their geochemical composition and display often enriched CaO concentrations (up to 33%). MnO enrichment is absent and rarely SiO_2-rich (>75%) rocks were deposited. Fe_2O_{3t} concentrations are generally low (with few exceptions), while MgO is in some samples enriched and reaches concentrations similar to the CaO (Table 1), which points to the abundance of dolomite. In contrast, the rocks at the base of the Nama Group are completely different and strongly enriched in SiO_2 (85-93%).

The Chemical Index of Alteration (CIA; after Nesbitt and Young 1982) is low for the diamictite with values between 56 and 63 and only slightly higher than the values of the four mentioned pebbles (Table 1). High CaO concentrations in the clastic rocks of the Holgat Formation exclude most of the samples from reliable calculations but the few samples with low CaO abundances point to a low value (56-65). Hence, the low CIA values point to a relatively low chemical alteration for the diamictite and clastic rocks of the Holgat Formation.

Trace element geochemistry of the clastic rocks

Volcanic and clastic sedimentary rocks can be geochemically characterised using the ratios of Zr/Ti versus Nb/Y (after Winchester and Floyd 1977; Fralick 2003; Lacassie et al. 2006; Van Staden et al. 2006; Bertolino et al. 2007), as these elements are strongly immobile. In Figure 5a samples from the Witputs diamictite matrix plot in a cluster, denoting a homogeneous composition. This is rather surprising for a glaciogenic rock as clustering should be seen only if there was a single homogenous source as sorting cannot play a major role if the rocks are immature. Diamictite or glaciogenic deposit which incorporates wide area of deglaciated craton surface rocks are expect to show a much broader spread of data (Young et al. 2000; McLennan et al.

2003). For comparison, data obtained from two other exposures of the Numees diamictite in this region (see Van Staden et al. 2006) are also shown. These data are sampled in exposures defined by McMillan (1968) as the 'upper tillite', or as the 'major tillite' by Martin (1965), one close to the type section of the Numees Formation (Van Staden et al. 2006). The geochemistry of the Witputs diamictite is different with a dominant alkaline source. The immature rocks of the Holgat Formation show a wider spread in their geochemistry, but with most of the samples pointing to a dominant felsic source (Fig. 5a), while the samples from the Nama Group (Kuibis Subgroup) are markedly high fractionated with a trend to alkaline sources.

Elements with a higher redox-potential such as Mo, Cd, V and other base metals enrich generally in an anoxic environment as do U/Th ratios (up to 1), due to U being less soluble under anoxic conditions (Calvert and Pedersen 1993). Such trends have been observed in glacial diamictites such as Hirnantian deposits from the Kalahari craton (Young et al. 2000) or Neoproterozoic deposits in China (Dobrzynski et al. 2004). However, no such trends are seen in these samples (see Table 1).

Th/Sc ratios are plotted against Zr/Sc ratios for the Witputs diamictite, the Sanddrif Member of the Holgat, and the lowermost Nama Group in Fig. 5b and are compared with data from the two other mentioned Numees Formation samples (green data points; Van Staden et al., 2006). The Witputs diamictite shows a cluster with high Th/Sc ratios, and Zr/Sc values indicate a major amount of recycled detritus with a characteristic clustered signature. The other exposures of the Numees diamictites (Van Staden et al. 2006) display different ratios hence are composed of different detrital material. All samples of the clastic Sanddrif Member show a wide range of both Th/Sc and Zr/Sc values reflecting the poor mixing of the detritus and the different, mainly felsic detritus with partly increased Zr/Sc ratios (> 30; Fig. 5b, Table 1).

Rare earth elements and Y geochemistry of the carbonates

REE+Y values given by Frimmel (2009) as criteria for environmental interpretation of carbonates would indicate for the carbonates at Witputs that the rocks were influenced by river water so deposited very close to the palaeoshoreline, with $(Y/Ho)_{SN}$ values comparable to PAAS (post Archaean Shale after Taylor and McLennan, 1985), the absence of a La/La* anomaly and with a significant influence of clastic material with Zr (> 4 ppm) (Table 2c), as confirmed by petrography. The samples at Witputs trend to show similarities to the proximal exposure analysed by Frimmel (2009) (Table 2c). The difference of the REE geochemistry of the carbonates at Witputs to samples from the proximal section of the Bloeddrif Member is that there is no correlation between Fe and total REE, as proposed by Frimmel (2009) for near-shore deposits. However, it might be that in the sampled carbonates at Witputs the clastic fraction is too strong and overprints any primary water signature.

ISOTOPE GEOCHEMISTRY

Carbon and Oxygen Isotopes in Carbonate Rocks

A total of seven samples were collected from the carbonate section with a sampling distance of approximately 1.2 m from the base upwards, avoiding the Mn-rich beds at the top of the section. The values for $\delta^{13}C_{VPDB}$ vary between -2.88 and -3.11. $\delta^{18}O_{VPDB}$ and $\delta^{18}O_{VSNOW}$ vary from -2.3 to -10.14 and 18.23 to 20.45, respectively, from bottom to top in these c. 12 m. The relatively constant values through the section are slightly different to previously published results from the

Bloeddrif Member sampled at different sections, especially in regard to O isotope values (Table 2a, b, Fölling and Frimmel 2002). The Mn/Sr, Fe/Sr and Ca/Sr ratios are generally higher than those in other sections (due to the lower than expected Sr concentrations; Table 2c), and are mostly well above the accepted thresholds for reliable chemostratigraphic proxies (after Fölling and Frimmel 2002). Frimmel (2008, 2009) points out the importance of local environmental influences for carbon isotopes in the Gariep Belt, demonstrating primary values diverging from secular sea water trends (Halverson et al. 2007, 2010). These variations are controlled by water composition (salinity and influx of river water) and by the occurrence of evaporites. The samples at Witputs comprise evaporite minerals and low Sr concentrations (Table 1).

Detrital Zircon Dating

The Witputs diamictite (NUM), the Sanddrif Member (HOL) and the Kanies Member (basal Nama Group) were sampled for detrital zircon age dating. The detrital zircons from the Nama Group were too few to represent a statistically valid sample, and too small (<30µm) to determine reliable ages using an LA-MC-ICP-MS. The results are compiled in Table 3, concordant results are listed at the top of every column, and probability plots are shown in Figure 1 of the data repository.

The 92 detrital zircon grains (<10% discordant) of the Witputs diamictite (NUM) show an unexpected $^{207}Pb/^{206}Pb$ age distribution (Fig. 6; Fig.1 data repository). The youngest detrital zircon grains are Mesoproterozoic in age, and more than 75% of the analysed detrital zircons have ages between 1.05 and 1.20 Ga. Most of the strongly discordant ages are Neoarchaean. The oldest concordant detrital zircon grains, which are round (Fig. 1 supplementary material), are Late Mesoarchaean to Neoarchaean in age (Table 3).

The Holgat Formation (HOL) sample is composed of sub-samples from different lithotypes sampled throughout the section, and the detrital zircon age spectrum is strikingly similar to that of the diamictite, with 78% of all detrital zircons being 1.0 -1.2 Ga in age (n=71 with < 10% discordance). Samples NUM and HOL are both devoid of any younger grains than 1.00 Ga. Both samples have minor amounts of detrital zircon grains with ages around 1.5 Ga and between 1.80 and 2.05 Ga. The oldest detrital zircon grains found in the Holgat Formation are Late Palaeoproterozoic in age.

INTERPRETATION AND DISCUSSION

Implication of the geochemical and isotope geochemical data

Detrital Zircon Populations and Source

Neoproterozoic grains are absent and most of the dated detrital zircon grains are related to locally occurring sources (Fig. 6a). Both samples show a minor peak of detritus with Late Palaeoproterozoic ages, which can be assigned to the Orange River Group and Vioolsdrif Suite rocks, or their equivalents, exposed further south and were possibly reworked from the Namaqua Metamorphic belt. The Archaean input, which is very low, can be explained through reworking of Mesoproterozoic rocks, which incorporate such detritus.

The lack of any Neoproterozoic grains is noteworthy, particularly given that in a previous study of diamictites of the Port Nolloth Group, two of which are classified as the Numees Formation (‘upper tillite’ after McMillan, 1968 or ‘major tillite’ after Martin, 1965), the youngest grain revealed an age of 784 +/-21 Ma (Fig. 6a; Van Staden et al., 2010a). It is also surprising as these are general interpreted as being glacial rocks, and so, as discussed should have a much broader age spectra (McLennan et al. 2003; Van Staden et al. 2010b; Nicoll et al. 2010).

Furthermore, no zircon ages related to the geographically closely related (c. 15 km) Neoproterozoic Rosh Pinah Formation volcanic event were found. These volcanic successions are dominated by felsic volcanic rocks with more than 1 km thickness (Kapok Formation after Martin 1965) and interpreted as being related to the rifting of the Adamastor Ocean. Similarly no detritus from the rift associated plutonic rocks of the Neoproterozoic Richtersveld Suite (Frimmel et al. 2001) were identified. This can be explained by (i) a tectonic style which did not exhume these buried successions, hence they were not exposed until 550 Ma, (slightly younger than the assumed age of the Sanddrif Member [Gaucher et al. 2005]); (ii) sediment transport directions which controlled the sediment transport and did not receive detritus from these sources, (iii) the fact that the basins were extremely restricted in their sizes and catchment areas as speculated by Martin (1965).

Carbonate rocks

The carbonate rocks at Witputs are correlated with the Kombuis Member of the Cango Caves Group (S Africa) and related to a cold climate event (e.g. Gaucher et al., 2005) and a near-global ice age event (Blanco et al., 2009). The C-Sr isotope values of the carbonate rocks at Witputs are compared with the basal 15 m of the Kombuis Member and other sections of the Bloeddrif Member in Fig. 7) with the secular curves for Sr and C isotopes after Halverson et al. (2007, 2010). We can observe slight differences between the three carbonate sections from the Gariep belt regarding their C isotopes for the first 15 m. Their starting point is quite similar, but the trends are then countercurrent for the distal and proximal section reasoned by their different depositional environment (Frimmel 2009). In Fig. 7 several attempts are made to fit the C isotope curve into the secular curve and this can be done during different points of time. However, at the proposed age at around 555 Ma (Gaucher et al. 2005) the Witputs samples do not fit unless there is a hiatus between the carbonate and clastic rocks at Witputs. However, Frimmel (2008) demonstrated that facies conditions could affect C and Sr isotope signatures, when rocks are deposited in smaller isolated basins with high salinity and the occurrence of evaporites. Furthermore, Frimmel (2009) showed for the proximal Bloeddrif Member carbonate rocks their coastal position affected the C isotope values as such that they do not reflect anymore the seawater composition but a mixture with river water. The samples from Witputs point to a similar trend and it is reasonable to argue that the REE concentrations are affected by the input of clastic material and overprinting of the carbonate signature. Moreover, geochemical values, which can demonstrate the effect of diagenesis and other post-depositional geological events affecting a primary chemostratigraphic signature, are mostly too high in the carbonate rocks at Witputs and point to such a disturbance in coincidence with the petrographic findings (Table 2).

If the Sr isotope values are interpreted as primary, a possible post-Marinoan and a pre-Gaskiers age could be inferred (Fig. 7), but this would be in contrast to the proposed age constraints by the clastic rocks based on microfossils. Hence, using Sr isotope data for the correlated Kombuis and Bloeddrif Members is not in accord with the proposed depositional age of the Kombuis Member. Correlating the Bloeddrif Member with the Kombuis Member would incriminate the validity of the Sr isotopes for the former in regard of the secular curve.

Combining the data with the acritarch assemblage interpreted as being younger than the ECAP, hence younger than 570-565 Ma (Grey et al. 2003; Grey and Calver 2007), then the carbonate deposit is not related to a (near-)global ice age, as no global or near-global ice event is observed for the time after 570-540 Ma on Earth and the evolution of Ediacaran fauna was flourishing, which is contradictive to one of the major arguments of the ‘snowball earth hypothesis’ (Hoffman and Schrag 2002).

Sedimentological interpretation

The massive diamictite does not show any lithological or petrographical changes. The larger clasts are rounded, while the matrix is dominated by angular grains. The lithoclasts are derived from metasedimentary rocks, and larger feldspar and quartz crystals have a (meta-)igneous origin. The deposit shows no indication for deposition in a glaciogenic environment. The detrital zircon population (n= 92; < 10% discordance) of the diamictite shows an absence of regionally and locally exposed Neoproterozoic rocks but is dominated by Mesoproterozoic detritus (Table 3). Hence, the detrital zircon population does not reflect a larger catchment area but simply the very local geology. Based on all these characteristics, the deposit is best described as a debris or mass flow, probably a palaeovalley infill. Using the classification of Sømme et al. (2009), the Witputs diamictite deposit relates to a small-scale sedimentary system with a short depositional history as suspected by Martin (1965).

The overlying carbonate rocks show influence of detrital minerals point to a proximal depositional setting. The rocks also show fine lamination and different grain sizes and were affected by hydrothermal alteration and fluid flow, which resulted in the crystallisation of muscovite, quartz and calcite in veins together with MnO and the enrichment in various base metals. These characteristics will have had a significant effect on the trace element geochemistry, thereby hampering Chemostratigraphic correlation.

The restricted detrital zircon population and the rapid lithological changes in the Sanddrif Member point to an unstable environment characterised by permanent facies changes. Frimmel et al. (2002) report for the upper part of the Holgat Formation a ‘flysch-deposit’ (foreland basin) deposited in fore-deep position (Frimmel and Fölling 2004) represented by widespread turbidite sedimentation. This is not observed at Witputs. Either the top of the Sanddrif Member has been eroded or, alternatively the Witputs represent a much shallower basin part, which is likely given the proximity of basement rock exposures. The basin developed during the closure of the ocean between the Kalahari and Río de la Plata cratons, which started approx. 580 Ma (Frimmel 2000; Gray et al. 2006). The envisaged depositional age of the Sanddrif Member according to its acritach assemblage is approximately 555 Ma (Gaucher et al. 2005). During such a long period, basin margins should be developing, and mixing as well as sorting should be a dominant sedimentary process. However, we observe poorly sorted rocks, with a dominance of local sources. This could be explained if there was a massive orogenic belt to the east, which blocked any sediment from the interior of the craton. The relatively immature upper successions of the Gariep basin can be explained through deposition in relatively small sub-basins, or possibly in a larger foreland basin, thus explaining extremely local source of detritus.

Implications for correlation

The combination of these new data and the data known from literature complicates possible correlation of the deposits at Witputs if they are assigned to global or near-global ice age events. We demonstrated that the diamictite at the bottom of the section at Witputs does not show any indication for a glaciogenic origin. Overlying carbonates rock are affected by fluid flow and significant clastic input and their geochemical characteristics point to a post-depositional disturbance of their isotope characteristics. A negative C isotope excursion in Neoproterozoic rocks, as observed here, is often related glaciations in the Snowball Earth context. Recently, the upper Doushantuo Formation, generally interpreted as 'cap carbonates', were dated by a ash layer with SHRIMP technique at 555.2 +/-6.1 Ma and the carbonate rocks show significant negative excursions as negative as -3 for $\delta^{13}C$ (Zhang et al. 2005). This negative excursion is difficult to interpret in terms of a major global glacial event as it is coeval with development of the Ediacaran fauna (dated at 555 +/- 0.3 Ma in the White Sea region of Russia, Martin et al. 2000).

Microfossil evidence tends to argue for a depositional age around 555 Ma for the Sanddrif Member (Gaucher et al. 2005). This leads to two options: (i) interpreting the entire succession at Witputs as conformable and therefore with an age between 555 and 560 Ma with the consequence that C-Sr isotope values cannot be used for correlation and the diamictite at the base is not related to a global or near-global ice age event or (ii) assign very different depositional ages to these three sedimentary rocks with a considerable hiatus (of several million years) in between them. Following option (i) the section cannot be correlated to a global or near-global ice age event in our current knowledge and correlation based on that criterion is not possible. Following option (ii) the microfossil assemblage in the Sanddrif Member does not date the Numees Formation, assuming the diamictite at the bottom of the section at Witputs is the Numees Formation.

CONCLUSIONS AND IMPLICATIONS FOR THE REGIONAL GEOLOGY

The Witputs section of the Gariep Belt (S Namibia) comprises a sequence of clastic and chemical sediments, which were interpreted in the literature as representative of global or near-global ice age events (e.g. Fölling and Frimmel 2002; Gaucher et al. 2005; Blanco et al. 2009; Frimmel 2009). They are therefore key exposures of Late Neoproterozoic age for cratonwide correlation. Detailed petrographic, geochemical and isotope geochemical studies were applied to these rocks to further characterize their provenance and age to reveal more arguments for such an attempt.

The petrographic, sedimentological or geochemical characteristics of the Witputs diamictite are indicative of debris flow deposits or palaeo-valley infill with no glaciogenic evidence, deposited in an oxic environment. The mineralogical and geochemical composition is homogeneous and dominated by felsic magmatic and felsic metamorphic detritus only, although the textural maturity is very low. This homogeneity is reflected in the detrital zircon age spectra with most ages falling between 1.0 and 1.3 Ga, representing the local geology and, therefore, atypical for a glacial diamictite or tillite related to a near-global ice age event. Therefore, we interpret a non-glacial origin for the deposit.

Paraconformable overlying carbonate rocks, earlier identified as ‘cap carbonates’ and therefore correlated regionally and globally, were attributed to the Bloeddrif Member of the Holgat Formation (e.g. Gaucher et al. 2005), show Mn (up to 60% MnO) and base metal precipitation (Zn, V, Co) and are recrystallised. Their $\delta^{13}C_{VPDB}$ isotope values are homogeneous around -3, while $\delta^{18}O_{VSMOW}$ values rise from 19.63 to 21.89 through the section and are different from those found in other section of the Bloeddrif Member. Major and trace element ratios reach values which indicate that C-O isotopes should be disturbed and/or do not reflect the primary seawater composition because of the syndepositional environmental setting. However, using the C-Sr isotope data for correlation with the recent published secular curve by Halverson et al. (2007, 2010) only a post-Marinoan age would fit well, as earlier proposed (Fölling and Frimmel, 2002). However, other possibilities can be assumed if the deposit is not related to a (near-)global ice age event or/and the C-Sr isotopes would be reinterpreted (Frimmel 2008, 2009).

The contact to the overlying late Ediacaran Sanddrif Member is not exposed and the rocks have a different dip direction to the underlying carbonate rocks. The c. 40 m thick section is characterised by rapid lithology changes including shales, calcareous sandstones and wackes, fine-grained conglomerates and rare clean quartz-rich sandstones. We interpret for this section a possible shallow water facies at the coastline. The geochemical signature is according to the different lithologies heterogeneous, and contains often a significant reworked component possibly inherited from the sources (Zr/Sc >30; Ti/Zr <15; Th/Sc 1-3). The detrital zircon population is as restricted in their spread as in the underlying diamictites. The youngest detrital zircon was dated at 1082.8 +/- 10 (2σ). Acritarchs found in the Sanddrif Member would point to an age younger than 570 Ma (Gaucher et al. 2005) or 565 Ma (Grey and Calver 2007), which is not in accord with the support of C-Sr isotope values if correlating them with the secular sea-water curve (Fig. 7).

If the carbonate rocks are interpreted as ‘cap carbonates’, then a Marinoan age would fit best the Sr isotope characteristics. The overlying rocks of the Sanddrif Member (Holgat Formation) could have a depositional age, according to the interpretation by Gaucher et al. (2005), of around 555 Ma. This hiatus might explain the restricted Mn and base metal mineralisation, which affected only the carbonate rocks.

ACKNOWLEDGEMENTS

JT and UZ acknowledge financial assistance from Marie Curie FP6 EXT Action. UZ thanks Marathon and Statoil for financial support. We are grateful to S. Siegesmund and M.A.S. Basei to be invited to this special volume. We acknowledge the review of an anonymous person and the thorough and inspiring comments by A. Prave, which enhanced the quality of the manuscript.

REFERENCES

Aftalion M, Bowes DR, Vrána S (1989) Early Carboniferous U–Pb zircon age of garnetiferous, perpotassic granulites, Blansk´y les massif, Czechoslovakia. N Jahrb Min Monats 4:145–152

Andersen T (2005) Detrital zircons as tracers of sedimentary provenance: limiting conditions from statistics and numerical simulation. Chem Geol 216: 249–270

Basei MAS, Siga Jr O, Masquelin H, Harara OM, Reis Neto JM, Preciozzi Porta F (2000) The Dom Feliciano Belt and the Rio de la Plata Craton: tectonic evolution and correlation with similar provinces of southwestern Africa. In: Cordani UG, Milani EJ, Thomas Filho A, Campos DA, (eds) Tectonic evolution of South America. 31st Intern Geol Congress, Rio de Janeiro 311-334

Basei MAS, Frimmel HE, Nutman AP, Preciozzi, F, Jacob J. (2005) A connection between the Neoproterozoic Dom Feliciano (Brazil/Uruguay) and Gariep (Namibia/South Africa) orogenic belts – evidence from a reconnaissance provenance study. Precambrian Res. 139:195-221

Basei MAS, Frimmel HE, Nutman, AP, Preciozzi, F. (2008) West Gondwana amalgamation based on detrital zircon ages from Neoproterozoic Ribeira and Dom Feliciano belts of South America and comparison with coeval sequences from SW Africa; Geol Soc London Spec Publ 294: 239-254

Bertolino SRL, Zimmermann U, Sattler F (2007) Mineralogy and geochemistry of bottom sediments from water reservoirs in the vicinity of Córdoba, Argentina: environmental and health constraints. Appl. Clay Sci. 36:206-220

Bhatia M, Crook KAW (1986) Trace element characteristics of graywackes and tectonic setting discrimination of sedimentary basins. Contrib. Mineral. Petrol. 92:181-193

Blanco, G., Rajesh, H.R., Gaucher, C., Germs, G.J.B., Chemale Jr., F., 2009. Provenance of the Arroyo del Soldado Group (Ediacaran to Cambrian, Uruguay): Implications for the paleogeographic evolution of southwestern Gondwana; Precambrian Res., 171, 57–73.

Borg G, Armstrong R (2002) Isotopic SHRIMP age dating of zircons from igneous basement and rhyolitic cover rocks at Skorpion, Southern Namibia. 11th Symposium of IAGOD and GEOCONGRESS, Windhuk, 4 pages

Borg G, Kärner K, Buxton M, Armstrong R, Van Der Merwe SW (2003) Geology of the Skorpion zinc deposit, southern Namibia. Economic Geology 98: 749–71

Calvert SE, Pedersen TF (1993) Geochemistry of recent oxic and anoxic marine sediments: Implications for the geological record. Marine Geology 113:67-88

Dobrzinski N, Bahlburg H, Strauss H, Zhang Q (2004) Geochemical climate proxies applied to the Neoproterozoic glacial succession on the Yangtze Platform, South China. In: Jenkins G, McMenamin M, Sohl L, McKay C (eds) The extreme Proterozoic: Geology, Geochemistry and Climate. American Geophysical Union Monograph Ser 146:13-32.

Fölling PG (2000) Chemostratigraphic correlation and Pb-Pb dating of carbonate sequences in the external Gariep Belt and Kango Inlier of the Saldania Belt in Namibia and South Africa. Unpublished PhD thesis, University of Capetown, Capetown, 1-251

Fölling PG, Frimmel HE (2002) Chemostratigraphic correlation of carbonate successions in the Gariep and Saldania Belts, Namibia and South Africa. Basin Research 13:1-37

Fralick P (2003) Geochemistry of clastic sedimentary rocks: ratio techniques. In: Lentz, D.R. (ed) Geochemistry of sediments and sedimentary rocks: Evolutionary Considerations to Mineral-Deposit-Forming Environments. Geol. Assoc. Can. Spec. Pap 4:85-104

Frimmel HE (2000) The Pan-African Gariep Belt in southwestern Namibia and western South Africa. Communications of the Geological Survey of Namibia, 12, 197-209

Frimmel HE (2008) An evaporitic facies in Neoproterozoic post-glacial carbonates: The Gifberg Group, South Africa. Gondwana Res 13:453-468

Frimmel, H.E. (2009) Trace element distribution in Neoproterozoic carbonates as palaeoenvironmental indicator. Chem Geol 258:338–353

Frimmel HE, Klötzli U, Siegfried P (1996) New Pb-Pb single zircon age constraints on the timing of the Neoproterozoic glaciation and continental break-up in Namibia. J Geol 104:459-469

Frimmel HE, Zartman RE, Spaeth A (2001) The Richtersveld igneous complex, South Africa; U-Pb zircon and geochemical evidence for the beginning of Neoproterozoic continental breakup. Journal of Geology 109:493-508.

Frimmel HE, Fölling PG, Eriksson P (2002) Neoproterozoic tectonic and climatic evolution recorded in the Gariep Belt, Namibia and South Africa. Basin Research, 14:55-67

Frimmel HE, Fölling PG (2004) Late Vendian Closure of the Adamaster Ocean: Timing of Tectonic Inversion and Syn-orogenic Sedimentation in the Gariep Basin. Gondwana Research 7:685-699

Gaucher C, Frimmel HE, Germs GJB (2005) Organic-walled microfossils and biostratigraphy of the upper Port Nolloth Group (Namibia): implications for latest Neoproterozoic glaciations. Geol Mag 142:539-559

Gaucher C, Sprechmann P (2009) Neoproterozoic acritarch evolution. In: Gaucher C, Sial AN, Halverson GP, Frimmel HE (eds) Neoproterozoic-Cambrian tectonics, global change and evolution: a focus on southwestern Gondwana. Developments in Precambrian Geology 16: 319-326

Germs GJB (1974) The Nama Group in South West Africa and its relationship to the Pan African geosyncline. The Journal of Geology 82:301-317

Germs GJB (1983) Implications of sedimentary facies and depositional environmental analysis of the Nama Group in South West Africa/Namibia. In: Miller R McG (ed) The evolution of the Damara Orogen of South West Africa/Namibia. Geological Society of South Africa, Spec. Publ. 11:89-114

Germs GJB (1995) The Neoproterozoic of southwestern Africa, with emphasis on platform stratigraphy and paleontology. Precambrian Res. 73:137-151

Germs GJB, Gresse PG (1991) The foreland basin of the Damara and Gariep orogens in Namaqualand and southern Namibia: stratigraphic correlations and basin dynamics. S. Afr. J. Geol. 94:159-169

Gray DR, Foster DA, Ben Goscombe B, Passchier CW, Trouw RAW (2006) $^{40}Ar/^{39}Ar$ thermochronology of the Pan-African Damara Orogen, Namibia, with implications for tectonothermal and geodynamic evolution. Precambr Res 150:49–72

Gresse PG, von Veh MW, Frimmel HE (2006) Namibian (Neoproterozoic) to Early Cambrian Sucessions. In: Johnson MR, Anhaeusser CR, Thomas, RJ (eds) The Geology of South Africa. Council of Geoscience, 395-420, Pretoria

Grey K, Walter Mr, Calver Cr (2003) Neoproterozoic biotic diversification: Snowball Earth or aftermath of the Acraman impact? Geology 31:459–62

Grey K, Calvert CR (2007) Correlating the Ediacaran of Australia. Geological Society, London, Special Publications, 286: 115-135

Halverson, G.P., Dudas, F.O., Maloof, A.C. and Bowring, S.A., 2007. Evolution of the Sr-87/Sr-86 composition of Neoproterozoic seawater. Palaeogeography Palaeoclimatology Palaeoecology, 256(3-4): 103-129.

Halverson GP, Wade BP, Hurtgen MT, Barovich KM (2010) Neoproterozoic chemostratigraphy. Precam Res (in press)

Hoffman PF, Li, ZX (2009) A palaeogeographic context for Neoproterozoic glaciation; Palaeogeography, Palaeoclimatology, Palaeoecology 277:158–172

Jackson SE, Pearson NJ, Griffin WL, Belousova EA (2004) The application of laser ablation-inductively coupled plasma-mass spectrometry to in situ U–Pb zircon geochronology. Chem Geol 211:47-69

Knoll A (2003) Life on a young planet: The first three Billion years of evolution on Earth. 1-277, Princeton University Press, New Jersey

Kröner A, Rankama, K (1972) Late Precambrian glaciogenic sedimentary rocks in southern Africa: A compilation with definitions and correlations; The Precambrian Research Unit, University of Cape Town, bulletin 11, 1-37

Lacassie JP, Hervé F, Roser B (2006) Sedimentary provenance study of the post-Early Permian to pre-Early Cretaceous metasedimentary Duque de York Complex, Chile. Rev. Geol. Chile 33: 199-219

Martin M (1965) The Precambrian Geology of South West Africa and Namaqualand; The Precambrian Research Unit, University of Cape Town, 1-159.

Martin MW, Grazhdankin DV, Bowring SA, Evans DAD, Fedonkin MA, Kirschvink JL (2000) Age of Neoproterozoic bilatarian body and trace fossils, White Sea, Russia: Implications for metazoan evolution. Science 288: 841–845

McLennan SM, Taylor SR, McCulloch MT, Maynard JB (1990) Geochemical and Nd-Sr isotopic composition of deep-sea turbidites: Crustal evolution and plate tectonic associations; Geochim. Cosmochim. Acta 54:2015-2050

McLennan SM, Bock B, Hemming SR, Horrowitz JA, Lev SM, McDaniel DK (2003) The roles of provenance and sedimentary processes in the geochemistry of sedimentary rocks. In: Lentz, RD (ed) Geochemistry of sediments and sedimentary rocks: Evolutionary Considerations to Mineral-Deposit-Forming Environments. Geological Association of Canada, GEOText 4:7-38

McLennan SM, Taylor SR, Hemming SR (2006) Composition, differentiation, and evolution of continental crust: Constraints from sedimentary rocks and heat flow. In: Brown M, Rushmer T (eds) Evolution and Differentiation of the Continental Crust. 92-134, Cambridge Univ. Press

McMillan M.D (1968) The geology of the Witputs-Sendlingsdrif area; The Precambrian Research Unit, University of Cape Town, 4:1-177

Menzies J, van der Meer JM, Rose J (2006) Till—as a glacial 'tectomict', its internal architecture, and the development of a 'typing' method for till differentiation; Geomorphology 75:172– 200

Murton JB, Bateman MD (2007) Syngenetic Sand Veins and Anti-Syngenetic Sand Wedges, Tuktoyaktuk Coastlands, Western Arctic Canada; Permafrost and Periglac. Process. 18:33–47

Nesbitt HW, Young YM (1982) Early Proterozoic climates and plate motions inferred from major element chemistry of lutites; Nature 299:715-717

Nicoll G, Straathof G, Tait J, Lo K, Ousmane N, El Moctar Dahmada M, Berndt J, Key R (2010) Provenance analysis and tectonic setting of the Neoproterozoic sediments within the Taoudeni Basin, Northern Mauritan Geophysical Research Abstracts 12:EGU2010-7094-2

Schermerhorn LJG, Stanton WI (1963) Tilloids in the West Congo geosyncline. Q. J. Geol. Soc.London 119, 201-234

Schneider N (1993) Das lumineszenzaktive Strukturinventar von Quarzphänokristen in Rhyolithen; Göttinger Arbeiten zur Geologie und Paläontologie, 60:1-81

Sømme TO, Helland-Hansen W, Martinsen OJ, Thurmond JB (2009) Relationships between morphological and sedimentological parameters in source-to-sink systems: a basis for predicting semi-quantitative characteristics in subsurface systems. Basin Res 21:361-387.

Stanistreet IG, Kukla PA, Henry G (1991) Sedimentary basinal responses to a Late Precambrian Wilson cycle: the Damara Orogen and Nama Foreland, Namibia. Journal of African Earth Science 13:141-156

Taylor SR, McLennan SM (1985) The Continental Crust: its Composition and Evolution. 1-298, Blackwell Scientific, Oxford

Van Staden A, Naidoo T, Zimmermann U, Germs GJB (2006) Provenance analysis of selected clastic rocks in Neoproterozoic to lower Palaeozoic successions of southern Africa from the Gariep Belt and the Kango Inlier. S. Afr. J. Geol. 109:215-232

Van Staden A, Zimmermann U, Gutzmer J, Germs GJB, Chemale Jr F (2010a) Detrital zircon dating and sedimentology of two Neoproterozoic diamictites from the Gariep belt (Namibia) and consequences for correlation. NGF Vinterkonferansen 11-13.1. 2010 Oslo.

Van Staden A, Zimmermann U, Gutzmer, J, Chemale Jr F, Germs GJB (2010b) First regional correlation of Lower Paleozoic successions from Argentina and South Africa using glacial diamictite deposits and its consequences for the regional geology. J Geol Soc London 167: 217-220

Van Vliet-Lanoe B (1989) Dynamics and extent of the Weichselian permafrost in Western Europe (substage 5e to stage 1);.Quaternary International 3/4:109–113.

Vandenberghe J, Zhiju C, Liang Z, Wei Z (2004) Thermal-contraction-crack Networks as Evidence for Late-Pleistocene Permafrost in Inner Mongolia, China; Permafrost and Periglac. Process. 15:21–29

Wiedenbeck M, Alle P, Corfu F, Griffin WL, Meier M, Oberli F, Von Quadt A, Roddick JC, Spiegel W (1995) Three natural zircon standards for U-Th-Pb and Lu-Hf, trace element and REE analyses. Geostand Newsl 19:1-23

Winchester JA, Floyd PA (1977) Geochemical discrimination of different magma series and their differentiation products using immobile elements. Chem. Geol. 20:325-343

Young GM, Minter WEL, Theron JN (2000) Geochemistry and palaeogeography of upper Ordovician glaciogenic sedimentary rocks in the Table Mountain Group, South Africa. Palaeogeography, Palaeoclimatology, Palaeoecology 214:323-345.

Zhang S, Jiang G, Zhang J, Song B, Kennedy MJ, Christie-Blick N (2005) U-Pb sensitive high-resolution ion microprobe ages from the Doushantup Formation in south china: Constraints on late Neoproterozoic glaciations. Geology, 33: 473-476.

Zimmermann U (2009) What was wrong with the Kalahari Craton?; Rodinia: Supercontinents, Superplumes and Scotland – FERMOR Meeting, Geological Society of London, Program and abstracts, 59

Zimmermann U, Chemale Jr F, Dussin IA, Justino D, Germs GJB, Blanco G (2008) Detrital zircon record of the Nama Group: implications for the Neoproterozoic to lower Palaeozoic palaeogeography of southern Africa. Actas VI South American Symposium on Isotope Geology, short paper, Bariloche (CD-ROM)

FIGURE CAPTIONS

Figure 1: a) Important Neoproterozoic orogenic belts in southwestern Gondwana (modified after Fölling 2000). - b) Schematic geological map of the sampling area; the basement comprises alaskitic and pegmatitic gneisses, mica schist, amphibolites, muscovite and adamellitic gneisses of the Gaidab Massif (after McMillan 1968); cl= indicates cleavage.

Figure 2: Stratigraphy of the Port Nolloth and Nama Groups after Germs (1995) and Gresse et al. (2006). Structural data and rock classification are from this study. Age constraints are compiled from Gaucher et al. (2005).

Figure 3: a) Satellite photograph of the sampling locality; b) photograph of the section; c) Close up of the diamictite at the base; d) carbonate rock with Mn alteration; e) Sanddrif Member; f) Contact between the Sanddrif Member and the base of the Nama Group.

Figure 4: Photomicrographs (under polarized light) of: a) the Witputs diamictite matrix; b) the Mn-rich carbonate rocks; c) the Sanddrif Member; d) the base of the Kuibis Subgroup.

Figure 5: Geochemical ratios for provenance analysis. a) Geochemical plot after Winchester and Floyd (1977); b) Th/Sc versus Zr/Sc after McLennan et al. (1990). The star indicates a typical upper continental crustal composition (after McLennan et al. 2006).

Figure 6: Schematic distribution of detrital zircon age spectra (see data in Table 3; CL imaging of selected important zircons in Fig. 1 supplementary material and probability plots in Fig. 2 supplementary material). a) Detrital zircon ages from the diamictite and the Sanddrif Member (Holgat Formation) at Witputs. The youngest zircon measured in the Numees Formation was sampled in northern South Africa (close to the type locality; see Van Staden et al., 2006 for locality; data for the Kaigas and Numees Formations from Van Staden et al., 2010a); b) Detrital zircon ages from the Rosenhof Member (Fish River Group) and the Nasep Member (Schwarzrand Group) from the southern Nama Basin both with palaeocurrents from the east (sample localities and palaeocurrents in Germs (1983, p 101, 106) and from Zimmermann et al. (2008).

Figure 7: Compilation of C-Sr isotope data for the Bloeddrif Member distal (B-D), Bloeddrif Member proximal (B-P), Kombuis Member (KB) and the carbonate rocks at Witputs (WP) for the first 15-30 m. The secular curves for C and Sr isotopes are taken from Halverson et al., (2007, 2010); ELP= Ediacaran Leiosphere Palynoflora

ECAP= Ediacaran Complex Acanthomorph Palynoflora (Grey et al. 2003); LELP= (Late Ediacaran Leiosphere Palynoflora (Gaucher and Sprechmann 2009). The isotope data for the Bloeddrif and Kombuis Members are from Fölling and Frimmel (2002), Frimmel and Fölling (2004).

TABLE CAPTIONS

Table 1: Selected geochemical data for the Witputs diamictite, Holgat Formation and the base of the Nama. Ce* and Eu* denote chondritic normalized anomaly values; 'N' denotes chondritic normalization after Taylor and McLennan (1985); %=weight percent; ppm=parts per million; unreliable CIA values are omitted (see Table 1 supplementary data for the complete geochemistry and calculated CIA values).

Table 2: Comparisons of C and O isotopes and geochemical data for the carbonate rocks sampled at Witputs and at Bloeddrif in northwest South Africa (data from Fölling and Frimmel 2002; Frimmel and Fölling 2004; Frimmel 2009). Threshold values for unaltered carbonate rocks according to Fölling and Frimmel (2002); *=distal and proximal samples from Bloeddrif Member with only the lower 20-30 m above the Numees Formation are taken into account for comparisons (Fölling and Frimmel 2002; Frimmel and Fölling 2004); #= data from Fölling and Frimmel (2002), as no data tables were available Ca/Sr ratio was not reported; §= Sr isotope values are given for the entire sampled sequence as samples were low in numbers. All rare earth element calculations after Frimmel (2009); samples are normalized to post-Archaean Australian shale values (indicated by SHN) adopted from Taylor and McLennan (1985).

Table 3: Complete U-Pb data for all measured zircons including discordant grains.

SUPPLEMENTARY DATA:

Figure 1: Selected pictures of detrital zircons with their ages. Spot sizes (green) between 20 and 30 μm. Images a-d and h from the Witputs diamictite; images e-g from the Holgat Formation. a) One of the youngest grains, derived from the Namaqua Metamorphic Belt; b) Early Mesoproterozoic magmatic zircon; c) Palaeoproterozoic grain from the arc-related magmatic rocks of the Orange River Group or Vioolsdrif Suite; d) Archaean grain; e) youngest grain derived from the Namaqua Metamorphic Belt; f) Early Mesoproterozoic magmatic zircon; g) Palaeoproterozoic grain from the arc-related magmatic rocks of the Orange River Group or Vioolsdrif Suite; h) Zircon grain population of the Witputs diamictite showing mainly angular to sub-angular grains.

Figure 2: Probability plots of the two detrital zircon samples at Witputs.

Table 1: Complete geochemical data for the entire section at S27°35’18.6’’ E16°41’09.8’’. The samples are ordered from the bottom of the section to the top, and from South to North. Ce* and Eu* denote chondritic normalized anomaly values; ‘N’ denotes chondritic normalization after Taylor and McLennan (1985); %=weight percent; ppm=parts per million; unreliable CIA values because of dilution caused by enrichment in silica or CaO are in grey.

Word file: Detailed description of the analytical methods.

Figure

Click here to download high resolution image

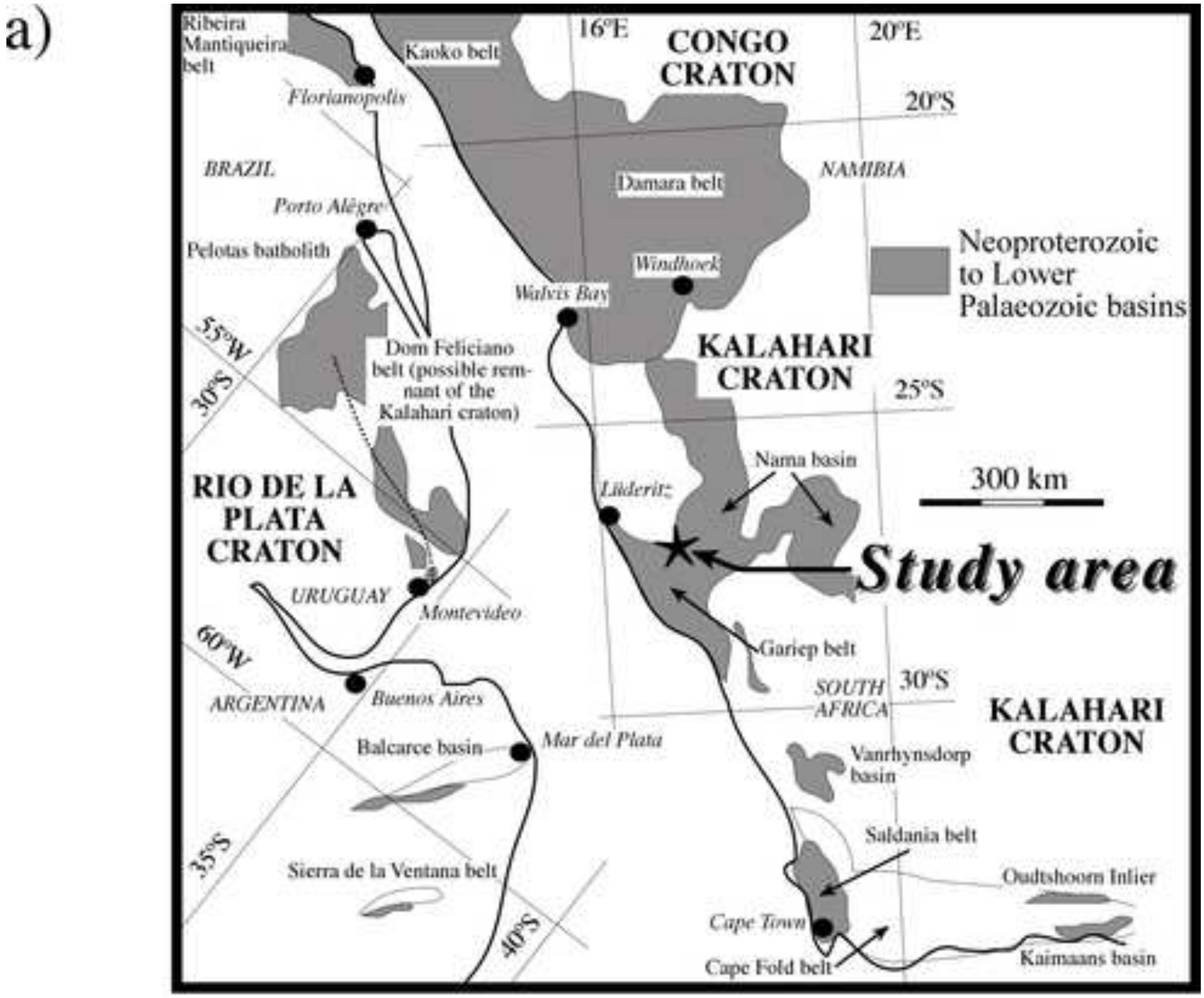

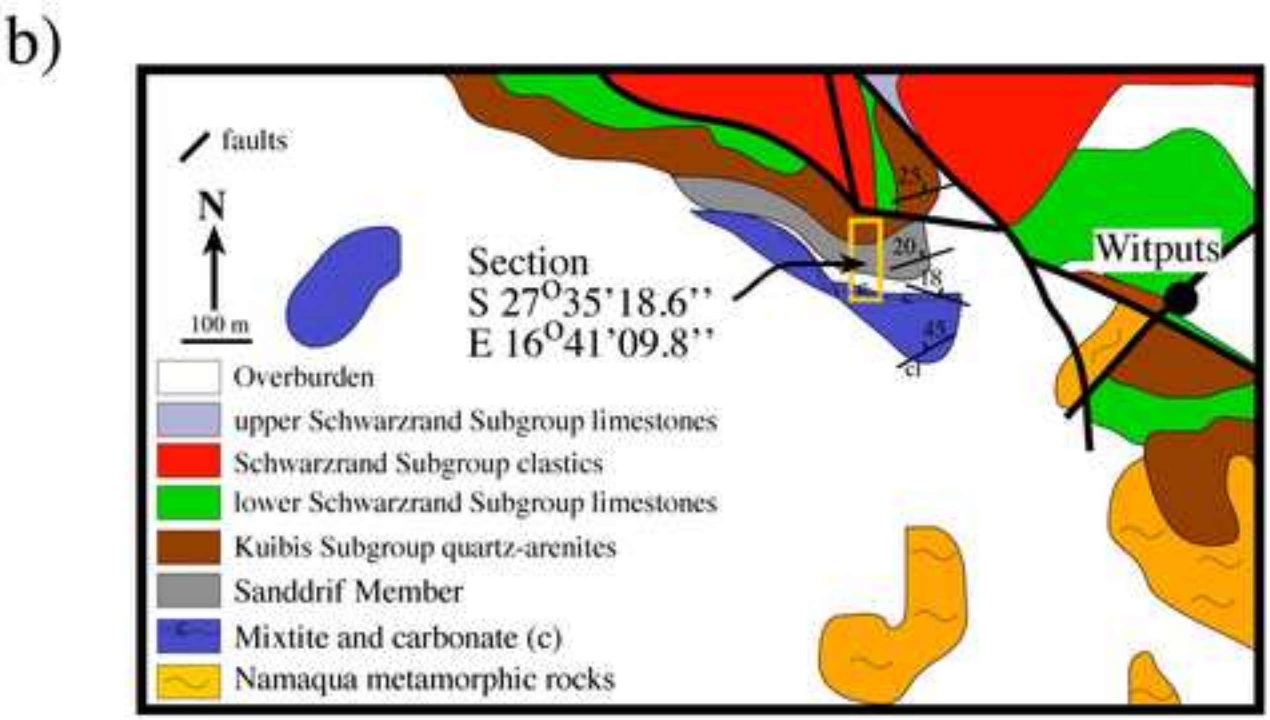

Fig 1: Zimmermann et al

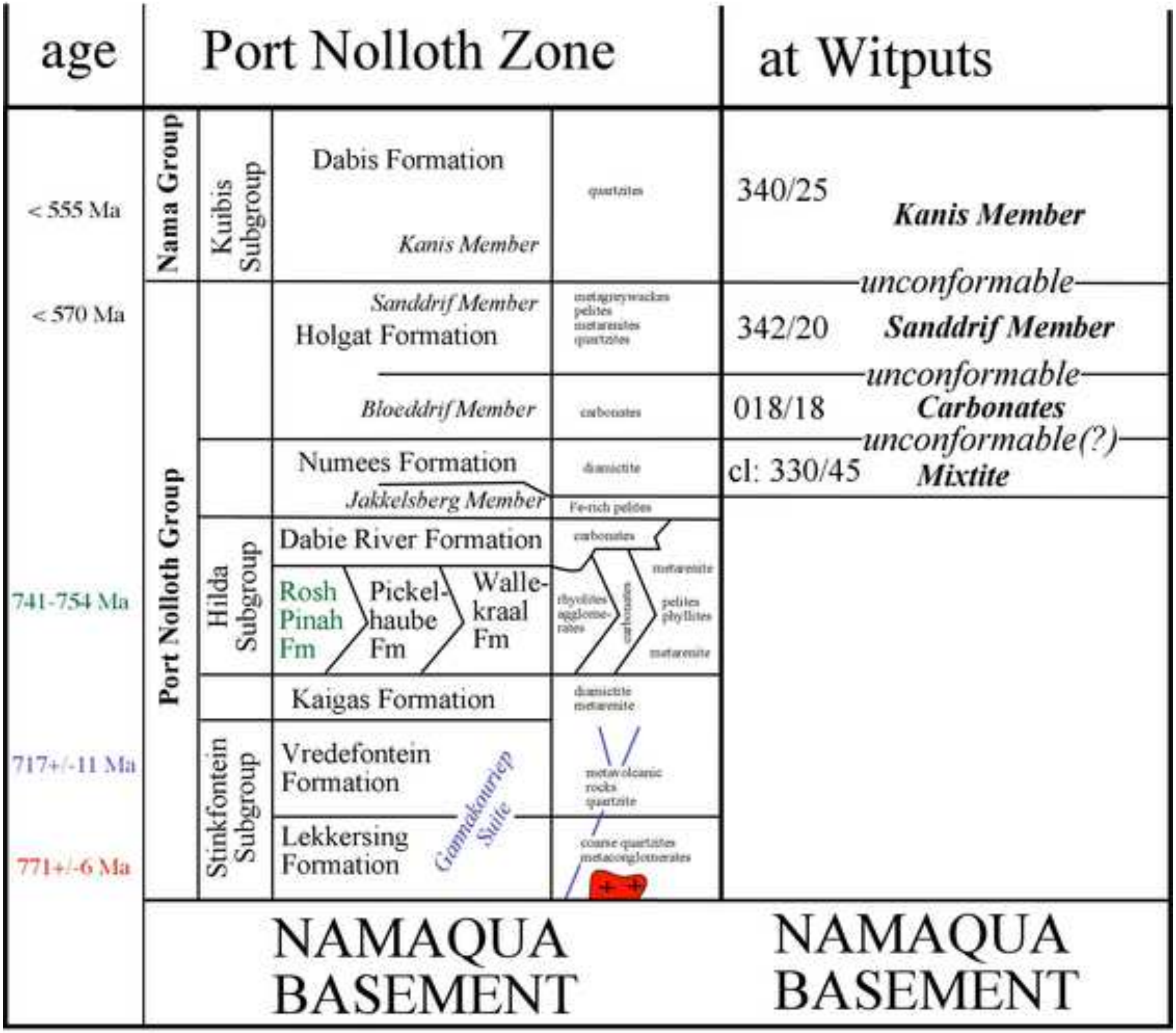

Figure 2: Zimmermann et al

Figure
Click here to download high resolution image

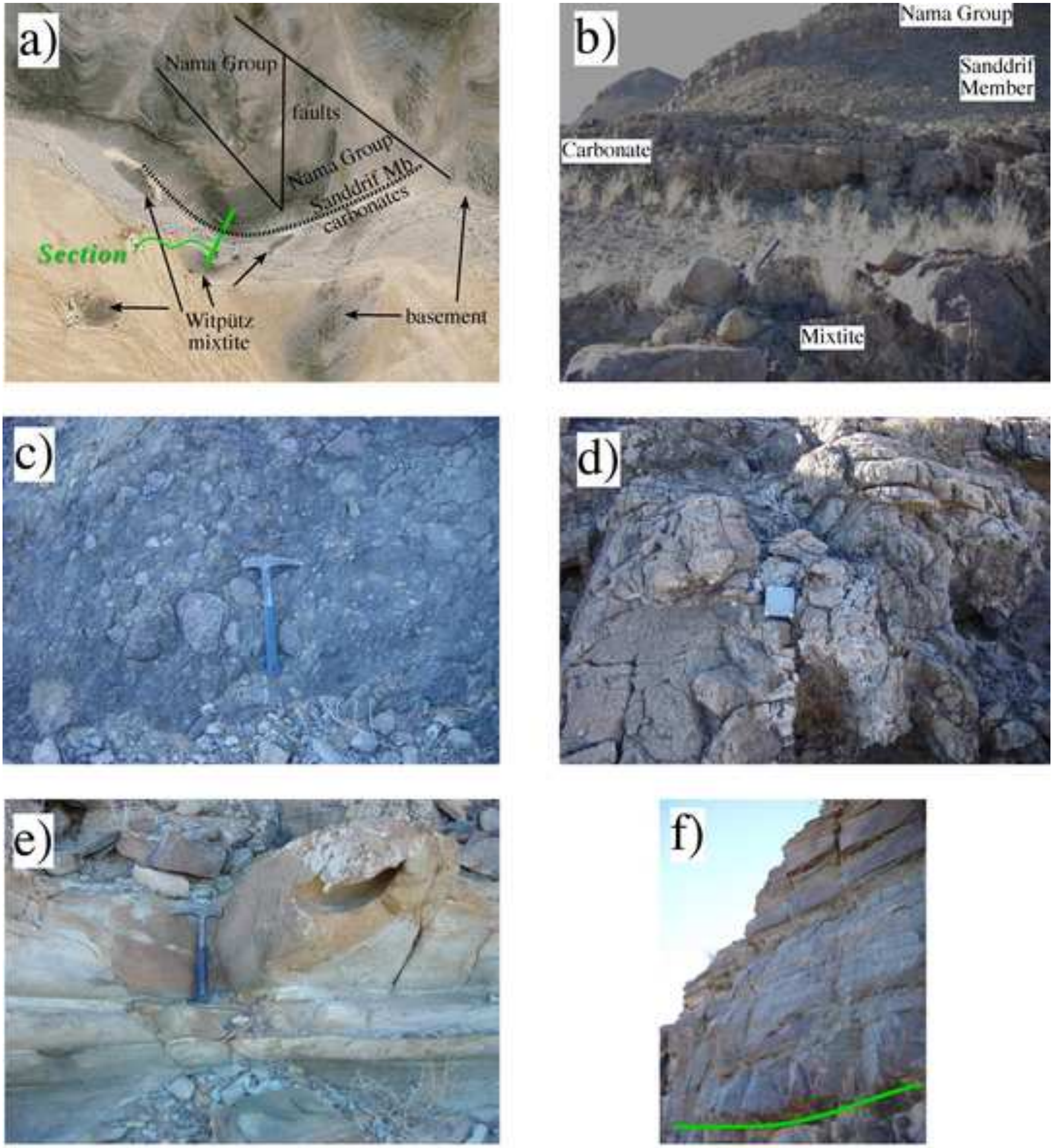

Figure 3: Zimmermann et al

Figure

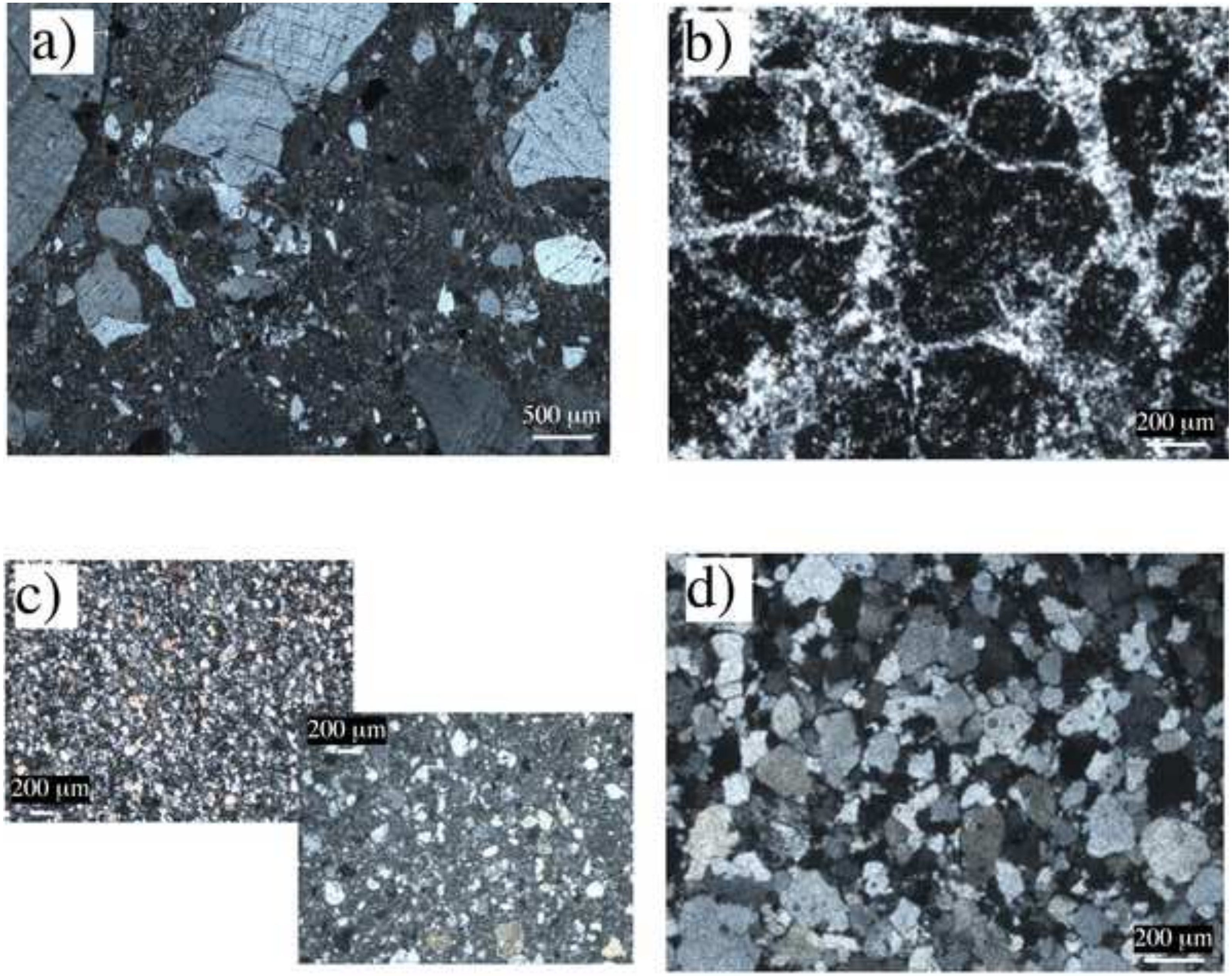

Figure 4: Zimmermann et al.

Figure

Click here to download high resolution image

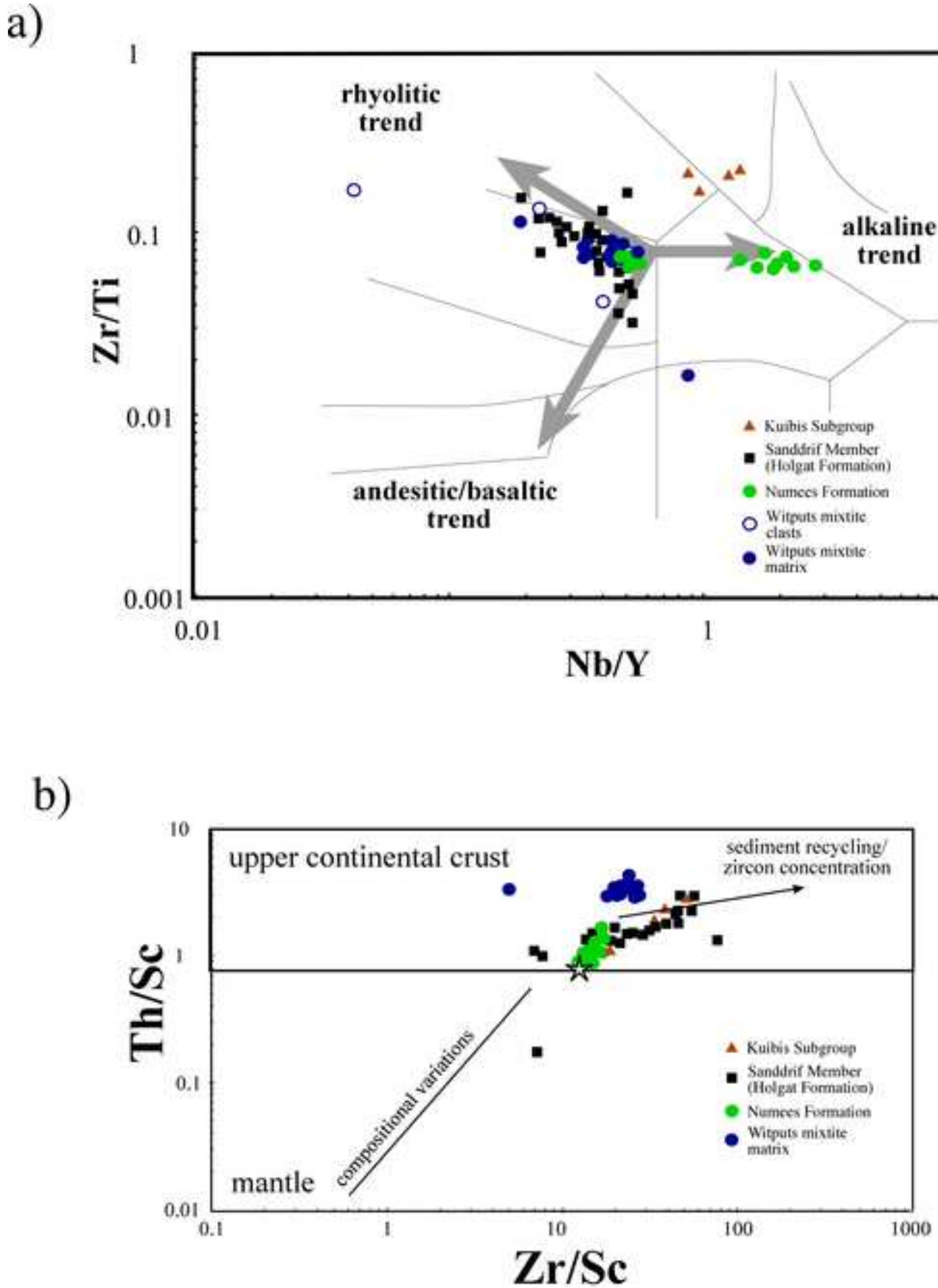

Fig. 5: Zimmermann et al

Figure
Click here to download high resolution image

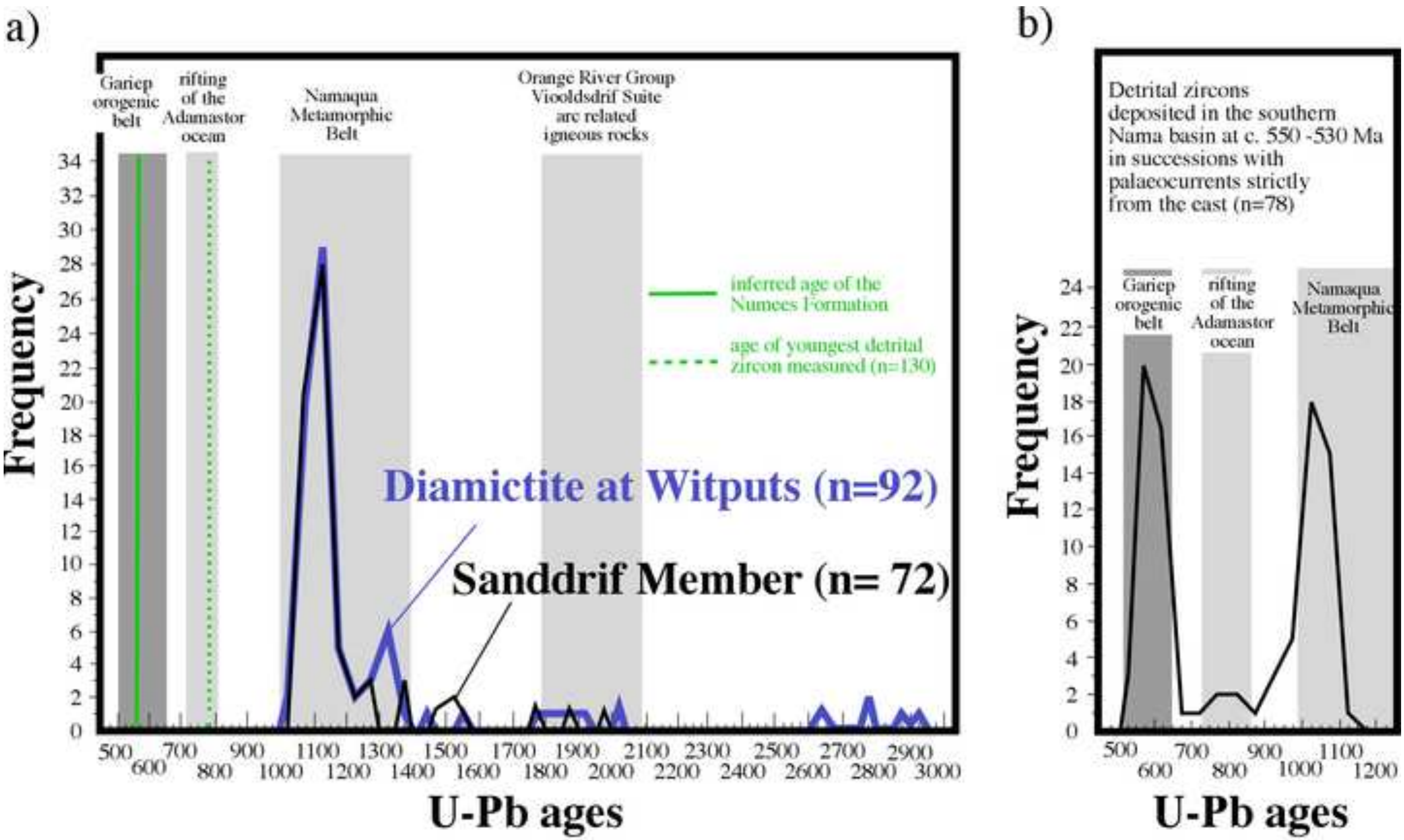

Figure 6: Zimmermann et al

Figure

Click here to download high resolution image

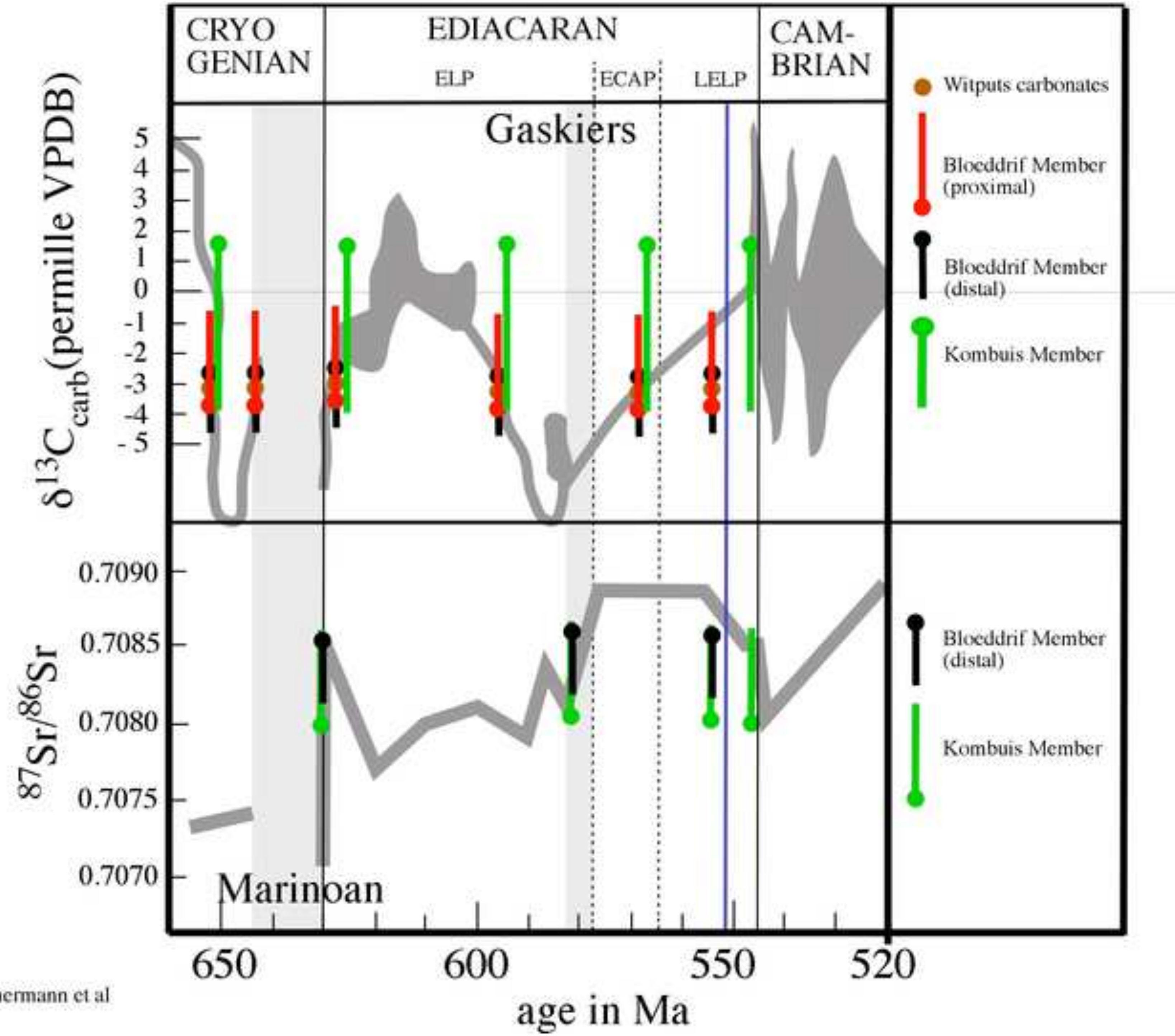

Fig. 7: Zimmermann et al

Table

SAMPLE	ROCK TYPE	CIA	SiO_2 %	Al_2O_3 %	Fe_2O_{3t} %	MgO %
diamictite	**bottom to top**					
DM1	coarse sand to silt	59	71.4	13.80	3.50	1.01
DM2	coarse sand to silt	59	74.9	12.54	2.51	0.80
DM3	coarse sand to silt	60	72.0	14.40	2.99	0.68
DM4	coarse sand to silt	63	70.1	16.53	3.02	0.61
DM5	coarse sand to silt	56	76.5	12.31	1.85	0.71
DM6	coarse sand to silt	63	69.1	14.97	3.96	0.77
DM7	coarse sand to silt	60	70.8	13.90	3.61	0.91
DM8	coarse sand to silt	60	70.1	14.31	3.62	1.06
DM9	coarse sand to silt	60	69.8	14.12	3.76	1.02
DM10	coarse sand to silt	60	70.3	14.35	3.59	1.11
DM11	coarse sand to silt	60	69.3	13.84	4.05	1.23
DM12	coarse sand to silt	59	67.6	14.93	3.74	0.70
DM13	coarse sand to silt	60	69.5	14.20	4.56	0.96
DM14	coarse sand to silt	62	72.7	14.30	3.60	0.96
DM15	coarse sand to silt	61	71.8	13.90	3.75	0.95
DM16	coarse sand to silt	61	70.4	14.20	3.77	0.89
DM17	coarse sand to silt	62	69.1	15.54	3.44	0.80
DM18	coarse sand to silt	59	70.9	14.08	3.57	1.16
DMP1	metamorphic	50	66.7	14.36	3.67	1.20
DMP2	igneous	55	69.9	13.90	2.58	0.74
DMP3	igneous	60	68.0	13.03	5.70	1.98
DMP4	igneous	57	69.5	14.60	3.23	0.85
carbonate and Mn-rich rocks						
C1	carbonate	3	5.7	1.74	0.70	17.53
C2	carbonate	1	5.1	1.04	0.63	20.21
C3	carbonate	1	4.8	0.89	0.67	10.75
C4	carbonate	1	4.9	0.97	0.58	16.03
C5	carbonate	2	5.5	0.95	0.53	20.98
C6	carbonate	1	4.9	0.87	0.53	10.62
CM7	Mn-rich	80	82.5	3.99	0.56	0.21
CM8	Mn-rich	33	78.3	0.88	0.54	0.38
CM9	Mn-rich	80	74.9	10.94	0.87	0.68
CM10	Mn-rich	77	59.1	2.32	0.34	0.05
CM11	Mn-rich	51	48.9	1.21	0.84	0.39
CM12	Mn-rich	53	57.9	1.39	0.92	0.25
CM13	Mn-rich	77	35.1	3.14	0.32	0.10
Holgat Formation	**Sanddrif Mb.**					
H1	arenite	61	61.4	15.90	6.34	4.64
H8	wacke	65	59.3	16.19	6.50	4.40
H11	shale	60	51.0	18.92	6.15	6.27
H12	wacke	17	52.9	7.09	1.86	1.50
H19	arenite	16	65.0	4.50	1.85	2.66
H20	marls	29	49.8	13.12	4.09	1.73

H26	wacke	60	68.1	12.64	1.88	1.79
H28	wacke	44	58.6	13.76	3.28	6.72
H29	marl	17	23.7	11.80	2.28	1.42
H34	arenite	56	76.5	12.31	1.85	0.71
H35	wacke	23	59.4	5.95	1.44	6.86
Nama Group	**Kanies Mb.**					
N2	quartzarenite	83	86.0	10.25	1.20	0.94
N3	quartzarenite	82	86.7	10.25	0.98	1.05

Table 1: Zimmermann et al.

CaO %	Na_2O %	K_2O %	TiO_2 %	P_2O_5 %	MnO %	LOI %	sum %	Ba ppm	Rb ppm	Sr ppm	Cs ppm	V ppm
0.40	2.23	4.88	0.42	0.140	0.040	1.6	99.4	713	233	88	4	44
0.34	1.85	4.53	0.36	0.150	0.020	1.5	99.6	632	199	86	3	37
0.54	2.05	4.72	0.31	0.110	0.130	1.8	99.7	671	201	106	3	35
0.38	2.21	4.91	0.35	0.153	0.084	1.4	99.8	711	211	102	4	36
0.54	2.42	4.39	0.27	0.110	0.030	1.6	100.7	166	37	433	2	22
0.28	1.53	5.49	0.47	0.459	0.040	2.3	99.4	677	261	81	5	165
0.24	1.76	5.36	0.44	0.160	0.040	2.0	99.2	677	255	96	4	49
0.30	1.92	5.30	0.45	0.170	0.030	1.8	99.1	793	254	82	3	45
0.31	2.04	5.22	0.44	0.180	0.040	2.5	99.5	768	251	84	5	49
0.35	2.04	5.10	0.45	0.160	0.040	1.9	99.4	744	248	79	4	46
0.39	1.91	5.05	0.44	0.160	0.030	2.3	98.7	284	32	21	4	12
0.42	2.42	5.25	0.42	0.209	0.059	2.6	98.3	667	234	93	4	49
0.40	1.83	5.25	0.43	0.140	0.050	1.9	99.3	678	218	88	5	43
0.31	1.75	4.83	0.44	0.170	0.060	1.9	101.0	703	221	76	3	39
0.36	1.92	4.85	0.42	0.150	0.040	1.8	100.0	650	218	78	4	40
0.34	1.87	4.99	0.42	0.170	0.060	2.1	99.2	701	230	82	4	34
0.36	1.71	5.59	0.45	0.282	0.030	1.9	99.2	835	262	87		59
0.44	1.89	5.30	0.45	0.180	0.040	2.1	100.1	701	258	94		49
3.14	3.17	3.07	0.45	0.129	0.061	4.6	100.5	706	114	92		54
0.34	2.30	6.38	0.27	0.120	0.030	1.9	98.5	672	235	171		24
0.58	1.71	4.32	0.99	0.100	0.100	2.3	98.8	531	227	76		80
0.40	2.40	6.02	0.34	0.150	0.060	1.5	99.1	651	238	166		23
29.85	0.04	0.60	0.07	0.170	1.210	42.2	99.8	119	27	204	0.7	14
33.41	0.21	0.44	0.08	0.224	1.706	39.2	102.3	141	21	149		11
41.48	0.14	0.34	0.08	0.062	1.207	41.2	101.6	104	18	150		9
35.10	0.16	0.53	0.08	0.102	2.988	39.2	100.6	194	32	163		10
29.64	0.04	0.23	0.06	0.280	1.590	41.2	101.1	129	18	158		10
36.56	0.16	0.48	0.06	0.077	1.949	44.4	100.5	72	30	171		11
0.26	0.07	0.38	0.03	0.240	9.800	3.0	101.1	3234	19	198	bdl	19
0.75	0.01	0.39	0.04	0.390	12.950	4.0	98.7	3878	17	423	bdl	24
0.89	0.18	0.73	0.08	0.522	6.156	3.1	99.1	1790	30	187	bdl	20
0.21	0.02	0.26	0.02	0.280	30.210	6.4	99.2	3207	11	317	bdl	28
0.41	0.01	0.36	0.06	0.310	37.770	8.0	98.3	1554	23	218	bdl	35
0.33	-0.01	0.59	0.09	0.290	30.650	7.7	100.1	1046	26	228	bdl	28
0.50	0.02	0.02	0.01	0.360	50.840	9.6	100.0	1233	10	350	bdl	38
2.36	0.56	4.39	0.74	0.160	0.030	2.3	98.8	792	185	58	7	82
1.51	0.58	4.64	0.82	0.170	0.030	6.6	100.8	818	196	50	7	86
2.65	0.14	6.96	0.76	0.200	0.020	7.4	100.5	930	230	40	14	98
17.42	1.06	2.03	0.41	0.120	0.060	15.6	100.0	507	89	306		38
11.93	0.92	0.66	0.48	0.060	0.080	12.6	100.7	151	36	163	1	31
14.94	1.10	2.62	0.47	0.087	0.063	11.2	99.2	270	80	194	4	47

2.09	0.95	2.88	0.20	0.102	0.027	7.7	98.3	434	79	41	8	22
6.60	0.33	4.74	0.50	0.103	0.040	6.0	100.7	734	152	49	1	56
29.57	0.94	1.59	0.32	0.082	0.080	28.9	100.7	225	53	272	2	27
0.54	2.42	4.39	0.27	0.110	0.030	12.2	111.3	770	86	91	5	44
9.19	0.64	2.23	0.30	0.090	0.060	14.8	101.0	655	76	114		31
0.12	0.60	0.85	0.04	0.037	0.015	0.9	101.0	163	20	17	1	260
0.05	0.67	1.02	0.03	0.025	0.012	0.8	101.5	172	25	17	1	212

Ni ppm	Co ppm	Cu ppm	Nb ppm	Ta ppm	Y ppm	Zr ppm	Hf ppm	Sc ppm	Th ppm	U ppm	Pb ppm	Ga ppm	Zn ppm
13	11	30	10.6	1.4	30.9	181	6	8.5	27.6	2.2	34.8	18.6	67
9	5	27	8.8	1.7	25.3	181	6	6.7	24.0	1.3	28.2	15.6	43
13	12	81	8	0.7	16.7	138	4	5.7	19.0	1.1	35.9	16.1	50
11	7	17	9.8	1.1	23.2	169	6	6.8	27.7	1.7	31.5	15.8	53
6	4	11.1.	6.3	1.1	33.9	173	3	6.0	17.0	1.3	26.8	7	14
60	13	9	69.3	11.2	17.6	181	6	8.7	27.3	2.4	39.5	19.6	68
13	10	16	11.8	0.6	21.3	184	6	8.2	27.1	2.5	26.3	18.8	52
13	11	23	10.9	2.3	25.8	183	5	8.0	26.2	2.6	37	19.2	60
13	11	20	10.3	1.2	22	183	6	8.2	28.2	2.4	25.2	18.8	56
13	10	18	11.4	1.1	33.8	185	5	8.6	27.1	2.0	24.3	19.7	62
3	1	6	5	1.3	5.7	42	6	8.5	27.5	1.2	7.2	0.9	7
14	12	36	10.8	1.7	23.6	182	6	8.3	28.8	2.6	29.8	17.7	56
11	9	41	11.4	2.1	25.5	177	6	8.7	27.1	2.6	39.2	18.7	63
10	10	24	11.6	0.6	27	181	6	8.8	28.6	2.0	34.5	19.7	65
10	9	12	11.6	2.3	29.2	177	6	9.2	27.4	1.6	29.2	19.8	67
10	9	60	11.7	1.0	28.6	177	6	8.6	29.1	2.1	36.6	19.9	61
13	11	25	10.5		25.5	191			29.3		38.6	20.4	58
13	9	17	11.1		27.1	185			28.1		24	18.7	57
11	2	13	13.9		27.5	196			22.9		12.4	14.5	49
8	5	22	7.4		180	254			93		39.2	20.8	49
16	7	34	16.5		42	229			8.7		25.3	17.7	130
8	2	68	7.9		35.2	251			99		44.3	22.5	69
56	94	7	1.5	0.1	4.4	19	1	2	1.5	2.4	4.3	2.9	298
56	162	11	4.1		5	35			4.9		39.9	2.8	277
39	106	10	4.3		7.7	45			1.8		28.9	3.2	171
106	322	10	3.8		6.2	41			2.7		30	3.8	372
43	107	11	3.7		8.7	56			2.9		24.3	3.7	401
51	142	20	3.5		6.5	34			2.3		25.1	3	319
185	571	18	3.9	0.2	9.5	38	bdl	1.7	0.9	8.7	26.3	1.3	502
454	1389	18	2.7	1.1	12.6	54	bdl	1.7	1.4	8.7	29.2	1.1	1055
245	751	16	5.1	0.4	8.2	43	bdl	2.0	2.2	5.2	21.6	2.6	415
532	1573	34	3.3	0.9	7.4	45	bdl	1.6	0.2	30.0	34.6	1	1822
367	974	61	4.5	0.3	8.4	53	bdl	2.9	0.9	66.0	78.3	4	2167
479	1379	34	6.7	0.4	10.2	55	bdl	2.7	1.8	28.0	40.9	2.3	1690
672	1840	84	4	0.3	14	60	bdl	2.5	0.2	71.8	64.1	1.5	3926
25	21	29	17	1.1	33.9	219	7	14.9	20.0	2.7	11.9	22.5	125
26	22	27	18	0.9	35.6	241	7	16.2	22.9	1.9	11.7	24.8	138
23	12	48	16.1	1.0	30.8	137	4	18.7	20.0	4.3	8.2	29.6	131
8	6	10	9.1		34.4	264			16.0		24.5	8.6	23
9	9	68	10.8	0.5	39.1	250	7	6.2	11.0	2.0	18.5	4	41
15	9	51	11.3	0.5	29.4	195	5	7.7	11.0	2.1	29.6	11.9	77

6	3	9	6.3	0.8	15.8	146	6	7.2	12.0	1.8	13.9	6.2	22
12	10	13	11.5	0.7	24.3	181	5	3.3	8.4	0.9	10.4	13.1	64
8	6	17	7.6	0.4	13.3	142	4	3.3	6.5	2.1	49	6.7	30
10	6	7	11	0.7	22.5	257	8	5.6	13.0	2.1	22.7	9.4	37
8	7	11	8.3		17.5	197			9.8		11.1	6.2	24
12	5	2	7.1	4.9	7.3	39	1	2.1	2.4	0.9	35.8	1.4	14
9	4	1	5.4	4.8	6	35	1	0.9	1.9	0.5	11.2	1.4	12

Mo ppm	**La** ppm	**Ce** ppm	**Pr** ppm	**Nd** ppm	**Sm** ppm	**Eu** ppm	**Gd** ppm	**Tb** ppm	**Dy** ppm	**Ho** ppm	**Er** ppm	**Tm** ppm	**Yb** ppm	**Lu** ppm	**Eu***
bdl	70	120		41	9.2	1.6		1.3					2.6	0.42	0.54
bdl	38	97		21	5.7	0.9		0.7					2.1	0.31	0.50
bdl	36	83		20	5.1	0.7		0.3					1.4	0.24	0.67
bdl	50	110		29	6.5	1.1		0.9					2.2	0.30	0.53
bdl	33	73		22	4.8	0.9		0.4					1.5	0.24	0.93
bdl	20	76		9	4.0	0.7		0.6					1.9	0.29	0.54
bdl	42	82		25	5.7	1.0		0.8					2.1	0.29	0.55
bdl	46	100		29	6.7	1.6		0.7					2.3	0.33	0.79
bdl	30	100		17	4.8	1.0		0.7					2.0	0.29	0.64
bdl	45	110		28	6.7	1.1		0.7					2.3	0.35	0.76
bdl	52	110		32	7.4	1.2		1.0					2.4	0.35	0.51
bdl	31	100		20	5.1	0.9		0.6					2.2	0.34	0.87
bdl	49	120		25	6.9	1.7		1.1					2.4	0.35	0.74
bdl	53	120		31	7.8	1.3		0.9					2.4	0.38	0.54
bdl	51	110		31	7.4	1.2		0.7					2.5	0.37	0.54
bdl	42	110		27	7.0	1.4		0.7					2.6	0.38	0.66

2.2	5	10	1	5	0.9	0.18	0.82	0.15	0.82	0.13	0.42	0.06	0.4	0.06	0.60
bdl	6	6		7	1.4	0.5		0.6					0.7	bdl	0.77
bdl	6	8		7	1.2	0.4		0.5					0.6	bdl	7.23
bdl	8	13		6	1.4	0.5		0.5					0.5	bdl	0.83
bdl	5	5		5	0.6	0.5		0.5					0.6	bdl	2.08
bdl	9	10		10	1.2	0.6		0.6					0.7	bdl	10.85
bdl	13	16		5	1.7	0.6		0.6					0.7	bdl	3.31
bdl	10	5		3	1.4	0.9		1.4					0.8	bdl	0.86
bdl	56	120		41	8.3	1.6		1.1					3.1	0.45	0.61
bdl	63	140		43	10.0	2.0		1.4					3.4	0.48	0.62
bdl	68	130		39	8.7	1.6		0.7					2.5	0.30	0.63
bdl	32	71		26	6.8	1.1		1.0					3.1	0.45	0.50
bdl	28	61		29	5.8	0.9		0.7					2.4	0.38	0.50

bdl	28	64	23	5.6	0.9	0.9	1.9	0.29	0.48
bdl	21	47	22	5.2	0.7	0.7	2.1	0.30	0.42
bdl	21	48	26	4.6	0.8	0.8	1.6	0.22	0.51
bdl	30	72	27	6.2	1.0	1.0	2.2	0.30	0.49
bdl	6	13	7	1.1	0.3	0.1	0.8	0.10	0.70
bdl	6	12	7	1.1	0.2	0.1	0.5	0.08	0.53

Ce*	La_N/Yb	K/Cs	U/Th	Nb/Y	Zr/Ti	Th/Sc	Zr/Sc	La/Sc	Ti/Zr
0.85	18.25	10127	0.08	0.34	0.07	3.25	21.33	8.26	13.89
1.28	12.23	12535	0.05	0.35	0.08	3.58	27.06	5.67	11.90
1.16	17.38	13046	0.06	0.48	0.07	3.33	24.25	6.32	13.36
1.10	15.36	10194	0.06	0.42	0.08	4.07	24.81	7.35	12.40
1.08	14.87	18221	0.08	0.19	0.11	2.83	28.90	5.50	9.33
1.95	7.11	9116	0.09	3.94	0.06	3.14	20.83	2.30	15.45
1.01	13.51	11123	0.09	0.55	0.07	3.30	22.49	5.12	14.30
1.07	13.51	14665	0.10	0.42	0.07	3.28	22.88	5.75	14.74
1.67	10.14	8666	0.09	0.47	0.07	3.44	22.32	3.66	14.41
1.21	13.22	10584	0.07	0.34	0.07	3.15	21.47	5.23	14.61
1.05	14.56	10480	0.04	0.88	0.02	3.24	4.92	6.08	63.11
1.59	9.52	10891	0.09	0.46	0.07	3.47	21.96	3.73	13.81
1.24	13.80	8716	0.10	0.45	0.07	3.11	20.39	5.63	14.53
1.12	14.98	13365	0.07	0.43	0.07	3.25	20.52	6.05	14.61
1.08	13.65	10065	0.06	0.40	0.07	2.98	19.23	5.49	14.23
1.29	10.92	10355	0.07	0.41	0.07	3.38	20.58	4.88	14.23
				0.41	0.07				
				0.41	0.07				
0.98	7.94								
0.43	5.99		9.67	0.41	0.21	0.53	22.35	3.65	4.73
0.57	7.10		6.21	0.21	0.22	0.82	31.65	3.71	4.46
0.82	10.27		2.36	0.62	0.09	1.10	21.45	3.80	11.60
0.44	5.86		150.00	0.45	0.37	0.13	27.81	3.25	2.69
0.48	9.07		73.33	0.54	0.15	0.31	18.10	3.24	6.85
0.64	12.55		15.56	0.66	0.10	0.67	20.30	4.81	9.85
0.27	8.45		359.00	0.29	1.01	0.08	24.16	4.00	0.99
1.04	12.10	5206	0.14	0.50	0.05	1.34	14.70	3.72	20.25
1.09	12.48	5502	0.08	0.51	0.05	1.41	14.89	3.88	20.38
0.96	18.33	4127	0.22	0.52	0.03	1.07	7.35	3.63	33.16
				0.26	0.11				9.32
1.05	6.98	5479	0.18	0.28	0.09	1.77	40.39	5.16	11.49
0.99	7.88	5443	0.19	0.38	0.07	1.43	25.31	3.64	14.55

1.08	9.96	2993	0.15	0.40	0.12	1.67	20.26	3.89	8.14
1.01	6.76	39355	0.11	0.47	0.06	2.55	54.88	6.36	16.68
1.00	8.87	6591	0.32	0.57	0.07	1.97	43.03	6.36	13.59
1.12	9.21	7288	0.16	0.49	0.16	2.32	45.91	5.36	6.30
				0.47	0.11				9.14
0.92	5.32	7089	0.38	0.97	0.15	1.14	18.71	3.00	6.56
0.86	8.38	8492	0.26	0.90	0.19	2.11	39.33	6.89	5.25

Table

SAMPLE	ROCK TYPE	CIA	SiO_2	Al_2O_3	Fe_2O_{3t}	MgO	CaO	Na_2O
			%	%	%	%	%	%
diamictite	**bottom to top**							
DM1	coarse sand to silt	59	71.4	13.80	3.50	1.01	0.40	2.23
DM2	coarse sand to silt	59	74.9	12.54	2.51	0.80	0.34	1.85
DM3	coarse sand to silt	60	72.0	14.40	2.99	0.68	0.54	2.05
DM4	coarse sand to silt	63	70.1	16.53	3.02	0.61	0.38	2.21
DM5	coarse sand to silt	56	76.5	12.31	1.85	0.71	0.54	2.42
DM6	coarse sand to silt	63	69.1	14.97	3.96	0.77	0.28	1.53
DM7	coarse sand to silt	60	70.8	13.90	3.61	0.91	0.24	1.76
DM8	coarse sand to silt	60	70.1	14.31	3.62	1.06	0.30	1.92
DM9	coarse sand to silt	60	69.8	14.12	3.76	1.02	0.31	2.04
DM10	coarse sand to silt	60	70.3	14.35	3.59	1.11	0.35	2.04
DM11	coarse sand to silt	60	69.3	13.84	4.05	1.23	0.39	1.91
DM12	coarse sand to silt	59	67.6	14.93	3.74	0.70	0.42	2.42
DM13	coarse sand to silt	60	69.5	14.20	4.56	0.96	0.40	1.83
DM14	coarse sand to silt	62	72.7	14.30	3.60	0.96	0.31	1.75
DM15	coarse sand to silt	61	71.8	13.90	3.75	0.95	0.36	1.92
DM16	coarse sand to silt	61	70.4	14.20	3.77	0.89	0.34	1.87
DM17	coarse sand to silt	62	69.1	15.54	3.44	0.80	0.36	1.71
DM18	coarse sand to silt	59	70.9	14.08	3.57	1.16	0.44	1.89
DMP1	metamorphic	50	66.7	14.36	3.67	1.20	3.14	3.17
DMP2	igneous	55	69.9	13.90	2.58	0.74	0.34	2.30
DMP3	igneous	60	68.0	13.03	5.70	1.98	0.58	1.71
DMP4	igneous	57	69.5	14.60	3.23	0.85	0.40	2.40
carbonate and Mn-rich rocks								
C1	carbonate	3	5.7	1.74	0.70	17.53	29.85	0.04
C2	carbonate	1	5.1	1.04	0.63	20.21	33.41	0.21
C3	carbonate	1	4.8	0.89	0.67	10.75	41.48	0.14
C4	carbonate	1	4.9	0.97	0.58	16.03	35.10	0.16
C5	carbonate	2	5.5	0.95	0.53	20.98	29.64	0.04
C6	carbonate	1	4.9	0.87	0.53	10.62	36.56	0.16
CM7	Mn-rich	80	82.5	3.99	0.56	0.21	0.26	0.07
CM8	Mn-rich	33	78.3	0.88	0.54	0.38	0.75	0.01
CM9	Mn-rich	80	74.9	10.94	0.87	0.68	0.89	0.18
CM10	Mn-rich	77	59.1	2.32	0.34	0.05	0.21	0.02
CM11	Mn-rich	51	48.9	1.21	0.84	0.39	0.41	0.01
CM12	Mn-rich	53	57.9	1.39	0.92	0.25	0.33	-0.01

CM13	Mn-rich	77	35.1	3.14	0.32	0.10	0.50	0.02
Holgat Formation	**Sanddrif Mb.**							
H1	arenite	61	61.4	15.90	6.34	4.64	2.36	0.56
H8	wacke	65	59.3	16.19	6.50	4.40	1.51	0.58
H11	shale	60	51.0	18.92	6.15	6.27	2.65	0.14
H12	wacke	17	52.9	7.09	1.86	1.50	17.42	1.06
H19	arenite	16	65.0	4.50	1.85	2.66	11.93	0.92
H20	marls	29	49.8	13.12	4.09	1.73	14.94	1.10
H26	wacke	60	68.1	12.64	1.88	1.79	2.09	0.95
H28	wacke	44	58.6	13.76	3.28	6.72	6.60	0.33
H29	marl	17	23.7	11.80	2.28	1.42	29.57	0.94
H34	arenite	56	76.5	12.31	1.85	0.71	0.54	2.42
H35	wacke	23	59.4	5.95	1.44	6.86	9.19	0.64
Nama Group	**Kanies Mb.**							
N2	quartzarenite	83	86.0	10.25	1.20	0.94	0.12	0.60
N3	quartzarenite	82	86.7	10.25	0.98	1.05	0.05	0.67

Table 1: Zimmermann et al.

K_2O %	TiO_2 %	P_2O_5 %	MnO %	LOI %	sum %	Ba ppm	Rb ppm	Sr ppm	Cs ppm	V ppm	Ni ppm	Co ppm	Cu ppm
4.88	0.42	0.140	0.040	1.6	99.4	713	233	88	4	44	13	11	30
4.53	0.36	0.150	0.020	1.5	99.6	632	199	86	3	37	9	5	27
4.72	0.31	0.110	0.130	1.8	99.7	671	201	106	3	35	13	12	81
4.91	0.35	0.153	0.084	1.4	99.8	711	211	102	4	36	11	7	17
4.39	0.27	0.110	0.030	1.6	100.7	166	37	433	2	22	6	4	11.1.
5.49	0.47	0.459	0.040	2.3	99.4	677	261	81	5	165	60	13	9
5.36	0.44	0.160	0.040	2.0	99.2	677	255	96	4	49	13	10	16
5.30	0.45	0.170	0.030	1.8	99.1	793	254	82	3	45	13	11	23
5.22	0.44	0.180	0.040	2.5	99.5	768	251	84	5	49	13	11	20
5.10	0.45	0.160	0.040	1.9	99.4	744	248	79	4	46	13	10	18
5.05	0.44	0.160	0.030	2.3	98.7	284	32	21	4	12	3	1	6
5.25	0.42	0.209	0.059	2.6	98.3	667	234	93	4	49	14	12	36
5.25	0.43	0.140	0.050	1.9	99.3	678	218	88	5	43	11	9	41
4.83	0.44	0.170	0.060	1.9	101.0	703	221	76	3	39	10	10	24
4.85	0.42	0.150	0.040	1.8	100.0	650	218	78	4	40	10	9	12
4.99	0.42	0.170	0.060	2.1	99.2	701	230	82	4	34	10	9	60
5.59	0.45	0.282	0.030	1.9	99.2	835	262	87		59	13	11	25
5.30	0.45	0.180	0.040	2.1	100.1	701	258	94		49	13	9	17
3.07	0.45	0.129	0.061	4.6	100.5	706	114	92		54	11	2	13
6.38	0.27	0.120	0.030	1.9	98.5	672	235	171		24	8	5	22
4.32	0.99	0.100	0.100	2.3	98.8	531	227	76		80	16	7	34
6.02	0.34	0.150	0.060	1.5	99.1	651	238	166		23	8	2	68
0.60	0.07	0.170	1.210	42.2	99.8	119	27	204	0.7	14	56	94	7
0.44	0.08	0.224	1.706	39.2	102.3	141	21	149		11	56	162	11
0.34	0.08	0.062	1.207	41.2	101.6	104	18	150		9	39	106	10
0.53	0.08	0.102	2.988	39.2	100.6	194	32	163		10	106	322	10
0.23	0.06	0.280	1.590	41.2	101.1	129	18	158		10	43	107	11
0.48	0.06	0.077	1.949	44.4	100.5	72	30	171		11	51	142	20
0.38	0.03	0.240	9.800	3.0	101.1	3234	19	198	bdl	19	185	571	18
0.39	0.04	0.390	12.950	4.0	98.7	3878	17	423	bdl	24	454	1389	18
0.73	0.08	0.522	6.156	3.1	99.1	1790	30	187	bdl	20	245	751	16
0.26	0.02	0.280	30.210	6.4	99.2	3207	11	317	bdl	28	532	1573	34
0.36	0.06	0.310	37.770	8.0	98.3	1554	23	218	bdl	35	367	974	61
0.59	0.09	0.290	30.650	7.7	100.1	1046	26	228	bdl	28	479	1379	34

0.02	0.01	0.360	50.840	9.6	100.0	1233	10	350	bdl	38	672	1840	84
4.39	0.74	0.160	0.030	2.3	98.8	792	185	58	7	82	25	21	29
4.64	0.82	0.170	0.030	6.6	100.8	818	196	50	7	86	26	22	27
6.96	0.76	0.200	0.020	7.4	100.5	930	230	40	14	98	23	12	48
2.03	0.41	0.120	0.060	15.6	100.0	507	89	306		38	8	6	10
0.66	0.48	0.060	0.080	12.6	100.7	151	36	163	1	31	9	9	68
2.62	0.47	0.087	0.063	11.2	99.2	270	80	194	4	47	15	9	51
2.88	0.20	0.102	0.027	7.7	98.3	434	79	41	8	22	6	3	9
4.74	0.50	0.103	0.040	6.0	100.7	734	152	49	1	56	12	10	13
1.59	0.32	0.082	0.080	28.9	100.7	225	53	272	2	27	8	6	17
4.39	0.27	0.110	0.030	12.2	111.3	770	86	91	5	44	10	6	7
2.23	0.30	0.090	0.060	14.8	101.0	655	76	114		31	8	7	11
0.85	0.04	0.037	0.015	0.9	101.0	163	20	17	1	260	12	5	2
1.02	0.03	0.025	0.012	0.8	101.5	172	25	17	1	212	9	4	1

Nb ppm	Ta ppm	Y ppm	Zr ppm	Hf ppm	Sc ppm	Th ppm	U ppm	Pb ppm	Ga ppm	Zn ppm	Mo ppm	La ppm	Ce ppm	Pr ppm	Nd ppm	Sm ppm
10.6	1.4	30.9	181	6	8.5	27.6	2.2	34.8	18.6	67	bdl	70	120		41	9.2
8.8	1.7	25.3	181	6	6.7	24.0	1.3	28.2	15.6	43	bdl	38	97		21	5.7
8	0.7	16.7	138	4	5.7	19.0	1.1	35.9	16.1	50	bdl	36	83		20	5.1
9.8	1.1	23.2	169	6	6.8	27.7	1.7	31.5	15.8	53	bdl	50	110		29	6.5
6.3	1.1	33.9	173	3	6.0	17.0	1.3	26.8	7	14	bdl	33	73		22	4.8
69.3	11.2	17.6	181	6	8.7	27.3	2.4	39.5	19.6	68	bdl	20	76		9	4.0
11.8	0.6	21.3	184	6	8.2	27.1	2.5	26.3	18.8	52	bdl	42	82		25	5.7
10.9	2.3	25.8	183	5	8.0	26.2	2.6	37	19.2	60	bdl	46	100		29	6.7
10.3	1.2	22	183	6	8.2	28.2	2.4	25.2	18.8	56	bdl	30	100		17	4.8
11.4	1.1	33.8	185	5	8.6	27.1	2.0	24.3	19.7	62	bdl	45	110		28	6.7
5	1.3	5.7	42	6	8.5	27.5	1.2	7.2	0.9	7	bdl	52	110		32	7.4
10.8	1.7	23.6	182	6	8.3	28.8	2.6	29.8	17.7	56	bdl	31	100		20	5.1
11.4	2.1	25.5	177	6	8.7	27.1	2.6	39.2	18.7	63	bdl	49	120		25	6.9
11.6	0.6	27	181	6	8.8	28.6	2.0	34.5	19.7	65	bdl	53	120		31	7.8
11.6	2.3	29.2	177	6	9.2	27.4	1.6	29.2	19.8	67	bdl	51	110		31	7.4
11.7	1.0	28.6	177	6	8.6	29.1	2.1	36.6	19.9	61	bdl	42	110		27	7.0
10.5		25.5	191			29.3		38.6	20.4	58						
11.1		27.1	185			28.1		24	18.7	57						
13.9		27.5	196			22.9		12.4	14.5	49						
7.4		180	254			93		39.2	20.8	49						
16.5		42	229			8.7		25.3	17.7	130						
7.9		35.2	251			99		44.3	22.5	69						
1.5	0.1	4.4	19	1	2	1.5	2.4	4.3	2.9	298	2.2	5	10	1	5	0.9
4.1		5	35			4.9		39.9	2.8	277						
4.3		7.7	45			1.8		28.9	3.2	171						
3.8		6.2	41			2.7		30	3.8	372						
3.7		8.7	56			2.9		24.3	3.7	401						
3.5		6.5	34			2.3		25.1	3	319						
3.9	0.2	9.5	38	bdl	1.7	0.9	8.7	26.3	1.3	502	bdl	6	6		7	1.4
2.7	1.1	12.6	54	bdl	1.7	1.4	8.7	29.2	1.1	1055	bdl	6	8		7	1.2
5.1	0.4	8.2	43	bdl	2.0	2.2	5.2	21.6	2.6	415	bdl	8	13		6	1.4
3.3	0.9	7.4	45	bdl	1.6	0.2	30.0	34.6	1	1822	bdl	5	5		5	0.6
4.5	0.3	8.4	53	bdl	2.9	0.9	66.0	78.3	4	2167	bdl	9	10		10	1.2
6.7	0.4	10.2	55	bdl	2.7	1.8	28.0	40.9	2.3	1690	bdl	13	16		5	1.7

4	0.3	14	60	bdl	2.5	0.2	71.8	64.1	1.5	3926	bdl	10	5	3	1.4
17	1.1	33.9	219	7	14.9	20.0	2.7	11.9	22.5	125	bdl	56	120	41	8.3
18	0.9	35.6	241	7	16.2	22.9	1.9	11.7	24.8	138	bdl	63	140	43	10.0
16.1	1.0	30.8	137	4	18.7	20.0	4.3	8.2	29.6	131	bdl	68	130	39	8.7
9.1		34.4	264			16.0		24.5	8.6	23					
10.8	0.5	39.1	250	7	6.2	11.0	2.0	18.5	4	41	bdl	32	71	26	6.8
11.3	0.5	29.4	195	5	7.7	11.0	2.1	29.6	11.9	77	bdl	28	61	29	5.8
6.3	0.8	15.8	146	6	7.2	12.0	1.8	13.9	6.2	22	bdl	28	64	23	5.6
11.5	0.7	24.3	181	5	3.3	8.4	0.9	10.4	13.1	64	bdl	21	47	22	5.2
7.6	0.4	13.3	142	4	3.3	6.5	2.1	49	6.7	30	bdl	21	48	26	4.6
11	0.7	22.5	257	8	5.6	13.0	2.1	22.7	9.4	37	bdl	30	72	27	6.2
8.3		17.5	197			9.8		11.1	6.2	24					
7.1	4.9	7.3	39	1	2.1	2.4	0.9	35.8	1.4	14	bdl	6	13	7	1.1
5.4	4.8	6	35	1	0.9	1.9	0.5	11.2	1.4	12	bdl	6	12	7	1.1

Eu	**Gd**	**Tb**	**Dy**	**Ho**	**Er**	**Tm**	**Yb**	**Lu**	**Eu***	**Ce***	**La$_N$/Yb**	**K/Cs**	**U/Th**	**Nb/**	**Zr/T**
ppm	ppm	ppm	ppm	ppm	ppm	ppm	ppm	ppm							
1.6		1.3					2.6	0.42	0.54	0.85	18.25	10127	0.08	0.34	0.07
0.9		0.7					2.1	0.31	0.50	1.28	12.23	12535	0.05	0.35	0.08
0.7		0.3					1.4	0.24	0.67	1.16	17.38	13046	0.06	0.48	0.07
1.1		0.9					2.2	0.30	0.53	1.10	15.36	10194	0.06	0.42	0.08
0.9		0.4					1.5	0.24	0.93	1.08	14.87	18221	0.08	0.19	0.11
0.7		0.6					1.9	0.29	0.54	1.95	7.11	9116	0.09	3.94	0.06
1.0		0.8					2.1	0.29	0.55	1.01	13.51	11123	0.09	0.55	0.07
1.6		0.7					2.3	0.33	0.79	1.07	13.51	14665	0.10	0.42	0.07
1.0		0.7					2.0	0.29	0.64	1.67	10.14	8666	0.09	0.47	0.07
1.1		0.7					2.3	0.35	0.76	1.21	13.22	10584	0.07	0.34	0.07
1.2		1.0					2.4	0.35	0.51	1.05	14.56	10480	0.04	0.88	0.02
0.9		0.6					2.2	0.34	0.87	1.59	9.52	10891	0.09	0.46	0.07
1.7		1.1					2.4	0.35	0.74	1.24	13.80	8716	0.10	0.45	0.07
1.3		0.9					2.4	0.38	0.54	1.12	14.98	13365	0.07	0.43	0.07
1.2		0.7					2.5	0.37	0.54	1.08	13.65	10065	0.06	0.40	0.07
1.4		0.7					2.6	0.38	0.66	1.29	10.92	10355	0.07	0.41	0.07
														0.41	0.07
														0.41	0.07
0.18	0.82	0.15	0.82	0.13	0.42	0.06	0.4	0.06	0.60	0.98	7.94				
0.5		0.6					0.7	bdl	0.77	0.43	5.99		9.67	0.41	0.21
0.4		0.5					0.6	bdl	7.23	0.57	7.10		6.21	0.21	0.22
0.5		0.5					0.5	bdl	0.83	0.82	10.27		2.36	0.62	0.09
0.5		0.5					0.6	bdl	2.08	0.44	5.86		150.00	0.45	0.37
0.6		0.6					0.7	bdl	10.85	0.48	9.07		73.33	0.54	0.15
0.6		0.6					0.7	bdl	3.31	0.64	12.55		15.56	0.66	0.10

0.9	1.4	0.8	bdl	0.86	0.27	8.45		359.00	0.29	1.01
1.6	1.1	3.1	0.45	0.61	1.04	12.10	5206	0.14	0.50	0.05
2.0	1.4	3.4	0.48	0.62	1.09	12.48	5502	0.08	0.51	0.05
1.6	0.7	2.5	0.30	0.63	0.96	18.33	4127	0.22	0.52	0.03
									0.26	0.11
1.1	1.0	3.1	0.45	0.50	1.05	6.98	5479	0.18	0.28	0.09
0.9	0.7	2.4	0.38	0.50	0.99	7.88	5443	0.19	0.38	0.07
0.9	0.9	1.9	0.29	0.48	1.08	9.96	2993	0.15	0.40	0.12
0.7	0.7	2.1	0.30	0.42	1.01	6.76	39355	0.11	0.47	0.06
0.8	0.8	1.6	0.22	0.51	1.00	8.87	6591	0.32	0.57	0.07
1.0	1.0	2.2	0.30	0.49	1.12	9.21	7288	0.16	0.49	0.16
									0.47	0.11
0.3	0.1	0.8	0.10	0.70	0.92	5.32	7089	0.38	0.97	0.15
0.2	0.1	0.5	0.08	0.53	0.86	8.38	8492	0.26	0.90	0.19

Th/Sc	Zr/S	La/S	Ti/Zr
3.25	21.33	8.26	13.89
3.58	27.06	5.67	11.90
3.33	24.25	6.32	13.36
4.07	24.81	7.35	12.40
2.83	28.90	5.50	9.33
3.14	20.83	2.30	15.45
3.30	22.49	5.12	14.30
3.28	22.88	5.75	14.74
3.44	22.32	3.66	14.41
3.15	21.47	5.23	14.61
3.24	4.92	6.08	63.11
3.47	21.96	3.73	13.81
3.11	20.39	5.63	14.53
3.25	20.52	6.05	14.61
2.98	19.23	5.49	14.23
3.38	20.58	4.88	14.23

0.53	22.35	3.65	4.73
0.82	31.65	3.71	4.46
1.10	21.45	3.80	11.60
0.13	27.81	3.25	2.69
0.31	18.10	3.24	6.85
0.67	20.30	4.81	9.85

0.08	24.16	4.00	0.99
1.34	14.70	3.72	20.25
1.41	14.89	3.88	20.38
1.07	7.35	3.63	33.16
			9.32
1.77	40.39	5.16	11.49
1.43	25.31	3.64	14.55
1.67	20.26	3.89	8.14
2.55	54.88	6.36	16.68
1.97	43.03	6.36	13.59
2.32	45.91	5.36	6.30
			9.14
1.14	18.71	3.00	6.56
2.11	39.33	6.89	5.25

Table

a)

		Witputs carbonate rocks						
		G116	G111	G112	G113	G114	G115	num9
strat. height		0.5 m	2 m	4 m	6 m	8 m	10 m	12 m
$d^{13}C_{VPDB}$	‰	-2.91	-2.88	-3.11	-3.00	-2.96	-3.07	-2.99
$d^{18}O_{VSMOW}$	‰	19.63	20.99	21.23	21.25	####	####	21.86

b)

		Bloeddrif distal*			Bloeddrif proximal*			Kombuis Member		
strat. height		1 m	8 m	30 m	1 m	10 m	30 m	1 m	22 m	30 m
$d^{13}C_{VPDB}$	‰	-2.3	-4.6	0.3	-3.3	-2.2	-1.1	1.61	-1.13	0
$d^{18}O_{VSMOW}$	‰	24.6	24.7	27.5	21.80	23.9	30	20.70	26.9	22.8
$^{87}Sr/^{86}Sr$		0.70852		0.70824				0.70804	0.709	0.70870

c)

		Witputs carb. rocks	Bloeddrif distal§	Bloeddrif proximal*	Kombuis Member#
SiO_2	wt%	4.8 - 5.7	0.78-3.14	1.7-4.1	< 1.45
Zr	ppm	19 - 34	2-16.4	5.1-8.1	< 7
Y	ppm	4.4 - 8.7	0.91	2.36	< 3
Sr	ppm	149 - 204	1078-2483	33-1291	700-3000
Mn/Sr (<10)		46 - 142	0.01-0.14	3.5-14.8	< 0.8
Fe/Sr (<50)		26 - 81	0.11-0.4	15.8-55.5	< 6.3
Ca/Sr (<1000)		1046 - 1982	188-360	3191-5637	n.d.
TOT S	wt%	0.01	high	high	
La	ppm	5	0.21	1.80	0.22
Ce	ppm	10	0.38	4.06	0.43
Pr	ppm	1	0.05	0.45	0.05
Nd	ppm	5	0.21	1.82	0.22
Sm	ppm	0.9	0.05	0.36	0.05
Eu	ppm	0.18	0.01	0.07	0.01
Gd	ppm	0.82	0.07	0.39	0.07
Tb	ppm	0.15	0.01	0.06	0.01
Dy	ppm	0.82	0.08	0.37	0.07
Ho	ppm	0.13	0.02	0.08	0.02
Er	ppm	0.42	0.06	0.23	0.05
Tm	ppm	0.06	0.01	0.03	0.01
Yb	ppm	0.4	0.04	0.20	0.04
Lu	ppm	0.06	0.01	0.03	0.01
$(Y/Ho)_{SHN}$		1.25	1.58	1.15	1.97
S REE	ppm	29.00	1.21	9.96	1.26
Al_2O_3	%	1.74	0.26	0.48	
Eu/Eu*		0.95	1.16	0.93	1.08
La/La*		0.89	2.17	1.25	1.75
Ce/Ce*		0.95	0.80	1.00	0.86
Gd/Gd*		0.86	-0.99	-1.16	-1.06
$(Nd/Yb)_{SHN}$		1.05	0.44	0.78	0.47

Table

NUMEES FORMATION

Samples	^{204}Pb	^{206}Pb	^{207}Pb	^{238}U	Pb ppm	U ppm	Ages $^{207}Pb/^{206}Pb$	2s abs	$^{206}Pb/^{238}U$	2s abs	$^{207}Pb/^{235}U$	2s abs	Discordance 206Pb-238U/ 207Pb-206Pb	206Pb-238U/ 207Pb-235U
Num_26	-94.9224	3.02501	0.20104	14.9231	14.80	100.81	1030.2	10.9	1078.5	23.0	1062.7	16.7	-5	-1
Num_23	56.3923	4.44951	0.297843	22.139	21.77	149.56	1041.2	10.1	1084.2	21.8	1070.0	15.8	-4	-1
Num_40	76.2473	15.1183	1.03728	72.8108	73.97	491.88	1077.5	10.0	1095.7	21.9	1089.6	15.9	-2	-1
Num_28	90.1634	4.35856	0.298453	20.9459	21.32	141.50	1079.0	13.9	1097.7	25.1	1091.5	18.9	-2	-1
Num_34	119.246	8.09164	0.556893	39.5044	39.59	266.87	1084.3	10.0	1084.5	23.7	1084.4	17.0	0	0
Num_38	352.489	3.68433	0.25575	18.2661	18.03	123.40	1087.3	10.0	1076.1	25.5	1079.8	18.2	1	0
NUM_79	71.5942	5.95841	0.411914	26.8071	33.06	174.81	1087.7	10.0	1100.4	19.3	1096.2	14.3	-1	0
NUM_60	74.905	4.74224	0.328209	20.3417	26.32	132.65	1089.5	10.0	1107.9	17.9	1101.7	13.5	-2	-1
NUM_109	-163.276	5.18637	0.357006	20.6827	36.49	200.21	1090.3	20.0	1082.8	24.3	1085.3	17.5	1	0
Num_24	-90.5175	3.01094	0.208147	15.2122	14.73	102.77	1090.4	10.3	1073.0	20.9	1078.7	15.5	2	1
NUM_57	215.077	4.12187	0.284071	18.0069	22.87	117.42	1091.3	10.0	1120.3	20.9	1110.5	15.2	-3	-1
NUM_88	390.937	4.15597	0.289583	18.7534	23.06	122.29	1092.1	10.0	1116.0	24.8	1107.9	17.5	-2	-1
Num_30	36.7709	7.17922	0.495816	35.5193	35.12	239.95	1092.5	10.0	1073.4	20.9	1079.7	15.4	2	1
NUM_108	-132.386	5.15298	0.355506	20.1419	36.25	194.97	1093.0	20.0	1100.6	24.0	1098.1	17.2	-1	0
NUM_111	136.864	2.88535	0.199479	10.7813	20.30	104.36	1096.7	20.9	1123.4	23.9	1114.3	17.1	-2	-1
NUM_82	199.054	1.82738	0.12811	8.3621	10.14	54.53	1097.1	15.4	1106.8	23.1	1103.6	18.3	-1	0
NUM_77	-137.479	2.47556	0.17199	11.1779	13.74	72.89	1097.2	12.1	1113.1	16.5	1107.7	13.5	-1	0
NUM_69	-7.71153	4.0905	0.286705	17.9856	22.70	117.29	1097.7	10.0	1104.9	17.0	1102.5	13.0	-1	0
NUM_61	33.6139	2.94744	0.206408	13.0556	16.36	85.14	1097.8	10.3	1097.5	21.4	1097.6	15.7	0	0
NUM_106	11.491	2.85141	0.196598	11.2111	20.06	108.52	1098.4	20.7	1094.2	24.5	1095.6	17.6	0	0
NUM_85	297.583	6.86184	0.477128	31.4147	38.08	204.86	1098.9	10.0	1109.3	23.1	1105.8	16.6	-1	0
NUM_137	75.1311	6.61623	0.457402	25.9443	46.55	251.14	1100.2	20.0	1115.2	25.9	1110.1	18.2	-1	0
NUM_76	28.6426	4.68285	0.326255	21.848	25.99	142.47	1101.8	10.0	1083.3	17.7	1089.5	13.6	2	1
NUM_46	5.15622	6.98253	0.486544	30.7874	38.75	200.77	1104.2	10.0	1111.7	17.2	1109.2	13.1	-1	0
NUM_45	85.4665	5.5018	0.383217	24.3975	30.53	159.10	1105.0	10.0	1096.2	16.4	1099.2	12.7	1	0
NUM_139	23.0018	1.52423	0.105609	6.1515	10.72	59.55	1105.1	36.2	1077.5	23.6	1086.7	19.8	2	1
NUM_102	13.8637	3.24482	0.22556	12.8446	22.83	124.33	1106.6	20.0	1089.5	23.9	1095.2	17.2	2	1
NUM_44	-117.433	5.95251	0.416683	26.0535	33.03	169.90	1107.7	10.0	1129.8	19.5	1122.3	14.4	-2	-1
NUM_43	241.121	3.03368	0.211633	13.7915	16.83	89.94	1108.0	10.0	1097.7	17.8	1101.2	13.5	1	0
NUM_75	192.039	6.58903	0.462047	29.7542	36.56	194.03	1108.6	10.0	1120.5	16.3	1116.5	12.6	-1	0
NUM_121	53.3362	4.73714	0.328393	17.9237	33.33	173.50	1109.1	20.0	1120.7	22.2	1116.7	16.0	-1	0
NUM_73	213.233	8.77164	0.613865	40.1193	48.67	261.62	1109.2	10.0	1107.1	20.0	1107.8	14.8	0	0
NUM_41	-187.071	7.85974	0.548811	35.1925	43.61	229.49	1109.5	10.0	1110.9	20.8	1110.4	15.2	0	0

NUM_99	38.706	4.11253	0.285591	15.6705	28.93	151.69	1110.0	20.0	1082.7	23.3	1091.8	16.9	2	1
NUM_42	51.8551	5.88748	0.408834	26.2039	32.67	170.88	1110.9	10.0	1108.9	18.3	1109.6	13.8	0	0
NUM_84	267.126	7.48045	0.524472	34.5975	41.51	225.61	1117.6	10.0	1099.5	20.0	1105.6	14.8	2	1
NUM_116	134.124	2.46631	0.172634	9.05382	17.35	87.64	1119.1	24.4	1148.2	27.0	1138.2	19.3	-3	-1
NUM_74	358.498	8.91223	0.626036	39.5218	49.45	257.72	1119.7	10.0	1132.8	23.2	1128.3	16.6	-1	0
NUM_100	259.081	2.39598	0.167082	8.97814	16.86	86.91	1121.6	24.0	1098.6	23.3	1106.4	17.4	2	1
NUM_65	-142.352	4.21426	0.296905	18.6419	23.39	121.57	1122.4	10.0	1091.9	20.6	1102.1	15.3	3	1
NUM_105	236.817	10.5513	0.739084	43.6843	74.23	422.86	1124.8	19.9	1031.6	26.1	1061.9	19.1	8	3
NUM_91	-62.5263	3.45242	0.242037	12.6796	24.29	122.74	1126.9	19.9	1105.3	27.7	1112.6	19.5	2	1
NUM_130	296.525	6.41952	0.452683	28.7052	45.16	277.86	1127.4	19.9	998.2	31.2	1039.5	22.7	11	4
NUM_83	162.858	7.11491	0.504734	32.5008	39.48	211.94	1130.0	10.0	1116.2	23.1	1120.9	16.6	1	0
NUM_115	61.5566	3.46512	0.243181	13.1542	24.38	127.33	1131.5	19.9	1124.9	26.7	1127.1	18.7	1	0
NUM_122	267.067	5.48279	0.386242	20.7682	38.57	201.03	1132.9	19.9	1115.8	23.0	1121.6	16.6	2	1
NUM_93	-22.4314	4.28735	0.302196	16.0478	30.16	155.34	1135.9	19.9	1089.4	28.9	1105.0	20.4	4	1
NUM_114	360.677	1.45607	0.10299	5.56072	10.24	53.83	1136.6	36.9	1109.8	26.5	1118.9	21.4	2	1
NUM_92	-114.133	3.84046	0.271008	14.5225	27.02	140.58	1139.1	19.9	1093.4	24.0	1108.8	17.3	4	1
Num_39	402.866	6.84703	0.484793	33.6902	33.50	227.60	1141.8	9.9	1078.3	21.7	1099.5	16.0	6	2
NUM_124	108.949	2.59393	0.182987	9.96284	18.25	96.44	1141.9	22.7	1110.8	23.0	1121.3	17.0	3	1
NUM_95	-144.017	2.10032	0.14876	7.78914	14.78	75.40	1143.8	27.4	1101.6	29.8	1115.9	21.8	4	1
NUM_113	125.534	2.62088	0.186471	9.95132	18.44	96.33	1144.5	23.3	1111.3	26.5	1122.6	19.2	3	1
NUM_119	-169.306	2.03444	0.144145	7.82264	14.31	75.72	1145.2	27.5	1104.3	22.2	1118.1	17.4	4	1
NUM_47	222.464	6.17685	0.440947	26.8391	34.28	175.02	1154.0	9.9	1130.6	18.6	1138.6	14.0	2	1
NUM_131	131.019	5.21512	0.374631	19.7535	36.69	191.21	1174.9	19.8	1142.9	26.3	1154.0	18.5	3	1
Num_31	552.986	14.3861	1.04122	69.4722	70.38	469.32	1185.4	9.9	1094.0	23.2	1125.0	17.0	8	3
NUM_71	130.439	7.71486	0.562348	34.2187	42.81	223.14	1191.0	9.9	1115.9	17.7	1141.7	13.6	6	2
NUM_128	69.1319	12.2159	0.885243	43.8748	85.94	424.70	1192.2	19.7	1193.6	25.2	1193.1	17.6	0	0
NUM_53	82.5686	10.0344	0.732369	40.6392	55.68	265.01	1196.0	9.9	1207.3	17.8	1203.3	13.3	-1	0
NUM_56	213.636	2.43695	0.177618	9.82921	13.52	64.10	1197.2	11.6	1204.6	28.7	1201.9	20.0	-1	0
NUM_112	15.1108	8.12311	0.590088	32.0804	57.15	310.53	1197.5	19.7	1070.6	22.5	1113.3	16.7	11	4
Num_33	587.901	10.873	0.794671	52.3552	53.20	353.69	1202.8	9.9	1091.5	24.4	1129.3	17.8	9	3
Num_29	19.3086	6.4191	0.463855	30.1672	31.41	203.80	1215.4	9.8	1110.0	23.4	1146.2	17.1	9	3
Num_27	60.8125	4.17264	0.306915	17.1872	20.41	116.11	1222.8	9.8	1270.3	26.6	1252.8	18.0	-4	-1
NUM_140	423.633	6.67207	0.488841	26.4565	46.94	256.09	1232.0	19.6	1094.8	29.7	1141.7	21.2	11	4
NUM_80	273.425	8.89752	0.667708	35.7086	49.37	232.86	1250.0	9.8	1226.8	23.1	1235.2	16.3	2	1
NUM_129	178.227	16.7899	1.258	56.8915	118.12	550.70	1257.2	19.6	1259.9	25.9	1258.9	17.7	0	0
NUM_97	266.202	5.426	0.407405	19.9263	38.17	192.88	1260.2	19.5	1079.1	37.9	1140.8	26.8	14	5
NUM_126	138.15	6.59838	0.497017	22.2559	46.42	215.43	1269.6	19.5	1262.7	26.0	1265.2	17.8	1	0
NUM_120	193.748	5.11285	0.386563	19.7079	35.97	190.77	1272.5	19.5	1098.5	21.8	1158.5	16.3	14	5

NUM_132	341.622	8.22106	0.622811	31.7908	57.84	307.73	1277.5	20.9	1121.7	23.2	1176.1	17.2	12	5
NUM_67	-95.5243	4.5127	0.344114	16.664	25.04	108.67	1292.4	9.7	1306.3	19.3	1301.1	13.9	-1	0
NUM_50	-1.84602	7.02605	0.541236	25.4477	38.99	165.95	1301.0	9.7	1326.0	26.0	1316.5	17.5	-2	-1
NUM_89	220.438	6.19186	0.476655	23.384	34.36	152.49	1301.0	9.7	1312.7	25.2	1308.3	17.1	-1	0
NUM_55	741.849	13.5579	1.04661	60.6732	75.23	395.65	1306.8	9.7	1088.5	18.4	1163.8	14.4	17	6
NUM_94	177.93	5.87392	0.451488	21.727	41.32	210.31	1311.5	19.4	1089.0	27.5	1165.8	20.1	17	7
Num_22	-83.2001	12.6226	0.977616	50.0888	61.76	338.38	1317.7	9.7	1344.4	27.6	1334.1	18.3	-2	-1
NUM_59	163.861	11.4197	0.894245	40.74	63.37	265.67	1332.1	9.7	1347.1	22.1	1341.3	15.3	-1	0
NUM_58	375.536	4.59017	0.359484	16.4727	25.47	107.42	1334.0	9.7	1328.2	23.9	1330.4	16.4	0	0
NUM_54	261.003	8.40107	0.658033	29.9922	46.62	195.58	1334.2	9.7	1354.3	21.6	1346.5	15.1	-2	-1
NUM_72	148.45	10.6268	0.841881	39.0505	58.97	254.65	1350.5	9.6	1343.9	23.3	1346.5	16.1	0	0
NUM_96	143.938	12.3219	0.978215	40.4452	86.68	391.50	1356.2	19.3	1204.6	33.1	1260.1	22.7	11	4
Num_37	434.77	2.81534	0.22324	13.354	13.77	90.21	1373.5	13.6	1099.1	23.3	1195.2	18.9	20	8
NUM_62	92.1018	3.50378	0.284012	13.5747	19.44	88.52	1394.9	9.6	1250.7	26.4	1304.8	18.4	10	4
Num_21	141.399	9.34908	0.763495	24.7321	45.74	167.08	1416.6	9.6	1304.6	27.6	1347.6	18.8	8	3
NUM_98	19.084	4.98711	0.410139	17.0138	35.08	164.69	1440.9	31.1	1199.1	34.6	1288.6	25.7	17	7
NUM_90	328.869	7.30589	0.609667	25.878	40.54	168.75	1458.6	9.5	1380.2	25.6	1411.3	17.4	5	2
NUM_104	856.203	8.21879	0.726233	31.4177	57.82	304.12	1551.9	31.0	1125.1	22.7	1280.6	19.9	27	12
NUM_49	25.3835	9.33506	0.823616	28.678	51.80	187.01	1562.0	9.4	1540.3	26.1	1549.5	17.0	1	1
NUM_70	15.2413	15.605	1.38401	53.9295	86.59	351.68	1564.4	9.4	1385.7	20.6	1457.7	14.8	11	5
NUM_81	722.989	3.36947	0.305086	15.1798	18.70	98.99	1579.1	23.9	1118.5	23.2	1286.5	24.6	29	13
Num_25	836.15	11.4671	1.01002	49.9775	56.10	337.62	1579.9	34.6	1216.2	27.1	1354.4	32.6	23	10
NUM_123	301.071	8.19426	0.737925	22.7873	57.65	220.58	1607.0	18.6	1472.9	31.4	1528.8	20.3	8	4
Num_32	181.626	17.9736	1.64514	62.134	87.94	419.75	1634.7	9.3	1476.6	31.9	1542.8	20.6	10	4
NUM_136	1774.58	12.5071	1.15784	52.9416	87.99	512.47	1658.7	18.5	1041.3	21.7	1261.1	17.7	37	17
NUM_64	1410.67	9.21857	0.869106	35.6097	51.15	232.21	1684.2	9.2	1244.4	23.2	1415.9	17.3	26	12
NUM_51	2256.62	26.6275	2.58693	91.914	147.76	599.38	1717.7	15.8	1377.0	30.3	1516.8	23.2	20	9
NUM_110	-154.656	7.81195	0.768961	18.4553	54.96	178.64	1770.9	18.3	1740.9	34.5	1754.6	20.5	2	1
NUM_127	54.8255	10.2602	1.02256	25.3178	72.18	245.07	1797.1	18.2	1680.8	33.0	1733.3	20.1	6	3
NUM_134	63.9909	4.80709	0.493987	10.9485	33.82	105.98	1849.7	18.1	1815.8	37.0	1831.7	21.4	2	1
NUM_118	1896.03	10.6508	1.10632	36.2876	74.93	351.26	1853.1	140.4	1226.8	28.6	1475.1	61.7	34	17
NUM_66	442.274	4.11838	0.429931	11.1081	22.85	72.44	1872.9	9.0	1685.8	37.9	1770.9	22.8	10	5
NUM_101	-62.6975	12.8044	1.34601	28.1799	90.08	272.78	1888.9	18.0	1830.1	39.5	1857.8	22.6	3	1
NUM_135	297.186	0.401269	0.0442079	1.5329	2.82	14.84	1921.9	189.1	1126.1	30.1	1432.2	80.7	41	21
NUM_48	1249.22	18.0849	1.9614	54.9864	100.35	358.57	1929.5	22.8	1538.6	35.0	1711.2	29.4	20	10
NUM_87	666.43	16.4799	1.78044	41.5674	91.45	271.06	1933.2	9.0	1896.8	29.5	1914.2	17.6	2	1
NUM_86	3768.6	15.6485	1.80071	67.3471	86.83	439.18	2015.0	25.8	1173.2	31.2	1507.5	31.8	42	22
NUM_117	-80.5194	7.79971	0.892104	15.0797	54.87	145.97	2042.3	17.7	2045.3	44.5	2043.8	23.8	0	0

NUM_103	-69.1167	26.5053	3.04501	57.8788	186.47	560.26	2059.5	17.6	1837.1	35.0	1943.8	20.7	11	5
NUM_63	2347.29	18.3158	2.33495	47.4149	101.64	309.20	2220.4	18.7	1766.9	46.2	1985.0	31.7	20	11
NUM_133	3796.31	28.8387	3.68005	73.2666	202.88	709.21	2233.6	22.5	1637.9	31.8	1916.8	21.8	27	15
NUM_107	296.652	18.4893	2.8535	41.0306	130.07	397.17	2557.5	16.7	1823.1	39.4	2192.0	23.8	29	17
NUM_78	13305	35.8105	5.72952	117.443	198.72	765.85	2598.4	48.8	1487.1	40.9	2009.0	56.3	43	26
NUM_138	266.966	5.05349	0.857535	10.1662	35.55	98.41	2704.8	16.5	2029.4	40.6	2385.2	23.1	25	15
Num_36	352.709	9.33838	1.61194	17.026	45.69	115.02	2740.6	8.2	2583.6	48.0	2672.6	23.1	6	3
Num_35	114.393	10.2804	1.79759	17.3375	50.30	117.12	2757.4	8.2	2720.9	52.3	2741.9	24.1	1	1
NUM_68	-22.6878	25.9171	4.57459	40.3903	143.82	263.39	2764.2	8.2	2726.6	34.8	2748.3	17.5	1	1
NUM_52	191.676	7.10421	1.25706	14.746	39.42	96.16	2782.0	8.2	2182.0	51.1	2507.1	27.0	22	13
NUM_125	98.373	11.7586	2.21422	15.5036	82.72	150.07	2885.5	16.2	2866.1	59.1	2877.5	26.0	1	0
NUM_125	275.653	9.89021	1.91775	12.6312	69.58	122.27	2929.1	16.2	2901.3	53.6	2917.7	23.8	1	1

HOLGAT FORMATION

							Ages						**Discordance**	
Samples	**^{204}Pb**	**^{206}Pb**	**^{207}Pb**	**^{238}U**	**Pb ppm**	**U ppm**	**^{207}Pb/^{206}Pb**	**2s abs**	**^{206}Pb/^{238}U**	**2s abs**	**^{207}Pb/^{235}U**	**2s abs**	**206Pb-238U/ 207Pb-206Pb**	**206Pb-238U/ 207Pb-235U**
HOL_31	100.182	4.95085	0.332939	20.8969	33.36	177.17	1082.8	10.0	1116.7	23.7	1105.3	16.8	-3	-1
HOL_72	-146.64	3.87069	0.260759	17.2293	26.08	146.07	1083.7	10.0	1107.6	24.2	1099.5	17.2	-2	-1
HOL_1	345.031	1.00547	0.0677678	4.11501	6.77	34.89	1086.5	26.3	1140.8	26.5	1122.2	24.5	-5	-2
HOL_30	37.9141	6.47095	0.436418	27.7308	43.60	235.11	1087.2	10.0	1066.3	31.4	1073.2	22.0	2	1
HOL_38	10.926	3.06075	0.206094	12.7559	20.62	108.15	1089.7	10.6	1100.8	24.1	1097.1	17.3	-1	0
HOL_79	-35.2488	7.35961	0.496775	32.0703	49.59	271.90	1090.1	10.0	1118.0	25.6	1108.6	18.0	-3	-1
HOL_68	-9.94066	2.12224	0.142917	9.44994	14.30	80.12	1090.4	14.3	1108.7	23.6	1102.5	18.1	-2	-1
HOL_59	-135.017	2.73395	0.184637	12.0723	18.42	102.35	1091.0	11.3	1121.8	25.6	1111.4	18.3	-3	-1
HOL_37	355.311	5.11814	0.345829	21.4343	34.48	181.72	1093.7	10.0	1075.6	32.4	1081.6	22.5	2	1
HOL_16	188.826	3.80607	0.257979	15.4015	25.64	130.58	1094.0	10.0	1117.0	24.3	1109.3	17.2	-2	-1
HOL_39	167.7	2.29938	0.15569	9.74681	15.49	82.64	1094.1	13.6	1085.5	23.3	1088.4	17.9	1	0
HOL_21	-140.028	5.25579	0.355457	21.4523	35.41	181.88	1094.4	10.0	1111.2	22.5	1105.6	16.2	-2	-1
HOL_78	10.5601	2.69868	0.182973	12.0164	18.18	101.88	1095.3	11.2	1119.3	25.6	1111.2	18.3	-2	-1
HOL_73	-210.279	2.18605	0.148037	9.51681	14.73	80.69	1096.0	14.0	1114.7	24.2	1108.4	18.4	-2	-1
HOL_33	-20.8544	9.17087	0.62197	37.8655	61.79	321.03	1097.0	10.0	1097.0	22.1	1097.0	16.1	0	0
HOL_25	-7.2203	3.29856	0.223469	13.7587	22.22	116.65	1097.1	10.0	1104.4	22.9	1101.9	16.5	-1	0
HOL_20	-94.0325	5.99812	0.406313	25.155	40.41	213.27	1097.3	10.0	1122.5	23.2	1113.9	16.5	-2	-1
HOL_32	-9.95178	2.12572	0.143962	9.26912	14.32	78.59	1097.9	14.8	962.4	36.4	1004.6	27.4	12	4
HOL_75	-126.124	2.90847	0.197137	12.6368	19.60	107.14	1098.4	10.6	1129.1	26.4	1118.7	18.6	-3	-1
HOL_26	10.1072	4.652	0.315426	19.4979	31.34	165.31	1099.4	10.0	1125.4	24.4	1116.6	17.2	-2	-1

HOL_58	-16.5922	1.54602	0.105546	6.79378	10.42	57.60	1100.0	18.4	1121.5	25.6	1114.2	20.7	-2	-1
HOL_2	152.638	2.91654	0.197783	11.7899	19.65	99.96	1101.2	10.8	1150.5	27.3	1133.6	19.0	-4	-1
HOL_82	194.719	2.73063	0.185539	12.2739	18.40	104.06	1101.4	11.7	1096.9	22.8	1098.4	17.0	0	0
HOL_60	-100.053	3.12238	0.210452	13.7912	21.04	116.92	1101.8	10.0	1110.2	26.2	1107.4	18.5	-1	0
HOL_18	-81.3813	1.98678	0.135095	8.19453	13.39	69.47	1104.0	14.4	1137.8	26.5	1126.2	19.7	-3	-1
HOL_15	-67.9998	1.87168	0.127271	7.73363	12.61	65.57	1106.4	15.7	1121.0	24.3	1116.0	19.0	-1	0
HOL_66	183.858	6.20229	0.421854	27.2705	41.79	231.20	1107.0	10.0	1100.8	22.1	1102.9	16.1	1	0
HOL_55	73.7947	2.16118	0.14711	9.47474	14.56	80.33	1107.2	13.7	1110.4	22.1	1109.4	17.2	0	0
HOL_65	-215.695	4.41132	0.300247	19.3639	29.72	164.17	1107.9	10.0	1117.0	21.8	1113.9	15.8	-1	0
HOL_23	-145.577	3.15787	0.213184	12.7899	21.28	108.43	1108.2	10.1	1102.7	24.7	1104.6	17.7	0	0
HOL_49 re	234.953	2.75093	0.187266	12.1231	18.53	102.78	1111.6	11.5	1125.1	22.6	1120.5	16.6	-1	0
HOL_9	208.529	1.69183	0.115289	7.06349	11.40	59.89	1112.4	16.8	1112.9	27.7	1112.7	21.4	0	0
HOL_48	82.1182	6.59191	0.451956	29.4275	44.41	249.49	1113.2	10.0	1120.9	25.0	1118.2	17.7	-1	0
HOL_62	-178.622	2.8018	0.190986	12.3075	18.88	104.35	1115.4	11.0	1120.3	22.5	1118.6	16.5	0	0
HOL_47	136.489	3.41302	0.233122	15.1134	23.00	128.13	1115.4	10.0	1120.9	24.3	1119.0	17.3	0	0
HOL_7	232.995	2.83023	0.193328	12.0493	19.07	102.16	1115.5	10.9	1119.6	29.3	1118.2	20.5	0	0
HOL_54	108.161	4.02342	0.275027	17.7363	27.11	150.37	1116.3	10.0	1113.3	22.5	1114.3	16.2	0	0
HOL_3	166.398	2.34284	0.159366	9.37097	15.79	79.45	1118.5	12.8	1141.0	24.0	1133.3	17.8	-2	-1
HOL_81	65.5582	6.89406	0.472287	28.4304	46.45	241.04	1119.9	10.0	1181.3	34.7	1159.8	23.1	-5	-2
HOL_44	156.967	3.99632	0.273521	17.1167	26.93	145.12	1119.9	10.0	1132.7	27.9	1128.3	19.4	-1	0
HOL_28	-43.5809	2.95894	0.203556	12.5058	19.94	106.03	1120.2	12.1	1100.9	24.7	1107.4	18.3	2	1
HOL_45	98.1697	1.99406	0.135785	8.73605	13.44	74.07	1122.7	15.0	1120.2	23.7	1121.1	18.5	0	0
HOL_34	227.159	4.1816	0.28915	17.1662	28.17	145.54	1126.6	11.5	1122.9	24.3	1124.2	17.7	0	0
HOL_43	96.1044	1.33953	0.0912289	5.93169	9.03	50.29	1129.2	20.5	1126.0	26.4	1127.1	22.1	0	0
HOL_8	241.716	1.86304	0.12831	7.9203	12.55	67.15	1130.8	15.1	1115.0	27.0	1120.3	20.5	1	0
HOL_46	331.748	3.70573	0.256003	16.3746	24.97	138.83	1132.5	10.0	1117.8	24.3	1122.8	17.3	1	0
HOL_29	-29.2947	1.61638	0.11164	6.94346	10.89	58.87	1132.5	17.7	1106.7	23.5	1115.4	19.6	2	1
HOL_6	575.012	2.39975	0.167049	9.91026	16.17	84.02	1143.6	12.3	1113.6	26.2	1123.8	19.2	3	1
HOL_4	31.1353	2.84911	0.197838	11.873	19.20	100.66	1148.5	10.8	1112.3	21.2	1124.6	15.8	3	1
HOL_11	138.849	8.43121	0.589419	36.0383	56.81	305.54	1157.7	9.9	1077.6	29.0	1104.5	20.6	7	2
HOL_17	70.7201	5.8035	0.416413	24.0406	39.10	203.82	1174.0	19.2	1116.9	23.7	1136.4	20.4	5	2
HOL_13	-34.0505	12.3097	0.869247	46.9726	82.94	398.24	1178.2	9.9	1207.5	26.0	1197.1	17.9	-2	-1
HOL_52	230.431	4.58427	0.326791	20.2397	30.89	171.60	1184.0	13.1	1127.2	22.3	1146.7	17.3	5	2
HOL_14	-152.269	1.5041	0.106711	5.79128	10.13	49.10	1194.5	17.5	1193.3	94.9	1193.7	61.0	0	0
HOL_77	21.5964	6.18234	0.440526	24.9633	41.65	211.64	1197.5	9.9	1222.4	24.5	1213.4	17.0	-2	-1
HOL_36	190.779	3.61786	0.259584	14.0355	24.38	119.00	1209.3	9.8	1212.9	25.4	1211.6	17.6	0	0
HOL_24	-217.182	1.72693	0.123947	6.524	11.64	55.31	1209.7	16.2	1215.1	24.9	1213.1	19.6	0	0
HOL_41	89.5673	3.1215	0.222421	13.7802	21.03	116.83	1210.1	20.6	1142.6	28.7	1166.2	23.7	6	2

HOL_76	272.478	8.01296	0.585249	35.783	53.99	303.37	1248.0	28.9	1113.0	25.5	1159.7	26.4	11	4
HOL_51a	366.411	1.30325	0.0960476	5.49998	8.78	46.63	1251.0	19.1	1086.6	36.0	1142.8	27.8	13	5
HOL_71sh	-88.0901	12.3369	0.905122	49.5761	83.12	420.31	1258.4	9.8	1237.5	34.3	1245.2	22.8	2	1
HOL_61	104.144	4.72823	0.350411	17.6037	31.86	149.25	1274.9	9.8	1319.6	28.5	1302.6	18.8	-4	-1
HOL_74	69.8107	4.02634	0.295411	18.0978	27.13	153.44	1281.3	28.8	1090.9	22.7	1156.4	25.4	15	6
HOL_70	22.8731	1.93594	0.145682	7.23657	13.04	61.35	1291.8	13.4	1326.4	27.9	1313.2	19.8	-3	-1
HOL_42 re	175.158	14.4854	1.11498	56.9858	97.60	483.14	1352.6	9.6	1246.6	29.0	1286.0	19.9	8	3
HOL_50	52.4382	5.89917	0.455006	20.9614	39.75	177.71	1353.3	9.6	1361.6	30.2	1358.4	19.7	-1	0
HOL_51b	175.164	7.01048	0.54998	26.1219	47.23	221.47	1358.8	9.6	1299.7	26.5	1322.2	18.1	4	2
HOL_12	366.527	8.98695	0.692638	46.471	60.55	393.99	1359.7	12.8	905.4	51.7	1048.4	40.3	33	14
HOL_63	68.5294	0.324046	0.0250782	1.11018	2.18	9.41	1379.3	60.2	1378.4	31.0	1378.7	49.7	0	0
HOL_10	309.249	5.65579	0.46904	17.0839	38.11	144.84	1493.5	9.5	1503.4	32.9	1499.3	20.6	-1	0
HOL_67	614.13	12.5013	1.04569	45.2581	84.23	383.71	1500.4	17.1	1332.0	33.4	1398.1	24.9	11	5
HOL_35	125.808	2.72987	0.230432	7.99839	18.39	67.81	1522.3	9.7	1554.1	30.6	1540.7	19.2	-2	-1
HOL_5	520.671	2.76363	0.234082	11.1778	18.62	94.77	1524.3	62.2	1175.4	44.7	1304.8	55.8	23	10
HOL_64	79.0467	6.14221	0.520383	19.0914	41.38	161.86	1534.4	9.4	1523.4	40.9	1528.0	24.8	1	0
HOL_40	35.9614	4.65887	0.39869	12.391	31.39	105.05	1543.2	9.4	1651.9	38.8	1604.6	22.8	-7	-3
HOL_69	-38.0872	8.01157	0.764957	21.3763	53.98	181.23	1752.8	9.1	1766.4	35.6	1760.2	20.8	-1	0
HOL_56	421.076	14.4598	1.43095	41.4953	97.43	351.80	1818.4	9.1	1637.9	36.1	1718.6	22.1	10	5
HOL_27	-183.804	9.55511	0.962832	22.2898	64.38	188.98	1850.0	9.0	1855.8	40.5	1853.1	22.8	0	0
HOL_19	41.3203	4.23695	0.456278	9.07048	28.55	76.90	1970.4	8.9	1997.0	45.4	1984.0	24.4	-1	-1
HOL_53	787.265	2.63769	0.288603	13.1908	17.77	111.83	2005.6	21.1	999.8	69.3	1369.8	57.7	50	27
HOL_22	351.543	0.305578	0.0782738	1.00114	2.06	8.49	3387.7	20.8	1358.5	35.1	2358.3	35.3	60	42

ages with discordances above 10% are in grey

Table 3: Zimmermann et al.

Table

NUMEES FORMATION

Samples	^{204}Pb	^{206}Pb	^{207}Pb	^{238}U	Pb ppm	U ppm	Ages ^{207}Pb/^{206}Pb	2s abs	^{206}Pb/^{238}U	2s abs	^{207}Pb/^{235}U	2s abs	Discordance 206Pb-238U/ 207Pb-206Pb	206Pb-238U/ 207Pb-235U
Num_26	-94.922	3.02501	0.20104	14.9231	14.80	100.81	1030.2	10.9	1078.5	23.0	1062.7	16.7	-5	-1
Num_23	56.3923	4.44951	0.297843	22.139	21.77	149.56	1041.2	10.1	1084.2	21.8	1070.0	15.8	-4	-1
Num_40	76.2473	15.1183	1.03728	72.8108	73.97	491.88	1077.5	10.0	1095.7	21.9	1089.6	15.9	-2	-1
Num_28	90.1634	4.35856	0.298453	20.9459	21.32	141.50	1079.0	13.9	1097.7	25.1	1091.5	18.9	-2	-1
Num_34	119.246	8.09164	0.556893	39.5044	39.59	266.87	1084.3	10.0	1084.5	23.7	1084.4	17.0	0	0
Num_38	352.489	3.68433	0.25575	18.2661	18.03	123.40	1087.3	10.0	1076.1	25.5	1079.8	18.2	1	0
NUM_79	71.5942	5.95841	0.411914	26.8071	33.06	174.81	1087.7	10.0	1100.4	19.3	1096.2	14.3	-1	0
NUM_60	74.905	4.74224	0.328209	20.3417	26.32	132.65	1089.5	10.0	1107.9	17.9	1101.7	13.5	-2	-1
NUM_109	-163.28	5.18637	0.357006	20.6827	36.49	200.21	1090.3	20.0	1082.8	24.3	1085.3	17.5	1	0
Num_24	-90.518	3.01094	0.208147	15.2122	14.73	102.77	1090.4	10.3	1073.0	20.9	1078.7	15.5	2	1
NUM_57	215.077	4.12187	0.284071	18.0069	22.87	117.42	1091.3	10.0	1120.3	20.9	1110.5	15.2	-3	-1
NUM_88	390.937	4.15597	0.289583	18.7534	23.06	122.29	1092.1	10.0	1116.0	24.8	1107.9	17.5	-2	-1
Num_30	36.7709	7.17922	0.495816	35.5193	35.12	239.95	1092.5	10.0	1073.4	20.9	1079.7	15.4	2	1
NUM_108	-132.39	5.15298	0.355506	20.1419	36.25	194.97	1093.0	20.0	1100.6	24.0	1098.1	17.2	-1	0
NUM_111	136.864	2.88535	0.199479	10.7813	20.30	104.36	1096.7	20.9	1123.4	23.9	1114.3	17.1	-2	-1
NUM_82	199.054	1.82738	0.12811	8.3621	10.14	54.53	1097.1	15.4	1106.8	23.1	1103.6	18.3	-1	0
NUM_77	-137.48	2.47556	0.17199	11.1779	13.74	72.89	1097.2	12.1	1113.1	16.5	1107.7	13.5	-1	0
NUM_69	-7.7115	4.0905	0.286705	17.9856	22.70	117.29	1097.7	10.0	1104.9	17.0	1102.5	13.0	-1	0
NUM_61	33.6139	2.94744	0.206408	13.0556	16.36	85.14	1097.8	10.3	1097.5	21.4	1097.6	15.7	0	0
NUM_106	11.491	2.85141	0.196598	11.2111	20.06	108.52	1098.4	20.7	1094.2	24.5	1095.6	17.6	0	0
NUM_85	297.583	6.86184	0.477128	31.4147	38.08	204.86	1098.9	10.0	1109.3	23.1	1105.8	16.6	-1	0
NUM_137	75.1311	6.61623	0.457402	25.9443	46.55	251.14	1100.2	20.0	1115.2	25.9	1110.1	18.2	-1	0
NUM_76	28.6426	4.68285	0.326255	21.848	25.99	142.47	1101.8	10.0	1083.3	17.7	1089.5	13.6	2	1
NUM_46	5.15622	6.98253	0.486544	30.7874	38.75	200.77	1104.2	10.0	1111.7	17.2	1109.2	13.1	-1	0
NUM_45	85.4665	5.5018	0.383217	24.3975	30.53	159.10	1105.0	10.0	1096.2	16.4	1099.2	12.7	1	0
NUM_139	23.0018	1.52423	0.105609	6.1515	10.72	59.55	1105.1	36.2	1077.5	23.6	1086.7	19.8	2	1
NUM_102	13.8637	3.24482	0.22556	12.8446	22.83	124.33	1106.6	20.0	1089.5	23.9	1095.2	17.2	2	1
NUM_44	-117.43	5.95251	0.416683	26.0535	33.03	169.90	1107.7	10.0	1129.8	19.5	1122.3	14.4	-2	-1
NUM_43	241.121	3.03368	0.211633	13.7915	16.83	89.94	1108.0	10.0	1097.7	17.8	1101.2	13.5	1	0
NUM_75	192.039	6.58903	0.462047	29.7542	36.56	194.03	1108.6	10.0	1120.5	16.3	1116.5	12.6	-1	0

NUM_121	53.3362	4.73714	0.328393	17.9237	33.33	173.50	1109.1	20.0	1120.7	22.2	1116.7	16.0	-1	0
NUM_73	213.233	8.77164	0.613865	40.1193	48.67	261.62	1109.2	10.0	1107.1	20.0	1107.8	14.8	0	0
NUM_41	-187.07	7.85974	0.548811	35.1925	43.61	229.49	1109.5	10.0	1110.9	20.8	1110.4	15.2	0	0
NUM_99	38.706	4.11253	0.285591	15.6705	28.93	151.69	1110.0	20.0	1082.7	23.3	1091.8	16.9	2	1
NUM_42	51.8551	5.88748	0.408834	26.2039	32.67	170.88	1110.9	10.0	1108.9	18.3	1109.6	13.8	0	0
NUM_84	267.126	7.48045	0.524472	34.5975	41.51	225.61	1117.6	10.0	1099.5	20.0	1105.6	14.8	2	1
NUM_116	134.124	2.46631	0.172634	9.05382	17.35	87.64	1119.1	24.4	1148.2	27.0	1138.2	19.3	-3	-1
NUM_74	358.498	8.91223	0.626036	39.5218	49.45	257.72	1119.7	10.0	1132.8	23.2	1128.3	16.6	-1	0
NUM_100	259.081	2.39598	0.167082	8.97814	16.86	86.91	1121.6	24.0	1098.6	23.3	1106.4	17.4	2	1
NUM_65	-142.35	4.21426	0.296905	18.6419	23.39	121.57	1122.4	10.0	1091.9	20.6	1102.1	15.3	3	1
NUM_105	236.817	10.5513	0.739084	43.6843	74.23	422.86	1124.8	19.9	1031.6	26.1	1061.9	19.1	8	3
NUM_91	-62.526	3.45242	0.242037	12.6796	24.29	122.74	1126.9	19.9	1105.3	27.7	1112.6	19.5	2	1
NUM_130	296.525	6.41952	0.452683	28.7052	45.16	277.86	1127.4	19.9	998.2	31.2	1039.5	22.7	11	4
NUM_83	162.858	7.11491	0.504734	32.5008	39.48	211.94	1130.0	10.0	1116.2	23.1	1120.9	16.6	1	0
NUM_115	61.5566	3.46512	0.243181	13.1542	24.38	127.33	1131.5	19.9	1124.9	26.7	1127.1	18.7	1	0
NUM_122	267.067	5.48279	0.386242	20.7682	38.57	201.03	1132.9	19.9	1115.8	23.0	1121.6	16.6	2	1
NUM_93	-22.431	4.28735	0.302196	16.0478	30.16	155.34	1135.9	19.9	1089.4	28.9	1105.0	20.4	4	1
NUM_114	360.677	1.45607	0.10299	5.56072	10.24	53.83	1136.6	36.9	1109.8	26.5	1118.9	21.4	2	1
NUM_92	-114.13	3.84046	0.271008	14.5225	27.02	140.58	1139.1	19.9	1093.4	24.0	1108.8	17.3	4	1
Num_39	402.866	6.84703	0.484793	33.6902	33.50	227.60	1141.8	9.9	1078.3	21.7	1099.5	16.0	6	2
NUM_124	108.949	2.59393	0.182987	9.96284	18.25	96.44	1141.9	22.7	1110.8	23.0	1121.3	17.0	3	1
NUM_95	-144.02	2.10032	0.14876	7.78914	14.78	75.40	1143.8	27.4	1101.6	29.8	1115.9	21.8	4	1
NUM_113	125.534	2.62088	0.186471	9.95132	18.44	96.33	1144.5	23.3	1111.3	26.5	1122.6	19.2	3	1
NUM_119	-169.31	2.03444	0.144145	7.82264	14.31	75.72	1145.2	27.5	1104.3	22.2	1118.1	17.4	4	1
NUM_47	222.464	6.17685	0.440947	26.8391	34.28	175.02	1154.0	9.9	1130.6	18.6	1138.6	14.0	2	1
NUM_131	131.019	5.21512	0.374631	19.7535	36.69	191.21	1174.9	19.8	1142.9	26.3	1154.0	18.5	3	1
Num_31	552.986	14.3861	1.04122	69.4722	70.38	469.32	1185.4	9.9	1094.0	23.2	1125.0	17.0	8	3
NUM_71	130.439	7.71486	0.562348	34.2187	42.81	223.14	1191.0	9.9	1115.9	17.7	1141.7	13.6	6	2
NUM_128	69.1319	12.2159	0.885243	43.8748	85.94	424.70	1192.2	19.7	1193.6	25.2	1193.1	17.6	0	0
NUM_53	82.5686	10.0344	0.732369	40.6392	55.68	265.01	1196.0	9.9	1207.3	17.8	1203.3	13.3	-1	0
NUM_56	213.636	2.43695	0.177618	9.82921	13.52	64.10	1197.2	11.6	1204.6	28.7	1201.9	20.0	-1	0
NUM_112	15.1108	8.12311	0.590088	32.0804	57.15	310.53	1197.5	19.7	1070.6	22.5	1113.3	16.7	11	4
Num_33	587.901	10.873	0.794671	52.3552	53.20	353.69	1202.8	9.9	1091.5	24.4	1129.3	17.8	9	3
Num_29	19.3086	6.4191	0.463855	30.1672	31.41	203.80	1215.4	9.8	1110.0	23.4	1146.2	17.1	9	3

Num_27	60.8125	4.17264	0.306915	17.1872	20.41	116.11	1222.8	9.8	1270.3	26.6	1252.8	18.0	-4	-1
NUM_140	423.633	6.67207	0.488841	26.4565	46.94	256.09	1232.0	19.6	1094.8	29.7	1141.7	21.2	11	4
NUM_80	273.425	8.89752	0.667708	35.7086	49.37	232.86	1250.0	9.8	1226.8	23.1	1235.2	16.3	2	1
NUM_129	178.227	16.7899	1.258	56.8915	118.12	550.70	1257.2	19.6	1259.9	25.9	1258.9	17.7	0	0
NUM_97	266.202	5.426	0.407405	19.9263	38.17	192.88	1260.2	19.5	1079.1	37.9	1140.8	26.8	14	5
NUM_126	138.15	6.59838	0.497017	22.2559	46.42	215.43	1269.6	19.5	1262.7	26.0	1265.2	17.8	1	0
NUM_120	193.748	5.11285	0.386563	19.7079	35.97	190.77	1272.5	19.5	1098.5	21.8	1158.5	16.3	14	5
NUM_132	341.622	8.22106	0.622811	31.7908	57.84	307.73	1277.5	20.9	1121.7	23.2	1176.1	17.2	12	5
NUM_67	-95.524	4.5127	0.344114	16.664	25.04	108.67	1292.4	9.7	1306.3	19.3	1301.1	13.9	-1	0
NUM_50	-1.846	7.02605	0.541236	25.4477	38.99	165.95	1301.0	9.7	1326.0	26.0	1316.5	17.5	-2	-1
NUM_89	220.438	6.19186	0.476655	23.384	34.36	152.49	1301.0	9.7	1312.7	25.2	1308.3	17.1	-1	0
NUM_55	741.849	13.5579	1.04661	60.6732	75.23	395.65	1306.8	9.7	1088.5	18.4	1163.8	14.4	17	6
NUM_94	177.93	5.87392	0.451488	21.727	41.32	210.31	1311.5	19.4	1089.0	27.5	1165.8	20.1	17	7
Num_22	-83.2	12.6226	0.977616	50.0888	61.76	338.38	1317.7	9.7	1344.4	27.6	1334.1	18.3	-2	-1
NUM_59	163.861	11.4197	0.894245	40.74	63.37	265.67	1332.1	9.7	1347.1	22.1	1341.3	15.3	-1	0
NUM_58	375.536	4.59017	0.359484	16.4727	25.47	107.42	1334.0	9.7	1328.2	23.9	1330.4	16.4	0	0
NUM_54	261.003	8.40107	0.658033	29.9922	46.62	195.58	1334.2	9.7	1354.3	21.6	1346.5	15.1	-2	-1
NUM_72	148.45	10.6268	0.841881	39.0505	58.97	254.65	1350.5	9.6	1343.9	23.3	1346.5	16.1	0	0
NUM_96	143.938	12.3219	0.978215	40.4452	86.68	391.50	1356.2	19.3	1204.6	33.1	1260.1	22.7	11	4
Num_37	434.77	2.81534	0.22324	13.354	13.77	90.21	1373.5	13.6	1099.1	23.3	1195.2	18.9	20	8
NUM_62	92.1018	3.50378	0.284012	13.5747	19.44	88.52	1394.9	9.6	1250.7	26.4	1304.8	18.4	10	4
Num_21	141.399	9.34908	0.763495	24.7321	45.74	167.08	1416.6	9.6	1304.6	27.6	1347.6	18.8	8	3
NUM_98	19.084	4.98711	0.410139	17.0138	35.08	164.69	1440.9	31.1	1199.1	34.6	1288.6	25.7	17	7
NUM_90	328.869	7.30589	0.609667	25.878	40.54	168.75	1458.6	9.5	1380.2	25.6	1411.3	17.4	5	2
NUM_104	856.203	8.21879	0.726233	31.4177	57.82	304.12	1551.9	31.0	1125.1	22.7	1280.6	19.9	27	12
NUM_49	25.3835	9.33506	0.823616	28.678	51.80	187.01	1562.0	9.4	1540.3	26.1	1549.5	17.0	1	1
NUM_70	15.2413	15.605	1.38401	53.9295	86.59	351.68	1564.4	9.4	1385.7	20.6	1457.7	14.8	11	5
NUM_81	722.989	3.36947	0.305086	15.1798	18.70	98.99	1579.1	23.9	1118.5	23.2	1286.5	24.6	29	13
Num_25	836.15	11.4671	1.01002	49.9775	56.10	337.62	1579.9	34.6	1216.2	27.1	1354.4	32.6	23	10
NUM_123	301.071	8.19426	0.737925	22.7873	57.65	220.58	1607.0	18.6	1472.9	31.4	1528.8	20.3	8	4
Num_32	181.626	17.9736	1.64514	62.134	87.94	419.75	1634.7	9.3	1476.6	31.9	1542.8	20.6	10	4
NUM_136	1774.58	12.5071	1.15784	52.9416	87.99	512.47	1658.7	18.5	1041.3	21.7	1261.1	17.7	37	17
NUM_64	1410.67	9.21857	0.869106	35.6097	51.15	232.21	1684.2	9.2	1244.4	23.2	1415.9	17.3	26	12
NUM_51	2256.62	26.6275	2.58693	91.914	147.76	599.38	1717.7	15.8	1377.0	30.3	1516.8	23.2	20	9

NUM_110	-154.66	7.81195	0.768961	18.4553	54.96	178.64	1770.9	18.3	1740.9	34.5	1754.6	20.5	2	1
NUM_127	54.8255	10.2602	1.02256	25.3178	72.18	245.07	1797.1	18.2	1680.8	33.0	1733.3	20.1	6	3
NUM_134	63.9909	4.80709	0.493987	10.9485	33.82	105.98	1849.7	18.1	1815.8	37.0	1831.7	21.4	2	1
NUM_118	1896.03	10.6508	1.10632	36.2876	74.93	351.26	1853.1	140.4	1226.8	28.6	1475.1	61.7	34	17
NUM_66	442.274	4.11838	0.429931	11.1081	22.85	72.44	1872.9	9.0	1685.8	37.9	1770.9	22.8	10	5
NUM_101	-62.698	12.8044	1.34601	28.1799	90.08	272.78	1888.9	18.0	1830.1	39.5	1857.8	22.6	3	1
NUM_135	297.186	0.40127	0.044208	1.5329	2.82	14.84	1921.9	189.1	1126.1	30.1	1432.2	80.7	41	21
NUM_48	1249.22	18.0849	1.9614	54.9864	100.35	358.57	1929.5	22.8	1538.6	35.0	1711.2	29.4	20	10
NUM_87	666.43	16.4799	1.78044	41.5674	91.45	271.06	1933.2	9.0	1896.8	29.5	1914.2	17.6	2	1
NUM_86	3768.6	15.6485	1.80071	67.3471	86.83	439.18	2015.0	25.8	1173.2	31.2	1507.5	31.8	42	22
NUM_117	-80.519	7.79971	0.892104	15.0797	54.87	145.97	2042.3	17.7	2045.3	44.5	2043.8	23.8	0	0
NUM_103	-69.117	26.5053	3.04501	57.8788	186.47	560.26	2059.5	17.6	1837.1	35.0	1943.8	20.7	11	5
NUM_63	2347.29	18.3158	2.33495	47.4149	101.64	309.20	2220.4	18.7	1766.9	46.2	1985.0	31.7	20	11
NUM_133	3796.31	28.8387	3.68005	73.2666	202.88	709.21	2233.6	22.5	1637.9	31.8	1916.8	21.8	27	15
NUM_107	296.652	18.4893	2.8535	41.0306	130.07	397.17	2557.5	16.7	1823.1	39.4	2192.0	23.8	29	17
NUM_78	13305	35.8105	5.72952	117.443	198.72	765.85	2598.4	48.8	1487.1	40.9	2009.0	56.3	43	26
NUM_138	266.966	5.05349	0.857535	10.1662	35.55	98.41	2704.8	16.5	2029.4	40.6	2385.2	23.1	25	15
Num_36	352.709	9.33838	1.61194	17.026	45.69	115.02	2740.6	8.2	2583.6	48.0	2672.6	23.1	6	3
Num_35	114.393	10.2804	1.79759	17.3375	50.30	117.12	2757.4	8.2	2720.9	52.3	2741.9	24.1	1	1
NUM_68	-22.688	25.9171	4.57459	40.3903	143.82	263.39	2764.2	8.2	2726.6	34.8	2748.3	17.5	1	1
NUM_52	191.676	7.10421	1.25706	14.746	39.42	96.16	2782.0	8.2	2182.0	51.1	2507.1	27.0	22	13
NUM_125	98.373	11.7586	2.21422	15.5036	82.72	150.07	2885.5	16.2	2866.1	59.1	2877.5	26.0	1	0
NUM_125	275.653	9.89021	1.91775	12.6312	69.58	122.27	2929.1	16.2	2901.3	53.6	2917.7	23.8	1	1

HOLGAT FORMATION

							Ages						Discordance	
Samples	**^{204}Pb**	**^{206}Pb**	**^{207}Pb**	**^{238}U**	**Pb ppm**	**U ppm**	**^{207}Pb/^{206}Pb**	**2s abs**	**^{206}Pb/^{238}U**	**2s abs**	**^{207}Pb/^{235}U**	**2s abs**	**206Pb-238U/ 207Pb-206Pb**	**206Pb-238U/ 207Pb-235U**
HOL_31	100.182	4.95085	0.332939	20.8969	33.36	177.17	1082.8	10.0	1116.7	23.7	1105.3	16.8	-3	-1
HOL_72	-146.64	3.87069	0.260759	17.2293	26.08	146.07	1083.7	10.0	1107.6	24.2	1099.5	17.2	-2	-1
HOL_1	345.031	1.00547	0.067768	4.11501	6.77	34.89	1086.5	26.3	1140.8	26.5	1122.2	24.5	-5	-2
HOL_30	37.9141	6.47095	0.436418	27.7308	43.60	235.11	1087.2	10.0	1066.3	31.4	1073.2	22.0	2	1
HOL_38	10.926	3.06075	0.206094	12.7559	20.62	108.15	1089.7	10.6	1100.8	24.1	1097.1	17.3	-1	0
HOL_79	-35.249	7.35961	0.496775	32.0703	49.59	271.90	1090.1	10.0	1118.0	25.6	1108.6	18.0	-3	-1

HOL_68	-9.9407	2.12224	0.142917	9.44994	14.30	80.12	1090.4	14.3	1108.7	23.6	1102.5	18.1	-2	-1
HOL_59	-135.02	2.73395	0.184637	12.0723	18.42	102.35	1091.0	11.3	1121.8	25.6	1111.4	18.3	-3	-1
HOL_37	355.311	5.11814	0.345829	21.4343	34.48	181.72	1093.7	10.0	1075.6	32.4	1081.6	22.5	2	1
HOL_16	188.826	3.80607	0.257979	15.4015	25.64	130.58	1094.0	10.0	1117.0	24.3	1109.3	17.2	-2	-1
HOL_39	167.7	2.29938	0.15569	9.74681	15.49	82.64	1094.1	13.6	1085.5	23.3	1088.4	17.9	1	0
HOL_21	-140.03	5.25579	0.355457	21.4523	35.41	181.88	1094.4	10.0	1111.2	22.5	1105.6	16.2	-2	-1
HOL_78	10.5601	2.69868	0.182973	12.0164	18.18	101.88	1095.3	11.2	1119.3	25.6	1111.2	18.3	-2	-1
HOL_73	-210.28	2.18605	0.148037	9.51681	14.73	80.69	1096.0	14.0	1114.7	24.2	1108.4	18.4	-2	-1
HOL_33	-20.854	9.17087	0.62197	37.8655	61.79	321.03	1097.0	10.0	1097.0	22.1	1097.0	16.1	0	0
HOL_25	-7.2203	3.29856	0.223469	13.7587	22.22	116.65	1097.1	10.0	1104.4	22.9	1101.9	16.5	-1	0
HOL_20	-94.033	5.99812	0.406313	25.155	40.41	213.27	1097.3	10.0	1122.5	23.2	1113.9	16.5	-2	-1
HOL_32	-9.9518	2.12572	0.143962	9.26912	14.32	78.59	1097.9	14.8	962.4	36.4	1004.6	27.4	12	4
HOL_75	-126.12	2.90847	0.197137	12.6368	19.60	107.14	1098.4	10.6	1129.1	26.4	1118.7	18.6	-3	-1
HOL_26	10.1072	4.652	0.315426	19.4979	31.34	165.31	1099.4	10.0	1125.4	24.4	1116.6	17.2	-2	-1
HOL_58	-16.592	1.54602	0.105546	6.79378	10.42	57.60	1100.0	18.4	1121.5	25.6	1114.2	20.7	-2	-1
HOL_2	152.638	2.91654	0.197783	11.7899	19.65	99.96	1101.2	10.8	1150.5	27.3	1133.6	19.0	-4	-1
HOL_82	194.719	2.73063	0.185539	12.2739	18.40	104.06	1101.4	11.7	1096.9	22.8	1098.4	17.0	0	0
HOL_60	-100.05	3.12238	0.210452	13.7912	21.04	116.92	1101.8	10.0	1110.2	26.2	1107.4	18.5	-1	0
HOL_18	-81.381	1.98678	0.135095	8.19453	13.39	69.47	1104.0	14.4	1137.8	26.5	1126.2	19.7	-3	-1
HOL_15	-68	1.87168	0.127271	7.73363	12.61	65.57	1106.4	15.7	1121.0	24.3	1116.0	19.0	-1	0
HOL_66	183.858	6.20229	0.421854	27.2705	41.79	231.20	1107.0	10.0	1100.8	22.1	1102.9	16.1	1	0
HOL_55	73.7947	2.16118	0.14711	9.47474	14.56	80.33	1107.2	13.7	1110.4	22.1	1109.4	17.2	0	0
HOL_65	-215.7	4.41132	0.300247	19.3639	29.72	164.17	1107.9	10.0	1117.0	21.8	1113.9	15.8	-1	0
HOL_23	-145.58	3.15787	0.213184	12.7899	21.28	108.43	1108.2	10.1	1102.7	24.7	1104.6	17.7	0	0
HOL_49 r	234.953	2.75093	0.187266	12.1231	18.53	102.78	1111.6	11.5	1125.1	22.6	1120.5	16.6	-1	0
HOL_9	208.529	1.69183	0.115289	7.06349	11.40	59.89	1112.4	16.8	1112.9	27.7	1112.7	21.4	0	0
HOL_48	82.1182	6.59191	0.451956	29.4275	44.41	249.49	1113.2	10.0	1120.9	25.0	1118.2	17.7	-1	0
HOL_62	-178.62	2.8018	0.190986	12.3075	18.88	104.35	1115.4	11.0	1120.3	22.5	1118.6	16.5	0	0
HOL_47	136.489	3.41302	0.233122	15.1134	23.00	128.13	1115.4	10.0	1120.9	24.3	1119.0	17.3	0	0
HOL_7	232.995	2.83023	0.193328	12.0493	19.07	102.16	1115.5	10.9	1119.6	29.3	1118.2	20.5	0	0
HOL_54	108.161	4.02342	0.275027	17.7363	27.11	150.37	1116.3	10.0	1113.3	22.5	1114.3	16.2	0	0
HOL_3	166.398	2.34284	0.159366	9.37097	15.79	79.45	1118.5	12.8	1141.0	24.0	1133.3	17.8	-2	-1
HOL_81	65.5582	6.89406	0.472287	28.4304	46.45	241.04	1119.9	10.0	1181.3	34.7	1159.8	23.1	-5	-2
HOL_44	156.967	3.99632	0.273521	17.1167	26.93	145.12	1119.9	10.0	1132.7	27.9	1128.3	19.4	-1	0

HOL_28	-43.581	2.95894	0.203556	12.5058	19.94	106.03	1120.2	12.1	1100.9	24.7	1107.4	18.3	2	1
HOL_45	98.1697	1.99406	0.135785	8.73605	13.44	74.07	1122.7	15.0	1120.2	23.7	1121.1	18.5	0	0
HOL_34	227.159	4.1816	0.28915	17.1662	28.17	145.54	1126.6	11.5	1122.9	24.3	1124.2	17.7	0	0
HOL_43	96.1044	1.33953	0.091229	5.93169	9.03	50.29	1129.2	20.5	1126.0	26.4	1127.1	22.1	0	0
HOL_8	241.716	1.86304	0.12831	7.9203	12.55	67.15	1130.8	15.1	1115.0	27.0	1120.3	20.5	1	0
HOL_46	331.748	3.70573	0.256003	16.3746	24.97	138.83	1132.5	10.0	1117.8	24.3	1122.8	17.3	1	0
HOL_29	-29.295	1.61638	0.11164	6.94346	10.89	58.87	1132.5	17.7	1106.7	23.5	1115.4	19.6	2	1
HOL_6	575.012	2.39975	0.167049	9.91026	16.17	84.02	1143.6	12.3	1113.6	26.2	1123.8	19.2	3	1
HOL_4	31.1353	2.84911	0.197838	11.873	19.20	100.66	1148.5	10.8	1112.3	21.2	1124.6	15.8	3	1
HOL_11	138.849	8.43121	0.589419	36.0383	56.81	305.54	1157.7	9.9	1077.6	29.0	1104.5	20.6	7	2
HOL_17	70.7201	5.8035	0.416413	24.0406	39.10	203.82	1174.0	19.2	1116.9	23.7	1136.4	20.4	5	2
HOL_13	-34.051	12.3097	0.869247	46.9726	82.94	398.24	1178.2	9.9	1207.5	26.0	1197.1	17.9	-2	-1
HOL_52	230.431	4.58427	0.326791	20.2397	30.89	171.60	1184.0	13.1	1127.2	22.3	1146.7	17.3	5	2
HOL_14	-152.27	1.5041	0.106711	5.79128	10.13	49.10	1194.5	17.5	1193.3	94.9	1193.7	61.0	0	0
HOL_77	21.5964	6.18234	0.440526	24.9633	41.65	211.64	1197.5	9.9	1222.4	24.5	1213.4	17.0	-2	-1
HOL_36	190.779	3.61786	0.259584	14.0355	24.38	119.00	1209.3	9.8	1212.9	25.4	1211.6	17.6	0	0
HOL_24	-217.18	1.72693	0.123947	6.524	11.64	55.31	1209.7	16.2	1215.1	24.9	1213.1	19.6	0	0
HOL_41	89.5673	3.1215	0.222421	13.7802	21.03	116.83	1210.1	20.6	1142.6	28.7	1166.2	23.7	6	2
HOL_76	272.478	8.01296	0.585249	35.783	53.99	303.37	1248.0	28.9	1113.0	25.5	1159.7	26.4	11	4
HOL_51a	366.411	1.30325	0.096048	5.49998	8.78	46.63	1251.0	19.1	1086.6	36.0	1142.8	27.8	13	5
HOL_71sl	-88.09	12.3369	0.905122	49.5761	83.12	420.31	1258.4	9.8	1237.5	34.3	1245.2	22.8	2	1
HOL_61	104.144	4.72823	0.350411	17.6037	31.86	149.25	1274.9	9.8	1319.6	28.5	1302.6	18.8	-4	-1
HOL_74	69.8107	4.02634	0.295411	18.0978	27.13	153.44	1281.3	28.8	1090.9	22.7	1156.4	25.4	15	6
HOL_70	22.8731	1.93594	0.145682	7.23657	13.04	61.35	1291.8	13.4	1326.4	27.9	1313.2	19.8	-3	-1
HOL_42 r	175.158	14.4854	1.11498	56.9858	97.60	483.14	1352.6	9.6	1246.6	29.0	1286.0	19.9	8	3
HOL_50	52.4382	5.89917	0.455006	20.9614	39.75	177.71	1353.3	9.6	1361.6	30.2	1358.4	19.7	-1	0
HOL_51b	175.164	7.01048	0.54998	26.1219	47.23	221.47	1358.8	9.6	1299.7	26.5	1322.2	18.1	4	2
HOL_12	366.527	8.98695	0.692638	46.471	60.55	393.99	1359.7	12.8	905.4	51.7	1048.4	40.3	33	14
HOL_63	68.5294	0.32405	0.025078	1.11018	2.18	9.41	1379.3	60.2	1378.4	31.0	1378.7	49.7	0	0
HOL_10	309.249	5.65579	0.46904	17.0839	38.11	144.84	1493.5	9.5	1503.4	32.9	1499.3	20.6	-1	0
HOL_67	614.13	12.5013	1.04569	45.2581	84.23	383.71	1500.4	17.1	1332.0	33.4	1398.1	24.9	11	5
HOL_35	125.808	2.72987	0.230432	7.99839	18.39	67.81	1522.3	9.7	1554.1	30.6	1540.7	19.2	-2	-1
HOL_5	520.671	2.76363	0.234082	11.1778	18.62	94.77	1524.3	62.2	1175.4	44.7	1304.8	55.8	23	10
HOL_64	79.0467	6.14221	0.520383	19.0914	41.38	161.86	1534.4	9.4	1523.4	40.9	1528.0	24.8	1	0

HOL_40	35.9614	4.65887	0.39869	12.391	31.39	105.05	1543.2	9.4	1651.9	38.8	1604.6	22.8	-7	-3
HOL_69	-38.087	8.01157	0.764957	21.3763	53.98	181.23	1752.8	9.1	1766.4	35.6	1760.2	20.8	-1	0
HOL_56	421.076	14.4598	1.43095	41.4953	97.43	351.80	1818.4	9.1	1637.9	36.1	1718.6	22.1	10	5
HOL_27	-183.8	9.55511	0.962832	22.2898	64.38	188.98	1850.0	9.0	1855.8	40.5	1853.1	22.8	0	0
HOL_19	41.3203	4.23695	0.456278	9.07048	28.55	76.90	1970.4	8.9	1997.0	45.4	1984.0	24.4	-1	-1
HOL_53	787.265	2.63769	0.288603	13.1908	17.77	111.83	2005.6	21.1	999.8	69.3	1369.8	57.7	50	27
HOL_22	351.543	0.30558	0.078274	1.00114	2.06	8.49	3387.7	20.8	1358.5	35.1	2358.3	35.3	60	42

ages with discordances above 10% are in grey

Table 3: Zimmermann et al.

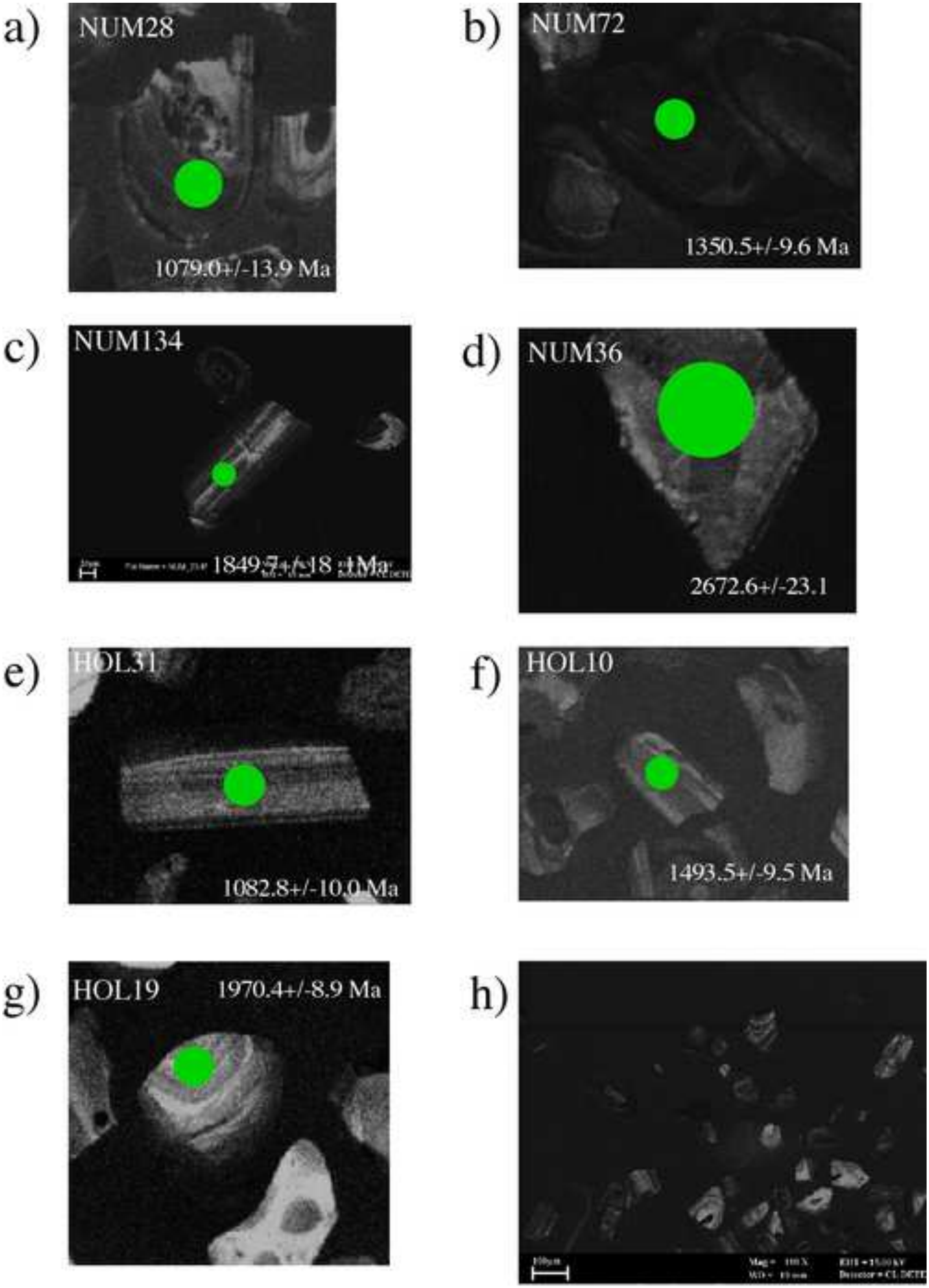

Figure 1 data repository: Zimmermann et al.

Electronic Supplementary Material

a)

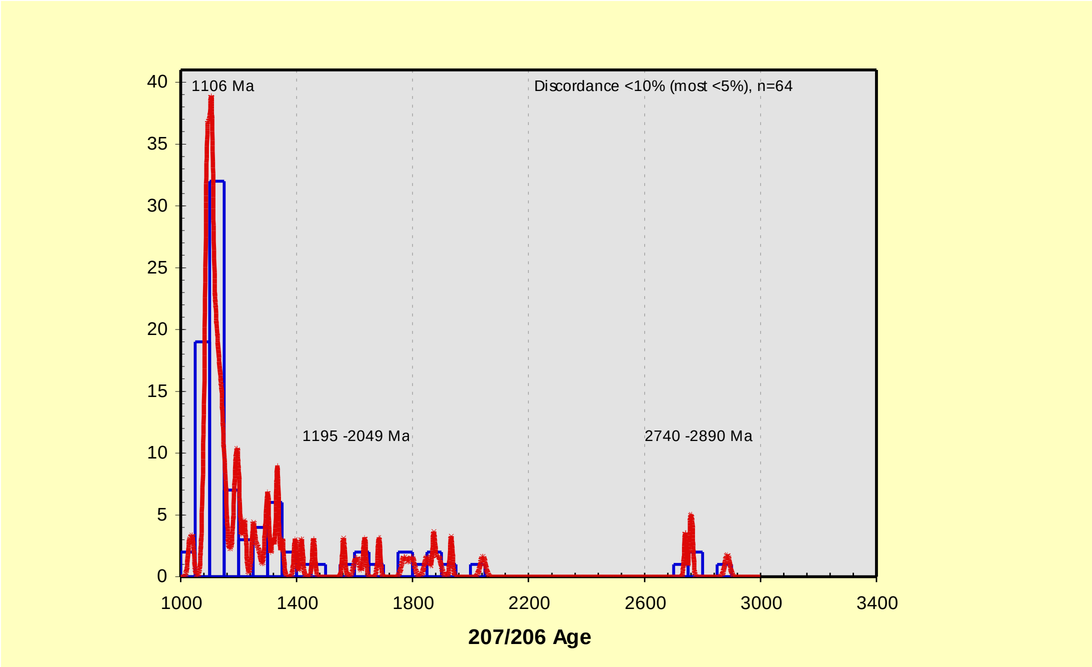

b)

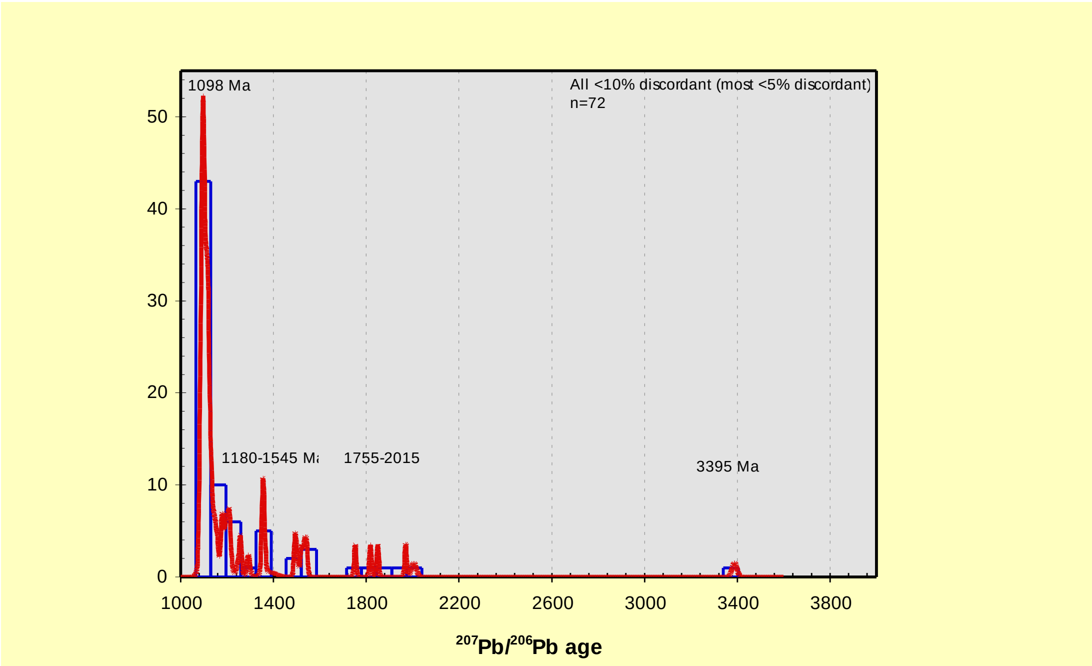

SAMPLE	ROCK TYPE	CIA	SiO_2 %	Al_2O_3 %	Fe_2O_{3t} %	MgO %	CaO %
diamictite							
DM1	coarse sand to silt	59	71.4	13.80	3.50	1.01	0.40
DM2	coarse sand to silt	59	74.9	12.54	2.51	0.80	0.34
DM3	coarse sand to silt	60	72.0	14.40	2.99	0.68	0.54
DM4	coarse sand to silt	63	70.1	16.53	3.02	0.61	0.38
DM5	coarse sand to silt	56	76.5	12.31	1.85	0.71	0.54
DM6	coarse sand to silt	63	69.1	14.97	3.96	0.77	0.28
DM7	coarse sand to silt	60	70.8	13.90	3.61	0.91	0.24
DM8	coarse sand to silt	60	70.1	14.31	3.62	1.06	0.30
DM9	coarse sand to silt	60	69.8	14.12	3.76	1.02	0.31
DM10	coarse sand to silt	60	70.3	14.35	3.59	1.11	0.35
DM11	coarse sand to silt	60	69.3	13.84	4.05	1.23	0.39
DM12	coarse sand to silt	59	67.6	14.93	3.74	0.70	0.42
DM13	coarse sand to silt	60	69.5	14.20	4.56	0.96	0.40
DM14	coarse sand to silt	62	72.7	14.30	3.60	0.96	0.31
DM15	coarse sand to silt	61	71.8	13.90	3.75	0.95	0.36
DM16	coarse sand to silt	61	70.4	14.20	3.77	0.89	0.34
DM17	coarse sand to silt	62	69.1	15.54	3.44	0.80	0.36
DM18	coarse sand to silt	59	70.9	14.08	3.57	1.16	0.44
DMP1	metamorphic	50	66.7	14.36	3.67	1.20	3.14
DMP2	igneous	55	69.9	13.90	2.58	0.74	0.34
DMP3	igneous	60	68.0	13.03	5.70	1.98	0.58
DMP4	igneous	57	69.5	14.60	3.23	0.85	0.40
carbonate and Mn-rich rocks							
C1	carbonate	3	5.7	1.74	0.70	17.53	29.85
C2	carbonate	1	5.1	1.04	0.63	20.21	33.41
C3	carbonate	1	4.8	0.89	0.67	10.75	41.48
C4	carbonate	1	4.9	0.97	0.58	16.03	35.10
C5	carbonate	2	5.5	0.95	0.53	20.98	29.64
C6	carbonate	1	4.9	0.87	0.53	10.62	36.56
CM7	Mn-rich	80	82.5	3.99	0.56	0.21	0.26
CM8	Mn-rich	33	78.3	0.88	0.54	0.38	0.75
CM9	Mn-rich	80	74.9	10.94	0.87	0.68	0.89
CM10	Mn-rich	77	59.1	2.32	0.34	0.05	0.21
CM11	Mn-rich	51	48.9	1.21	0.84	0.39	0.41
CM12	Mn-rich	53	57.9	1.39	0.92	0.25	0.33
CM13	Mn-rich	77	35.1	3.14	0.32	0.10	0.50
HOLGAT FORMATION	**Sanddrif Mb.**						
H1	arenite	61	61.4	15.90	6.34	4.64	2.36
H2	marl	16	22.9	12.25	2.39	1.20	33.90
H3	arenite	27	54.9	11.81	2.31	1.63	15.61
H4	arenite	20	42.8	11.82	2.05	1.21	24.45
H5	wacke	33	62.6	8.96	2.18	4.21	7.30
H6	arenite	19	63.1	6.21	1.37	2.10	12.23

H7	marls	21	41.5	12.01	2.31	1.39	23.03
H8	wacke	65	59.3	16.19	6.50	4.40	1.51
H9	shale	35	59.9	10.78	4.27	3.33	8.91
H10	shale	46	52.4	15.00	7.04	3.09	6.30
H11	shale	60	51.0	18.92	6.15	6.27	2.65
H12	wacke	17	52.9	7.09	1.86	1.50	17.42
H13	wacke	29	47.7	13.28	3.87	1.52	15.53
H14	wacke	27	45.1	12.44	2.11	3.63	16.18
H15	wacke	39	64.3	8.69	2.71	5.38	5.29
H16	arenite	25	49.2	11.91	2.42	1.56	18.35
H17	arenite	35	53.4	13.01	2.75	2.26	11.07
H18	arenite	23	49.3	11.61	1.76	1.27	19.56
H19	arenite	16	65.0	4.50	1.85	2.66	11.93
H20	marls	29	49.8	13.12	4.09	1.73	14.94
H21	wacke	23	61.5	7.23	1.94	3.15	11.38
H22	wacke	19	55.2	6.89	2.54	3.61	13.92
H23	wacke	9	48.6	4.34	1.15	0.98	23.17
H24	marl	24	41.8	12.67	2.91	1.80	19.64
H25	wacke	27	49.5	12.67	2.27	1.85	16.96
H26	wacke	60	68.1	12.64	1.88	1.79	2.09
H27	wacke	37	54.3	13.86	3.22	2.54	9.60
H28	wacke	44	58.6	13.76	3.28	6.72	6.60
H29	marl	17	23.7	11.80	2.28	1.42	29.57
H30	marl	26	38.5	12.10	2.56	8.03	17.66
H31	wacke	31	47.7	12.53	2.39	4.03	13.25
H32	wacke	30	46.9	12.51	2.44	4.11	13.74
H33	wacke	32	59.5	8.30	2.28	6.01	7.22
H34	arenite	56	76.5	12.31	1.85	0.71	0.54
H35	wacke	23	59.4	5.95	1.44	6.86	9.19
H36	wacke	37	46.2	13.86	4.50	3.67	10.01
Nama Group	**Kanies Mb.**						
N1	quartzarenite	52	95.1	2.14	0.47	0.43	0.33
N2	quartzarenite	83	86.0	10.25	1.20	0.94	0.12
N3	quartzarenite	82	86.7	10.25	0.98	1.05	0.05
N4	quartzarenite	53	92.2	2.29	0.66	0.88	0.37

Table 1 supplementary data: Zimmermann et al.

Na_2O %	K_2O %	TiO_2 %	P_2O_5 %	MnO %	LOI %	sum %	Ba ppm	Rb ppm	Sr ppm	Cs ppm	V ppm	Ni ppm
2.23	4.88	0.42	0.140	0.040	1.6	99.4	713	233	88	4	44	13
1.85	4.53	0.36	0.150	0.020	1.5	99.6	632	199	86	3	37	9
2.05	4.72	0.31	0.110	0.130	1.8	99.7	671	201	106	3	35	13
2.21	4.91	0.35	0.153	0.084	1.4	99.8	711	211	102	4	36	11
2.42	4.39	0.27	0.110	0.030	1.6	100.7	166	37	433	2	22	6
1.53	5.49	0.47	0.459	0.040	2.3	99.4	677	261	81	5	165	60
1.76	5.36	0.44	0.160	0.040	2.0	99.2	677	255	96	4	49	13
1.92	5.30	0.45	0.170	0.030	1.8	99.1	793	254	82	3	45	13
2.04	5.22	0.44	0.180	0.040	2.5	99.5	768	251	84	5	49	13
2.04	5.10	0.45	0.160	0.040	1.9	99.4	744	248	79	4	46	13
1.91	5.05	0.44	0.160	0.030	2.3	98.7	284	32	21	4	12	3
2.42	5.25	0.42	0.209	0.059	2.6	98.3	667	234	93	4	49	14
1.83	5.25	0.43	0.140	0.050	1.9	99.3	678	218	88	5	43	11
1.75	4.83	0.44	0.170	0.060	1.9	101.0	703	221	76	3	39	10
1.92	4.85	0.42	0.150	0.040	1.8	100.0	650	218	78	4	40	10
1.87	4.99	0.42	0.170	0.060	2.1	99.2	701	230	82	4	34	10
1.71	5.59	0.45	0.282	0.030	1.9	99.2	835	262	87		59	13
1.89	5.30	0.45	0.180	0.040	2.1	100.1	701	258	94		49	13
3.17	3.07	0.45	0.129	0.061	4.6	100.5	706	114	92		54	11
2.30	6.38	0.27	0.120	0.030	1.9	98.5	672	235	171		24	8
1.71	4.32	0.99	0.100	0.100	2.3	98.8	531	227	76		80	16
2.40	6.02	0.34	0.150	0.060	1.5	99.1	651	238	166		23	8
0.04	0.60	0.07	0.170	1.210	42.2	99.8	119	27	204	0.7	14	56
0.21	0.44	0.08	0.224	1.706	39.2	102.3	141	21	149		11	56
0.14	0.34	0.08	0.062	1.207	41.2	101.6	104	18	150		9	39
0.16	0.53	0.08	0.102	2.988	39.2	100.6	194	32	163		10	106
0.04	0.23	0.06	0.280	1.590	41.2	101.1	129	18	158		10	43
0.16	0.48	0.06	0.077	1.949	44.4	100.5	72	30	171		11	51
0.07	0.38	0.03	0.240	9.800	3.0	101.1	3234	19	198	bdl	19	185
0.01	0.39	0.04	0.390	12.950	4.0	98.7	3878	17	423	bdl	24	454
0.18	0.73	0.08	0.522	6.156	3.1	99.1	1790	30	187	bdl	20	245
0.02	0.26	0.02	0.280	30.210	6.4	99.2	3207	11	317	bdl	28	532
0.01	0.36	0.06	0.310	37.770	8.0	98.3	1554	23	218	bdl	35	367
-0.01	0.59	0.09	0.290	30.650	7.7	100.1	1046	26	228	bdl	28	479
0.02	0.02	0.01	0.360	50.840	9.6	100.0	1233	10	350	bdl	38	672
0.56	4.39	0.74	0.160	0.030	2.3	98.8	792	185	58	7	82	25
0.91	1.83	0.55	0.084	0.159	22.0	98.2	310	75	515	2	43	9
1.57	0.94	0.54	0.080	0.096	12.2	101.7	167	36	167	1	34	9
1.53	1.03	0.30	0.131	0.121	15.9	101.3	154	40	355		32	8
1.98	1.91	0.57	0.150	0.090	11.0	100.9	355	88	143	4	49	9
2.11	0.82	0.35	0.090	0.070	12.4	100.8	120	34	185	1	32	7

1.60	1.19	0.32	0.069	0.116	15.8	99.4	172	47	349	1	32	9
0.58	4.64	0.82	0.170	0.030	6.6	100.8	818	196	50	7	86	26
0.25	2.88	0.41	0.090	0.050	10.0	100.9	484	128	187	5	53	18
0.98	3.98	0.71	0.080	0.070	9.9	99.6	626	156	112	5	70	27
0.14	6.96	0.76	0.200	0.020	7.4	100.5	930	230	40	14	98	23
1.06	2.03	0.41	0.120	0.060	15.6	100.0	507	89	306		38	8
1.02	3.05	0.52	0.092	0.064	11.6	98.2	488	111	200	6	53	14
1.02	2.40	0.43	0.094	0.079	17.6	101.1	434	65	134	2	35	9
0.15	3.56	0.46	0.140	0.030	9.5	100.3	723	151	51	8	53	13
1.09	1.23	0.47	0.074	0.119	12.8	99.2	195	47	189	2	36	10
1.20	2.32	0.68	0.157	0.106	11.3	98.2	341	94	110	4	52	11
1.16	1.04	0.37	0.075	0.122	13.2	99.5	155	41	147	1	32	6
0.92	0.66	0.48	0.060	0.080	12.6	100.7	151	36	163	1	31	9
1.10	2.62	0.47	0.087	0.063	11.2	99.2	270	80	194	4	47	15
0.77	2.28	0.33	0.100	0.050	13.0	101.7	726	91	86	2	34	9
0.50	2.33	0.38	0.100	0.050	16.4	101.9	773	95	226	3	41	11
1.22	0.87	0.21	0.070	0.060	20.6	101.3	166	38	442	bdl	27	7
0.69	2.85	0.38	0.085	0.069	15.6	98.5	685	90	235	2	41	11
1.04	0.92	0.42	0.066	0.115	13.0	98.8	138	36	164	3	31	9
0.95	2.88	0.20	0.102	0.027	7.7	98.3	434	79	41	8	22	6
0.38	4.87	0.50	0.107	0.036	9.2	98.6	760	149	43	9	55	12
0.33	4.74	0.50	0.103	0.040	6.0	100.7	734	152	49	1	56	12
0.94	1.59	0.32	0.082	0.080	28.9	100.7	225	53	272	2	27	8
0.55	2.12	0.26	0.072	0.074	16.9	98.8	424	62	116		27	9
0.20	3.05	0.34	0.090	0.104	15.5	99.1	490	74	63	4	36	8
0.18	3.07	0.35	0.086	0.106	15.3	98.8	646	92	62	4	33	9
0.37	3.28	0.46	0.140	0.060	12.5	100.1	820	97	95	4	43	10
2.42	4.39	0.27	0.110	0.030	12.2	111.3	770	86	91	5	44	10
0.64	2.23	0.30	0.090	0.060	14.8	101.0	655	76	114		31	8
0.32	4.73	0.68	0.111	0.059	15.0	99.2	736	167	87	9	66	17
0.42	0.60	0.03	0.020	0.010	0.7	100.3	118	21	22	1	272	9
0.60	0.85	0.04	0.037	0.015	0.9	101.0	163	20	17	1	260	12
0.67	1.02	0.03	0.025	0.012	0.8	101.5	172	25	17	1	212	9
0.40	0.64	0.03	0.020	0.010	0.9	98.4	124	20	30	1	284	8

Co	Cu	Nb	Ta	Y	Zr	Hf	Sc	Th	U	Pb	Ga	Zn	Mo
ppm	ppm	ppm	ppm	ppm	ppm	ppm	ppm	ppm	ppm	ppm	ppm	ppm	ppm
11	30	10.6	1.4	30.9	181	6	8.5	27.6	2.2	34.8	18.6	67	bdl
5	27	8.8	1.7	25.3	181	6	6.7	24.0	1.3	28.2	15.6	43	bdl
12	81	8	0.7	16.7	138	4	5.7	19.0	1.1	35.9	16.1	50	bdl
7	17	9.8	1.1	23.2	169	6	6.8	27.7	1.7	31.5	15.8	53	bdl
4	11.1.	6.3	1.1	33.9	173	3	6.0	17.0	1.3	26.8	7	14	bdl
13	9	69.3	11.2	17.6	181	6	8.7	27.3	2.4	39.5	19.6	68	bdl
10	16	11.8	0.6	21.3	184	6	8.2	27.1	2.5	26.3	18.8	52	bdl
11	23	10.9	2.3	25.8	183	5	8.0	26.2	2.6	37	19.2	60	bdl
11	20	10.3	1.2	22	183	6	8.2	28.2	2.4	25.2	18.8	56	bdl
10	18	11.4	1.1	33.8	185	5	8.6	27.1	2.0	24.3	19.7	62	bdl
1	6	5	1.3	5.7	42	6	8.5	27.5	1.2	7.2	0.9	7	bdl
12	36	10.8	1.7	23.6	182	6	8.3	28.8	2.6	29.8	17.7	56	bdl
9	41	11.4	2.1	25.5	177	6	8.7	27.1	2.6	39.2	18.7	63	bdl
10	24	11.6	0.6	27	181	6	8.8	28.6	2.0	34.5	19.7	65	bdl
9	12	11.6	2.3	29.2	177	6	9.2	27.4	1.6	29.2	19.8	67	bdl
9	60	11.7	1.0	28.6	177	6	8.6	29.1	2.1	36.6	19.9	61	bdl
11	25	10.5		25.5	191			29.3		38.6	20.4	58	
9	17	11.1		27.1	185			28.1		24	18.7	57	
2	13	13.9		27.5	196			22.9		12.4	14.5	49	
5	22	7.4		180	254			93		39.2	20.8	49	
7	34	16.5		42	229			8.7		25.3	17.7	130	
2	68	7.9		35.2	251			99		44.3	22.5	69	
94	7	1.5	0.1	4.4	19	1	2	1.5	2.4	4.3	2.9	298	2.2
162	11	4.1		5	35			4.9		39.9	2.8	277	
106	10	4.3		7.7	45			1.8		28.9	3.2	171	
322	10	3.8		6.2	41			2.7		30	3.8	372	
107	11	3.7		8.7	56			2.9		24.3	3.7	401	
142	20	3.5		6.5	34			2.3		25.1	3	319	
571	18	3.9	0.2	9.5	38	bdl	1.7	0.9	8.7	26.3	1.3	502	bdl
1389	18	2.7	1.1	12.6	54	bdl	1.7	1.4	8.7	29.2	1.1	1055	bdl
751	16	5.1	0.4	8.2	43	bdl	2.0	2.2	5.2	21.6	2.6	415	bdl
1573	34	3.3	0.9	7.4	45	bdl	1.6	0.2	30.0	34.6	1	1822	bdl
974	61	4.5	0.3	8.4	53	bdl	2.9	0.9	66.0	78.3	4	2167	bdl
1379	34	6.7	0.4	10.2	55	bdl	2.7	1.8	28.0	40.9	2.3	1690	bdl
1840	84	4	0.3	14	60	bdl	2.5	0.2	71.8	64.1	1.5	3926	bdl
21	29	17	1.1	33.9	219	7	14.9	20.0	2.7	11.9	22.5	125	bdl
7	97	9.7	0.5	44.5	246	5	5.3	10.0	2.5	46.4	8.9	26	bdl
9	107	11.3	1.1	39.5	320	10	6.1	15.0	2.8	23.1	4.7	37	bdl
6	40	7.1		29.4	210			13.2		30	6.2	31	
6	73	12.8	0.5	38.6	291	8	7.1	16.0	2.0	17.9	10.2	24	bdl
5	95	8.5	0.6	32.2	229	7	4.3	11.0	1.9	20.3	5.6	14	bdl

9	36	7.5	0.7	30.1	212	5	4.6	9.0	1.5	26.7	7.6	37	bdl
22	27	18	0.9	35.6	241	7	16.2	22.9	1.9	11.7	24.8	138	bdl
16	41	10.7	1.2	23.3	82	2	10.0	10.0	0.8	20.7	17	101	bdl
22	25	16.8	1.2	32.6	194	5	13.3	17.0	2.2	16.4	20.9	125	bdl
12	48	16.1	1.0	30.8	137	4	18.7	20.0	4.3	8.2	29.6	131	bdl
6	10	9.1		34.4	264			16.0		24.5	8.6	23	
11	21	11.8	1.3	30.4	194	5	8.5	11.0	1.7	19	13.3	67	bdl
9	5	10.2	0.6	28.2	250	7	4.7	12.0	2.1	23.5	7.5	31	bdl
12	12	11.1	0.8	24.3	178	5	7.3	11.0	1.8	10.9	13	65	bdl
8	58	9.7	0.7	39	322	9	5.5	16.0	1.9	20.5	6	39	bdl
10	63	13.4	1.0	40.2	368	11	7.4	20.8	3.0	15	10.2	30	bdl
3	77	8	0.7	35.3	251	8	4.4	12.0	1.3	20.7	4	19	bdl
9	68	10.8	0.5	39.1	250	7	6.2	11.0	2.0	18.5	4	41	bdl
9	51	11.3	0.5	29.4	195	5	7.7	11.0	2.1	29.6	11.9	77	bdl
7	7	9.5	0.4	22.6	164	5	4.2	8.6	1.7	10.2	9	25	bdl
9	8	9.7	0.4	26.5	179	5	5.9	9.1	2.1	10.9	11	32	bdl
7	13	6.5	0.4	34.3	179	4	3.1	6.6	0.9	27	6.4	14	bdl
8	7	9.1	0.7	28	188	5	5.5	9.0	1.6	11.5	10.7	32	bdl
8	68	10.5	0.5	39.5	252	4	3.2	4.2	1.3	18.8	4.1	41	bdl
3	9	6.3	0.8	15.8	146	6	7.2	12.0	1.8	13.9	6.2	22	bdl
9	14	11.7	0.5	23	188	5	7.3	11.0	1.7	10.7	12.8	60	bdl
10	13	11.5	0.7	24.3	181	5	3.3	8.4	0.9	10.4	13.1	64	bdl
6	17	7.6	0.4	13.3	142	4	3.3	6.5	2.1	49	6.7	30	bdl
6	47	7.3		14.2	151			7.8		34.9	6.7	35	
4	21	8.5	0.5	21.8	154	4	4.6	7.6	1.2	26.6	7.7	36	bdl
6	24	9.8	0.7	21.4	159	5	4.5	7.6	1.3	27.8	7.2	34	bdl
6	7	10.7	0.7	22.3	251	8	5.3	12.0	2.6	10.6	9.4	35	bdl
6	7	11	0.7	22.5	257	8	5.6	13.0	2.1	22.7	9.4	37	bdl
7	11	8.3		17.5	197			9.8		11.1	6.2	24	
14	16	15.1	1.3	31.1	201	6	10.0	13.0	2.4	10	14.8	78	bdl

3	1	6.2	4.8	4.5	36	1	0.7	1.9	0.3	10.5	0.6	5	bdl
5	2	7.1	4.9	7.3	39	1	2.1	2.4	0.9	35.8	1.4	14	bdl
4	1	5.4	4.8	6	35	1	0.9	1.9	0.5	11.2	1.4	12	bdl
3	1	6.8	4.6	5.3	35	1	1.0	1.8	0.4	14.6	0.8	8	bdl

La	**Ce**	**Pr**	**Nd**	**Sm**	**Eu**	**Gd**	**Tb**	**Dy**	**Ho**	**Er**	**Tm**	**Yb**	**Lu**	**Eu***	**Ce***
ppm	ppm	ppm	ppm	ppm	ppm	ppm	ppm	ppm	ppm	ppm	ppm	ppm	ppm		
70	120		41	9.2	1.6		1.3					2.6	0.42	0.54	0.85
38	97		21	5.7	0.9		0.7					2.1	0.31	0.50	1.28
36	83		20	5.1	0.7		0.3					1.4	0.24	0.67	1.16
50	110		29	6.5	1.1		0.9					2.2	0.30	0.53	1.10
33	73		22	4.8	0.9		0.4					1.5	0.24	0.93	1.08
20	76		9	4.0	0.7		0.6					1.9	0.29	0.54	1.95
42	82		25	5.7	1.0		0.8					2.1	0.29	0.55	1.01
46	100		29	6.7	1.6		0.7					2.3	0.33	0.79	1.07
30	100		17	4.8	1.0		0.7					2.0	0.29	0.64	1.67
45	110		28	6.7	1.1		0.7					2.3	0.35	0.76	1.21
52	110		32	7.4	1.2		1.0					2.4	0.35	0.51	1.05
31	100		20	5.1	0.9		0.6					2.2	0.34	0.87	1.59
49	120		25	6.9	1.7		1.1					2.4	0.35	0.74	1.24
53	120		31	7.8	1.3		0.9					2.4	0.38	0.54	1.12
51	110		31	7.4	1.2		0.7					2.5	0.37	0.54	1.08
42	110		27	7.0	1.4		0.7					2.6	0.38	0.66	1.29
5	10	1	5	0.9	0.18	0.82	0.15	0.82	0.13	0.42	0.06	0.4	0.06	0.60	0.98
6	6		7	1.4	0.5		0.6					0.7	bdl	0.77	0.43
6	8		7	1.2	0.4		0.5					0.6	bdl	7.23	0.57
8	13		6	1.4	0.5		0.5					0.5	bdl	0.83	0.82
5	5		5	0.6	0.5		0.5					0.6	bdl	2.08	0.44
9	10		10	1.2	0.6		0.6					0.7	bdl	10.85	0.48
13	16		5	1.7	0.6		0.6					0.7	bdl	3.31	0.64
10	5		3	1.4	0.9		1.4					0.8	bdl	0.86	0.27
56	120		41	8.3	1.6		1.1					3.1	0.45	0.61	1.04
27	51		23	5.6	0.9		1.0					2.7	0.40	0.47	0.89
30	70		28	7.9	1.3		1.1					3.2	0.48	0.51	1.08
34	79		33	8.9	1.1		1.2					3.0	0.45	0.39	1.07
26	62		30	7.5	1.0		0.8					2.3	0.32	0.44	1.06

25	57	25	5.9	0.9	0.6	2.0	0.28	0.50	1.04
63	140	43	10.0	2.0	1.4	3.4	0.48	0.62	1.09
29	49	19	4.3	0.9	0.4	1.8	0.25	1.07	0.83
50	94	38	7.6	1.3	0.7	2.8	0.43	0.57	0.90
68	130	39	8.7	1.6	0.7	2.5	0.30	0.63	0.96
31	66	26	6.4	1.0	0.7	2.5	0.38	0.51	1.00
28	62	25	6.3	1.0	0.7	2.0	0.31	0.52	1.03
28	61	21	5.5	0.8	0.6	2.0	0.30	0.47	1.05
36	76	28	7.4	1.2	0.9	3.2	0.48	0.52	1.01
52	110	43	10.0	1.6	1.3	3.5	0.51	0.51	1.01
31	66	28	6.6	1.3	0.9	2.7	0.39	0.62	0.99
32	71	26	6.8	1.1	1.0	3.1	0.45	0.50	1.05
28	61	29	5.8	0.9	0.7	2.4	0.38	0.50	0.99
21	49	22	4.9	0.8	0.4	1.6	0.25	0.81	1.05
26	58	24	5.0	1.1	0.8	1.9	0.28	0.66	1.03
21	49	25	5.5	0.9	0.8	1.9	0.27	0.50	1.03
25	55	24	5.0	1.0	0.7	2.1	0.29	0.62	1.01
14	28	13	2.7	0.5	0.7	1.4	0.18	0.49	0.93
28	64	23	5.6	0.9	0.9	1.9	0.29	0.48	1.08
29	63	25	5.6	0.9	0.9	2.0	0.30	0.48	1.02
21	47	22	5.2	0.7	0.7	2.1	0.30	0.42	1.01
21	48	26	4.6	0.8	0.8	1.6	0.22	0.51	1.00
20	46	16	4.5	0.8	0.4	1.5	0.23	0.90	1.09
19	45	18	4.4	0.8	0.6	1.6	0.21	0.57	1.09
28	65	26	5.9	0.8	0.6	2.1	0.31	0.64	1.07
30	72	27	6.2	1.0	1.0	2.2	0.30	0.49	1.12
31	65	25	6.5	1.4	0.6	2.6	0.39	0.72	1.00
5	11	7	1.0	0.3	0.1	0.4	0.05	0.75	0.88
6	13	7	1.1	0.3	0.1	0.8	0.10	0.70	0.92
6	12	7	1.1	0.2	0.1	0.5	0.08	0.53	0.86
5	10	6	0.9	0.2	0.1	0.5	0.07	0.61	0.89

La_N/Yb	K/Cs	U/Th	Nb/Y	Zr/Ti	Th/Sc	Zr/Sc	La/Sc	Ti/Zr
18.25	10127	0.08	0.34	0.07	3.25	21.33	8.26	13.89
12.23	12535	0.05	0.35	0.08	3.58	27.06	5.67	11.90
17.38	13046	0.06	0.48	0.07	3.33	24.25	6.32	13.36
15.36	10194	0.06	0.42	0.08	4.07	24.81	7.35	12.40
14.87	18221	0.08	0.19	0.11	2.83	28.90	5.50	9.33
7.11	9116	0.09	3.94	0.06	3.14	20.83	2.30	15.45
13.51	11123	0.09	0.55	0.07	3.30	22.49	5.12	14.30
13.51	14665	0.10	0.42	0.07	3.28	22.88	5.75	14.74
10.14	8666	0.09	0.47	0.07	3.44	22.32	3.66	14.41
13.22	10584	0.07	0.34	0.07	3.15	21.47	5.23	14.61
14.56	10480	0.04	0.88	0.02	3.24	4.92	6.08	63.11
9.52	10891	0.09	0.46	0.07	3.47	21.96	3.73	13.81
13.80	8716	0.10	0.45	0.07	3.11	20.39	5.63	14.53
14.98	13365	0.07	0.43	0.07	3.25	20.52	6.05	14.61
13.65	10065	0.06	0.40	0.07	2.98	19.23	5.49	14.23
10.92	10355	0.07	0.41	0.07	3.38	20.58	4.88	14.23
			0.41	0.07				
			0.41	0.07				
7.94								
5.99		9.67	0.41	0.21	0.53	22.35	3.65	4.73
7.10		6.21	0.21	0.22	0.82	31.65	3.71	4.46
10.27		2.36	0.62	0.09	1.10	21.45	3.80	11.60
5.86		150.00	0.45	0.37	0.13	27.81	3.25	2.69
9.07		73.33	0.54	0.15	0.31	18.10	3.24	6.85
12.55		15.56	0.66	0.10	0.67	20.30	4.81	9.85
8.45		359.00	0.29	1.01	0.08	24.16	4.00	0.99
12.10	5206	0.14	0.50	0.05	1.34	14.70	3.72	20.25
6.76	7591	0.25	0.22	0.07	1.89	46.42	5.09	13.35
6.34	7761	0.19	0.29	0.10	2.46	52.39	4.92	10.09
			0.24	0.12				8.53
7.66	3964	0.13	0.33	0.09	2.25	40.99	4.79	11.74
7.64	6807	0.17	0.26	0.11	2.56	53.16	6.05	9.18

8.45	9878	0.17	0.25	0.11	1.96	46.17	5.43	9.06
12.48	5502	0.08	0.51	0.05	1.41	14.89	3.88	20.38
10.89	4781	0.08	0.46	0.03	1.00	8.17	2.90	30.09
12.16	6606	0.13	0.52	0.05	1.28	14.58	3.79	21.83
18.33	4127	0.22	0.52	0.03	1.07	7.35	3.63	33.16
			0.26	0.11				9.32
8.38	4216	0.15	0.39	0.06	1.29	22.79	3.65	15.97
9.46	9965	0.18	0.36	0.10	2.55	53.15	5.96	10.34
9.46	3694	0.16	0.46	0.06	1.51	24.40	3.84	15.48
7.60	5084	0.12	0.25	0.11	2.91	58.58	6.55	8.82
9.98	4817	0.14	0.33	0.09	2.81	49.78	6.99	11.00
7.76	8633	0.11	0.23	0.11	2.73	57.14	7.05	8.89
6.98	5479	0.18	0.28	0.09	1.77	40.39	5.16	11.49
7.88	5443	0.19	0.38	0.07	1.43	25.31	3.64	14.55
8.87	9463	0.20	0.42	0.08	2.05	39.07	5.00	12.06
9.25	6447	0.23	0.37	0.08	1.54	30.32	4.41	12.73
7.47		0.14	0.19	0.14	2.13	57.74	6.77	7.03
8.04	11816	0.18	0.33	0.08	1.64	34.11	4.55	12.24
6.76	2551	0.31	0.27	0.10	1.31	78.63	4.38	10.10
9.96	2993	0.15	0.40	0.12	1.67	20.26	3.89	8.14
9.80	4492	0.15	0.51	0.06	1.51	25.75	3.97	15.98
6.76	39355	0.11	0.47	0.06	2.55	54.88	6.36	16.68
8.87	6591	0.32	0.57	0.07	1.97	43.03	6.36	13.59
			0.51	0.10				10.16
9.01	6325	0.16	0.39	0.08	1.65	33.50	4.35	13.19
8.02	6377	0.17	0.46	0.08	1.69	35.40	4.22	13.10
9.01	6807	0.22	0.48	0.09	2.26	47.38	5.28	10.98
9.21	7288	0.16	0.49	0.16	2.32	45.91	5.36	6.30
			0.47	0.11				9.14
8.06	4359	0.18	0.49	0.05	1.30	20.05	3.10	20.33
9.12	4981	0.16	1.38	0.20	2.71	52.00	7.71	4.94
5.32	7089	0.38	0.97	0.15	1.14	18.71	3.00	6.56
8.38	8492	0.26	0.90	0.19	2.11	39.33	6.89	5.25
6.62	5313	0.22	1.28	0.19	1.80	34.90	4.90	5.15

SAMPLE	ROCK TYPE	CIA	SiO_2 %	Al_2O_3 %	Fe_2O_{3t} %	MgO %	CaO %	Na_2O %
diamictite								
DM1	coarse sand to silt	59	71.4	13.80	3.50	1.01	0.40	2.23
DM2	coarse sand to silt	59	74.9	12.54	2.51	0.80	0.34	1.85
DM3	coarse sand to silt	60	72.0	14.40	2.99	0.68	0.54	2.05
DM4	coarse sand to silt	63	70.1	16.53	3.02	0.61	0.38	2.21
DM5	coarse sand to silt	56	76.5	12.31	1.85	0.71	0.54	2.42
DM6	coarse sand to silt	63	69.1	14.97	3.96	0.77	0.28	1.53
DM7	coarse sand to silt	60	70.8	13.90	3.61	0.91	0.24	1.76
DM8	coarse sand to silt	60	70.1	14.31	3.62	1.06	0.30	1.92
DM9	coarse sand to silt	60	69.8	14.12	3.76	1.02	0.31	2.04
DM10	coarse sand to silt	60	70.3	14.35	3.59	1.11	0.35	2.04
DM11	coarse sand to silt	60	69.3	13.84	4.05	1.23	0.39	1.91
DM12	coarse sand to silt	59	67.6	14.93	3.74	0.70	0.42	2.42
DM13	coarse sand to silt	60	69.5	14.20	4.56	0.96	0.40	1.83
DM14	coarse sand to silt	62	72.7	14.30	3.60	0.96	0.31	1.75
DM15	coarse sand to silt	61	71.8	13.90	3.75	0.95	0.36	1.92
DM16	coarse sand to silt	61	70.4	14.20	3.77	0.89	0.34	1.87
DM17	coarse sand to silt	62	69.1	15.54	3.44	0.80	0.36	1.71
DM18	coarse sand to silt	59	70.9	14.08	3.57	1.16	0.44	1.89
DMP1	metamorphic	50	66.7	14.36	3.67	1.20	3.14	3.17
DMP2	igneous	55	69.9	13.90	2.58	0.74	0.34	2.30
DMP3	igneous	60	68.0	13.03	5.70	1.98	0.58	1.71
DMP4	igneous	57	69.5	14.60	3.23	0.85	0.40	2.40
carbonate and Mn-rich rocks								
C1	carbonate	3	5.7	1.74	0.70	17.53	29.85	0.04
C2	carbonate	1	5.1	1.04	0.63	20.21	33.41	0.21
C3	carbonate	1	4.8	0.89	0.67	10.75	41.48	0.14
C4	carbonate	1	4.9	0.97	0.58	16.03	35.10	0.16
C5	carbonate	2	5.5	0.95	0.53	20.98	29.64	0.04
C6	carbonate	1	4.9	0.87	0.53	10.62	36.56	0.16
CM7	Mn-rich	80	82.5	3.99	0.56	0.21	0.26	0.07
CM8	Mn-rich	33	78.3	0.88	0.54	0.38	0.75	0.01
CM9	Mn-rich	80	74.9	10.94	0.87	0.68	0.89	0.18
CM10	Mn-rich	77	59.1	2.32	0.34	0.05	0.21	0.02
CM11	Mn-rich	51	48.9	1.21	0.84	0.39	0.41	0.01
CM12	Mn-rich	53	57.9	1.39	0.92	0.25	0.33	-0.01

CM13	Mn-rich	77	35.1	3.14	0.32	0.10	0.50	0.02
HOLGAT FORMATIC	**Sanddrif Mb.**							
H1	arenite	61	61.4	15.90	6.34	4.64	2.36	0.56
H2	marl	16	22.9	12.25	2.39	1.20	33.90	0.91
H3	arenite	27	54.9	11.81	2.31	1.63	15.61	1.57
H4	arenite	20	42.8	11.82	2.05	1.21	24.45	1.53
H5	wacke	33	62.6	8.96	2.18	4.21	7.30	1.98
H6	arenite	19	63.1	6.21	1.37	2.10	12.23	2.11
H7	marls	21	41.5	12.01	2.31	1.39	23.03	1.60
H8	wacke	65	59.3	16.19	6.50	4.40	1.51	0.58
H9	shale	35	59.9	10.78	4.27	3.33	8.91	0.25
H10	shale	46	52.4	15.00	7.04	3.09	6.30	0.98
H11	shale	60	51.0	18.92	6.15	6.27	2.65	0.14
H12	wacke	17	52.9	7.09	1.86	1.50	17.42	1.06
H13	wacke	29	47.7	13.28	3.87	1.52	15.53	1.02
H14	wacke	27	45.1	12.44	2.11	3.63	16.18	1.02
H15	wacke	39	64.3	8.69	2.71	5.38	5.29	0.15
H16	arenite	25	49.2	11.91	2.42	1.56	18.35	1.09
H17	arenite	35	53.4	13.01	2.75	2.26	11.07	1.20
H18	arenite	23	49.3	11.61	1.76	1.27	19.56	1.16
H19	arenite	16	65.0	4.50	1.85	2.66	11.93	0.92
H20	marls	29	49.8	13.12	4.09	1.73	14.94	1.10
H21	wacke	23	61.5	7.23	1.94	3.15	11.38	0.77
H22	wacke	19	55.2	6.89	2.54	3.61	13.92	0.50
H23	wacke	9	48.6	4.34	1.15	0.98	23.17	1.22
H24	marl	24	41.8	12.67	2.91	1.80	19.64	0.69
H25	wacke	27	49.5	12.67	2.27	1.85	16.96	1.04
H26	wacke	60	68.1	12.64	1.88	1.79	2.09	0.95
H27	wacke	37	54.3	13.86	3.22	2.54	9.60	0.38
H28	wacke	44	58.6	13.76	3.28	6.72	6.60	0.33
H29	marl	17	23.7	11.80	2.28	1.42	29.57	0.94
H30	marl	26	38.5	12.10	2.56	8.03	17.66	0.55
H31	wacke	31	47.7	12.53	2.39	4.03	13.25	0.20
H32	wacke	30	46.9	12.51	2.44	4.11	13.74	0.18
H33	wacke	32	59.5	8.30	2.28	6.01	7.22	0.37
H34	arenite	56	76.5	12.31	1.85	0.71	0.54	2.42
H35	wacke	23	59.4	5.95	1.44	6.86	9.19	0.64
H36	wacke	37	46.2	13.86	4.50	3.67	10.01	0.32

Nama Group	**Kanies Mb.**								
N1	quartzarenite	52	95.1	2.14	0.47	0.43	0.33	0.42
N2	quartzarenite	83	86.0	10.25	1.20	0.94	0.12	0.60
N3	quartzarenite	82	86.7	10.25	0.98	1.05	0.05	0.67
N4	quartzarenite	53	92.2	2.29	0.66	0.88	0.37	0.40

Table 1 supplementary data: Zimmermann et al.

K_2O	TiO_2	P_2O_5	MnO	LOI	sum	Ba	Rb	Sr	Cs	V	Ni	Co	Cu
%	%	%	%	%	%	ppm	ppm	ppm	ppm	ppm	ppm	ppm	ppm
4.88	0.42	0.140	0.040	1.6	99.4	713	233	88	4	44	13	11	30
4.53	0.36	0.150	0.020	1.5	99.6	632	199	86	3	37	9	5	27
4.72	0.31	0.110	0.130	1.8	99.7	671	201	106	3	35	13	12	81
4.91	0.35	0.153	0.084	1.4	99.8	711	211	102	4	36	11	7	17
4.39	0.27	0.110	0.030	1.6	100.7	166	37	433	2	22	6	4	11.1.
5.49	0.47	0.459	0.040	2.3	99.4	677	261	81	5	165	60	13	9
5.36	0.44	0.160	0.040	2.0	99.2	677	255	96	4	49	13	10	16
5.30	0.45	0.170	0.030	1.8	99.1	793	254	82	3	45	13	11	23
5.22	0.44	0.180	0.040	2.5	99.5	768	251	84	5	49	13	11	20
5.10	0.45	0.160	0.040	1.9	99.4	744	248	79	4	46	13	10	18
5.05	0.44	0.160	0.030	2.3	98.7	284	32	21	4	12	3	1	6
5.25	0.42	0.209	0.059	2.6	98.3	667	234	93	4	49	14	12	36
5.25	0.43	0.140	0.050	1.9	99.3	678	218	88	5	43	11	9	41
4.83	0.44	0.170	0.060	1.9	101.0	703	221	76	3	39	10	10	24
4.85	0.42	0.150	0.040	1.8	100.0	650	218	78	4	40	10	9	12
4.99	0.42	0.170	0.060	2.1	99.2	701	230	82	4	34	10	9	60
5.59	0.45	0.282	0.030	1.9	99.2	835	262	87		59	13	11	25
5.30	0.45	0.180	0.040	2.1	100.1	701	258	94		49	13	9	17
3.07	0.45	0.129	0.061	4.6	100.5	706	114	92		54	11	2	13
6.38	0.27	0.120	0.030	1.9	98.5	672	235	171		24	8	5	22
4.32	0.99	0.100	0.100	2.3	98.8	531	227	76		80	16	7	34
6.02	0.34	0.150	0.060	1.5	99.1	651	238	166		23	8	2	68
0.60	0.07	0.170	1.210	42.2	99.8	119	27	204	0.7	14	56	94	7
0.44	0.08	0.224	1.706	39.2	102.3	141	21	149		11	56	162	11
0.34	0.08	0.062	1.207	41.2	101.6	104	18	150		9	39	106	10
0.53	0.08	0.102	2.988	39.2	100.6	194	32	163		10	106	322	10
0.23	0.06	0.280	1.590	41.2	101.1	129	18	158		10	43	107	11
0.48	0.06	0.077	1.949	44.4	100.5	72	30	171		11	51	142	20
0.38	0.03	0.240	9.800	3.0	101.1	3234	19	198	bdl	19	185	571	18
0.39	0.04	0.390	12.950	4.0	98.7	3878	17	423	bdl	24	454	1389	18
0.73	0.08	0.522	6.156	3.1	99.1	1790	30	187	bdl	20	245	751	16
0.26	0.02	0.280	30.210	6.4	99.2	3207	11	317	bdl	28	532	1573	34
0.36	0.06	0.310	37.770	8.0	98.3	1554	23	218	bdl	35	367	974	61
0.59	0.09	0.290	30.650	7.7	100.1	1046	26	228	bdl	28	479	1379	34

0.02	0.01	0.360	50.840	9.6	100.0	1233	10	350	bdl	38	672	1840	84
4.39	0.74	0.160	0.030	2.3	98.8	792	185	58	7	82	25	21	29
1.83	0.55	0.084	0.159	22.0	98.2	310	75	515	2	43	9	7	97
0.94	0.54	0.080	0.096	12.2	101.7	167	36	167	1	34	9	9	107
1.03	0.30	0.131	0.121	15.9	101.3	154	40	355		32	8	6	40
1.91	0.57	0.150	0.090	11.0	100.9	355	88	143	4	49	9	6	73
0.82	0.35	0.090	0.070	12.4	100.8	120	34	185	1	32	7	5	95
1.19	0.32	0.069	0.116	15.8	99.4	172	47	349	1	32	9	9	36
4.64	0.82	0.170	0.030	6.6	100.8	818	196	50	7	86	26	22	27
2.88	0.41	0.090	0.050	10.0	100.9	484	128	187	5	53	18	16	41
3.98	0.71	0.080	0.070	9.9	99.6	626	156	112	5	70	27	22	25
6.96	0.76	0.200	0.020	7.4	100.5	930	230	40	14	98	23	12	48
2.03	0.41	0.120	0.060	15.6	100.0	507	89	306		38	8	6	10
3.05	0.52	0.092	0.064	11.6	98.2	488	111	200	6	53	14	11	21
2.40	0.43	0.094	0.079	17.6	101.1	434	65	134	2	35	9	9	5
3.56	0.46	0.140	0.030	9.5	100.3	723	151	51	8	53	13	12	12
1.23	0.47	0.074	0.119	12.8	99.2	195	47	189	2	36	10	8	58
2.32	0.68	0.157	0.106	11.3	98.2	341	94	110	4	52	11	10	63
1.04	0.37	0.075	0.122	13.2	99.5	155	41	147	1	32	6	3	77
0.66	0.48	0.060	0.080	12.6	100.7	151	36	163	1	31	9	9	68
2.62	0.47	0.087	0.063	11.2	99.2	270	80	194	4	47	15	9	51
2.28	0.33	0.100	0.050	13.0	101.7	726	91	86	2	34	9	7	7
2.33	0.38	0.100	0.050	16.4	101.9	773	95	226	3	41	11	9	8
0.87	0.21	0.070	0.060	20.6	101.3	166	38	442	bdl	27	7	7	13
2.85	0.38	0.085	0.069	15.6	98.5	685	90	235	2	41	11	8	7
0.92	0.42	0.066	0.115	13.0	98.8	138	36	164	3	31	9	8	68
2.88	0.20	0.102	0.027	7.7	98.3	434	79	41	8	22	6	3	9
4.87	0.50	0.107	0.036	9.2	98.6	760	149	43	9	55	12	9	14
4.74	0.50	0.103	0.040	6.0	100.7	734	152	49	1	56	12	10	13
1.59	0.32	0.082	0.080	28.9	100.7	225	53	272	2	27	8	6	17
2.12	0.26	0.072	0.074	16.9	98.8	424	62	116		27	9	6	47
3.05	0.34	0.090	0.104	15.5	99.1	490	74	63	4	36	8	4	21
3.07	0.35	0.086	0.106	15.3	98.8	646	92	62	4	33	9	6	24
3.28	0.46	0.140	0.060	12.5	100.1	820	97	95	4	43	10	6	7
4.39	0.27	0.110	0.030	12.2	111.3	770	86	91	5	44	10	6	7
2.23	0.30	0.090	0.060	14.8	101.0	655	76	114		31	8	7	11
4.73	0.68	0.111	0.059	15.0	99.2	736	167	87	9	66	17	14	16

0.60	0.03	0.020	0.010	0.7	100.3	118	21	22	1	272	9	3	1
0.85	0.04	0.037	0.015	0.9	101.0	163	20	17	1	260	12	5	2
1.02	0.03	0.025	0.012	0.8	101.5	172	25	17	1	212	9	4	1
0.64	0.03	0.020	0.010	0.9	98.4	124	20	30	1	284	8	3	1

Nb	**Ta**	**Y**	**Zr**	**Hf**	**Sc**	**Th**	**U**	**Pb**	**Ga**	**Zn**	**Mo**	**La**	**Ce**	**Pr**	**Nd**	**Sm**
ppm	ppm	ppm	ppm	ppm	ppm	ppm	ppm	ppm	ppm	ppm	ppm	ppm	ppm	ppm	ppm	ppm
10.6	1.4	30.9	181	6	8.5	27.6	2.2	34.8	18.6	67	bdl	70	120		41	9.2
8.8	1.7	25.3	181	6	6.7	24.0	1.3	28.2	15.6	43	bdl	38	97		21	5.7
8	0.7	16.7	138	4	5.7	19.0	1.1	35.9	16.1	50	bdl	36	83		20	5.1
9.8	1.1	23.2	169	6	6.8	27.7	1.7	31.5	15.8	53	bdl	50	110		29	6.5
6.3	1.1	33.9	173	3	6.0	17.0	1.3	26.8	7	14	bdl	33	73		22	4.8
69.3	11.2	17.6	181	6	8.7	27.3	2.4	39.5	19.6	68	bdl	20	76		9	4.0
11.8	0.6	21.3	184	6	8.2	27.1	2.5	26.3	18.8	52	bdl	42	82		25	5.7
10.9	2.3	25.8	183	5	8.0	26.2	2.6	37	19.2	60	bdl	46	100		29	6.7
10.3	1.2	22	183	6	8.2	28.2	2.4	25.2	18.8	56	bdl	30	100		17	4.8
11.4	1.1	33.8	185	5	8.6	27.1	2.0	24.3	19.7	62	bdl	45	110		28	6.7
5	1.3	5.7	42	6	8.5	27.5	1.2	7.2	0.9	7	bdl	52	110		32	7.4
10.8	1.7	23.6	182	6	8.3	28.8	2.6	29.8	17.7	56	bdl	31	100		20	5.1
11.4	2.1	25.5	177	6	8.7	27.1	2.6	39.2	18.7	63	bdl	49	120		25	6.9
11.6	0.6	27	181	6	8.8	28.6	2.0	34.5	19.7	65	bdl	53	120		31	7.8
11.6	2.3	29.2	177	6	9.2	27.4	1.6	29.2	19.8	67	bdl	51	110		31	7.4
11.7	1.0	28.6	177	6	8.6	29.1	2.1	36.6	19.9	61	bdl	42	110		27	7.0
10.5		25.5	191			29.3		38.6	20.4	58						
11.1		27.1	185			28.1		24	18.7	57						
13.9		27.5	196			22.9		12.4	14.5	49						
7.4		180	254			93		39.2	20.8	49						
16.5		42	229			8.7		25.3	17.7	130						
7.9		35.2	251			99		44.3	22.5	69						
1.5	0.1	4.4	19	1	2	1.5	2.4	4.3	2.9	298	2.2	5	10	1	5	0.9
4.1		5	35			4.9		39.9	2.8	277						
4.3		7.7	45			1.8		28.9	3.2	171						
3.8		6.2	41			2.7		30	3.8	372						
3.7		8.7	56			2.9		24.3	3.7	401						
3.5		6.5	34			2.3		25.1	3	319						
3.9	0.2	9.5	38	bdl	1.7	0.9	8.7	26.3	1.3	502	bdl	6	6		7	1.4
2.7	1.1	12.6	54	bdl	1.7	1.4	8.7	29.2	1.1	1055	bdl	6	8		7	1.2
5.1	0.4	8.2	43	bdl	2.0	2.2	5.2	21.6	2.6	415	bdl	8	13		6	1.4
3.3	0.9	7.4	45	bdl	1.6	0.2	30.0	34.6	1	1822	bdl	5	5		5	0.6
4.5	0.3	8.4	53	bdl	2.9	0.9	66.0	78.3	4	2167	bdl	9	10		10	1.2
6.7	0.4	10.2	55	bdl	2.7	1.8	28.0	40.9	2.3	1690	bdl	13	16		5	1.7

4	0.3	14	60	bdl	2.5	0.2	71.8	64.1	1.5	3926	bdl	10	5	3	1.4
17	1.1	33.9	219	7	14.9	20.0	2.7	11.9	22.5	125	bdl	56	120	41	8.3
9.7	0.5	44.5	246	5	5.3	10.0	2.5	46.4	8.9	26	bdl	27	51	23	5.6
11.3	1.1	39.5	320	10	6.1	15.0	2.8	23.1	4.7	37	bdl	30	70	28	7.9
7.1		29.4	210			13.2		30	6.2	31					
12.8	0.5	38.6	291	8	7.1	16.0	2.0	17.9	10.2	24	bdl	34	79	33	8.9
8.5	0.6	32.2	229	7	4.3	11.0	1.9	20.3	5.6	14	bdl	26	62	30	7.5
7.5	0.7	30.1	212	5	4.6	9.0	1.5	26.7	7.6	37	bdl	25	57	25	5.9
18	0.9	35.6	241	7	16.2	22.9	1.9	11.7	24.8	138	bdl	63	140	43	10.0
10.7	1.2	23.3	82	2	10.0	10.0	0.8	20.7	17	101	bdl	29	49	19	4.3
16.8	1.2	32.6	194	5	13.3	17.0	2.2	16.4	20.9	125	bdl	50	94	38	7.6
16.1	1.0	30.8	137	4	18.7	20.0	4.3	8.2	29.6	131	bdl	68	130	39	8.7
9.1		34.4	264			16.0		24.5	8.6	23					
11.8	1.3	30.4	194	5	8.5	11.0	1.7	19	13.3	67	bdl	31	66	26	6.4
10.2	0.6	28.2	250	7	4.7	12.0	2.1	23.5	7.5	31	bdl	28	62	25	6.3
11.1	0.8	24.3	178	5	7.3	11.0	1.8	10.9	13	65	bdl	28	61	21	5.5
9.7	0.7	39	322	9	5.5	16.0	1.9	20.5	6	39	bdl	36	76	28	7.4
13.4	1.0	40.2	368	11	7.4	20.8	3.0	15	10.2	30	bdl	52	110	43	10.0
8	0.7	35.3	251	8	4.4	12.0	1.3	20.7	4	19	bdl	31	66	28	6.6
10.8	0.5	39.1	250	7	6.2	11.0	2.0	18.5	4	41	bdl	32	71	26	6.8
11.3	0.5	29.4	195	5	7.7	11.0	2.1	29.6	11.9	77	bdl	28	61	29	5.8
9.5	0.4	22.6	164	5	4.2	8.6	1.7	10.2	9	25	bdl	21	49	22	4.9
9.7	0.4	26.5	179	5	5.9	9.1	2.1	10.9	11	32	bdl	26	58	24	5.0
6.5	0.4	34.3	179	4	3.1	6.6	0.9	27	6.4	14	bdl	21	49	25	5.5
9.1	0.7	28	188	5	5.5	9.0	1.6	11.5	10.7	32	bdl	25	55	24	5.0
10.5	0.5	39.5	252	4	3.2	4.2	1.3	18.8	4.1	41	bdl	14	28	13	2.7
6.3	0.8	15.8	146	6	7.2	12.0	1.8	13.9	6.2	22	bdl	28	64	23	5.6
11.7	0.5	23	188	5	7.3	11.0	1.7	10.7	12.8	60	bdl	29	63	25	5.6
11.5	0.7	24.3	181	5	3.3	8.4	0.9	10.4	13.1	64	bdl	21	47	22	5.2
7.6	0.4	13.3	142	4	3.3	6.5	2.1	49	6.7	30	bdl	21	48	26	4.6
7.3		14.2	151			7.8		34.9	6.7	35					
8.5	0.5	21.8	154	4	4.6	7.6	1.2	26.6	7.7	36	bdl	20	46	16	4.5
9.8	0.7	21.4	159	5	4.5	7.6	1.3	27.8	7.2	34	bdl	19	45	18	4.4
10.7	0.7	22.3	251	8	5.3	12.0	2.6	10.6	9.4	35	bdl	28	65	26	5.9
11	0.7	22.5	257	8	5.6	13.0	2.1	22.7	9.4	37	bdl	30	72	27	6.2
8.3		17.5	197			9.8		11.1	6.2	24					
15.1	1.3	31.1	201	6	10.0	13.0	2.4	10	14.8	78	bdl	31	65	25	6.5

6.2	4.8	4.5	36	1	0.7	1.9	0.3	10.5	0.6	5	bdl	5	11	7	1.0
7.1	4.9	7.3	39	1	2.1	2.4	0.9	35.8	1.4	14	bdl	6	13	7	1.1
5.4	4.8	6	35	1	0.9	1.9	0.5	11.2	1.4	12	bdl	6	12	7	1.1
6.8	4.6	5.3	35	1	1.0	1.8	0.4	14.6	0.8	8	bdl	5	10	6	0.9

Eu	Gd	Tb	Dy	Ho	Er	Tm	Yb	Lu	Eu*	Ce*	La_N/Yb	K/Cs	U/Th	Nb/	Zr/T
ppm	ppm	ppm	ppm	ppm	ppm	ppm	ppm	ppm							
1.6		1.3					2.6	0.42	0.54	0.85	18.25	10127	0.08	0.34	0.07
0.9		0.7					2.1	0.31	0.50	1.28	12.23	12535	0.05	0.35	0.08
0.7		0.3					1.4	0.24	0.67	1.16	17.38	13046	0.06	0.48	0.07
1.1		0.9					2.2	0.30	0.53	1.10	15.36	10194	0.06	0.42	0.08
0.9		0.4					1.5	0.24	0.93	1.08	14.87	18221	0.08	0.19	0.11
0.7		0.6					1.9	0.29	0.54	1.95	7.11	9116	0.09	3.94	0.06
1.0		0.8					2.1	0.29	0.55	1.01	13.51	11123	0.09	0.55	0.07
1.6		0.7					2.3	0.33	0.79	1.07	13.51	14665	0.10	0.42	0.07
1.0		0.7					2.0	0.29	0.64	1.67	10.14	8666	0.09	0.47	0.07
1.1		0.7					2.3	0.35	0.76	1.21	13.22	10584	0.07	0.34	0.07
1.2		1.0					2.4	0.35	0.51	1.05	14.56	10480	0.04	0.88	0.02
0.9		0.6					2.2	0.34	0.87	1.59	9.52	10891	0.09	0.46	0.07
1.7		1.1					2.4	0.35	0.74	1.24	13.80	8716	0.10	0.45	0.07
1.3		0.9					2.4	0.38	0.54	1.12	14.98	13365	0.07	0.43	0.07
1.2		0.7					2.5	0.37	0.54	1.08	13.65	10065	0.06	0.40	0.07
1.4		0.7					2.6	0.38	0.66	1.29	10.92	10355	0.07	0.41	0.07
														0.41	0.07
														0.41	0.07
0.18	0.82	0.15	0.82	0.13	0.42	0.06	0.4	0.06	0.60	0.98	7.94				
0.5		0.6					0.7	bdl	0.77	0.43	5.99		9.67	0.41	0.21
0.4		0.5					0.6	bdl	7.23	0.57	7.10		6.21	0.21	0.22
0.5		0.5					0.5	bdl	0.83	0.82	10.27		2.36	0.62	0.09
0.5		0.5					0.6	bdl	2.08	0.44	5.86		150.00	0.45	0.37
0.6		0.6					0.7	bdl	10.85	0.48	9.07		73.33	0.54	0.15
0.6		0.6					0.7	bdl	3.31	0.64	12.55		15.56	0.66	0.10

0.9	1.4	0.8	bdl	0.86	0.27	8.45		359.00	0.29	1.01
1.6	1.1	3.1	0.45	0.61	1.04	12.10	5206	0.14	0.50	0.05
0.9	1.0	2.7	0.40	0.47	0.89	6.76	7591	0.25	0.22	0.07
1.3	1.1	3.2	0.48	0.51	1.08	6.34	7761	0.19	0.29	0.10
									0.24	0.12
1.1	1.2	3.0	0.45	0.39	1.07	7.66	3964	0.13	0.33	0.09
1.0	0.8	2.3	0.32	0.44	1.06	7.64	6807	0.17	0.26	0.11
0.9	0.6	2.0	0.28	0.50	1.04	8.45	9878	0.17	0.25	0.11
2.0	1.4	3.4	0.48	0.62	1.09	12.48	5502	0.08	0.51	0.05
0.9	0.4	1.8	0.25	1.07	0.83	10.89	4781	0.08	0.46	0.03
1.3	0.7	2.8	0.43	0.57	0.90	12.16	6606	0.13	0.52	0.05
1.6	0.7	2.5	0.30	0.63	0.96	18.33	4127	0.22	0.52	0.03
									0.26	0.11
1.0	0.7	2.5	0.38	0.51	1.00	8.38	4216	0.15	0.39	0.06
1.0	0.7	2.0	0.31	0.52	1.03	9.46	9965	0.18	0.36	0.10
0.8	0.6	2.0	0.30	0.47	1.05	9.46	3694	0.16	0.46	0.06
1.2	0.9	3.2	0.48	0.52	1.01	7.60	5084	0.12	0.25	0.11
1.6	1.3	3.5	0.51	0.51	1.01	9.98	4817	0.14	0.33	0.09
1.3	0.9	2.7	0.39	0.62	0.99	7.76	8633	0.11	0.23	0.11
1.1	1.0	3.1	0.45	0.50	1.05	6.98	5479	0.18	0.28	0.09
0.9	0.7	2.4	0.38	0.50	0.99	7.88	5443	0.19	0.38	0.07
0.8	0.4	1.6	0.25	0.81	1.05	8.87	9463	0.20	0.42	0.08
1.1	0.8	1.9	0.28	0.66	1.03	9.25	6447	0.23	0.37	0.08
0.9	0.8	1.9	0.27	0.50	1.03	7.47		0.14	0.19	0.14
1.0	0.7	2.1	0.29	0.62	1.01	8.04	11816	0.18	0.33	0.08
0.5	0.7	1.4	0.18	0.49	0.93	6.76	2551	0.31	0.27	0.10
0.9	0.9	1.9	0.29	0.48	1.08	9.96	2993	0.15	0.40	0.12
0.9	0.9	2.0	0.30	0.48	1.02	9.80	4492	0.15	0.51	0.06
0.7	0.7	2.1	0.30	0.42	1.01	6.76	39355	0.11	0.47	0.06
0.8	0.8	1.6	0.22	0.51	1.00	8.87	6591	0.32	0.57	0.07
									0.51	0.10
0.8	0.4	1.5	0.23	0.90	1.09	9.01	6325	0.16	0.39	0.08
0.8	0.6	1.6	0.21	0.57	1.09	8.02	6377	0.17	0.46	0.08
0.8	0.6	2.1	0.31	0.64	1.07	9.01	6807	0.22	0.48	0.09
1.0	1.0	2.2	0.30	0.49	1.12	9.21	7288	0.16	0.49	0.16
									0.47	0.11
1.4	0.6	2.6	0.39	0.72	1.00	8.06	4359	0.18	0.49	0.05

0.3	0.1	0.4	0.05	0.75	0.88	9.12	4981	0.16	1.38	0.20
0.3	0.1	0.8	0.10	0.70	0.92	5.32	7089	0.38	0.97	0.15
0.2	0.1	0.5	0.08	0.53	0.86	8.38	8492	0.26	0.90	0.19
0.2	0.1	0.5	0.07	0.61	0.89	6.62	5313	0.22	1.28	0.19

Th/Sc	Zr/S	La/S	Ti/Zr
3.25	21.33	8.26	13.89
3.58	27.06	5.67	11.90
3.33	24.25	6.32	13.36
4.07	24.81	7.35	12.40
2.83	28.90	5.50	9.33
3.14	20.83	2.30	15.45
3.30	22.49	5.12	14.30
3.28	22.88	5.75	14.74
3.44	22.32	3.66	14.41
3.15	21.47	5.23	14.61
3.24	4.92	6.08	63.11
3.47	21.96	3.73	13.81
3.11	20.39	5.63	14.53
3.25	20.52	6.05	14.61
2.98	19.23	5.49	14.23
3.38	20.58	4.88	14.23

0.53	22.35	3.65	4.73
0.82	31.65	3.71	4.46
1.10	21.45	3.80	11.60
0.13	27.81	3.25	2.69
0.31	18.10	3.24	6.85
0.67	20.30	4.81	9.85

0.08	24.16	4.00	0.99
1.34	14.70	3.72	20.25
1.89	46.42	5.09	13.35
2.46	52.39	4.92	10.09
			8.53
2.25	40.99	4.79	11.74
2.56	53.16	6.05	9.18
1.96	46.17	5.43	9.06
1.41	14.89	3.88	20.38
1.00	8.17	2.90	30.09
1.28	14.58	3.79	21.83
1.07	7.35	3.63	33.16
			9.32
1.29	22.79	3.65	15.97
2.55	53.15	5.96	10.34
1.51	24.40	3.84	15.48
2.91	58.58	6.55	8.82
2.81	49.78	6.99	11.00
2.73	57.14	7.05	8.89
1.77	40.39	5.16	11.49
1.43	25.31	3.64	14.55
2.05	39.07	5.00	12.06
1.54	30.32	4.41	12.73
2.13	57.74	6.77	7.03
1.64	34.11	4.55	12.24
1.31	78.63	4.38	10.10
1.67	20.26	3.89	8.14
1.51	25.75	3.97	15.98
2.55	54.88	6.36	16.68
1.97	43.03	6.36	13.59
			10.16
1.65	33.50	4.35	13.19
1.69	35.40	4.22	13.10
2.26	47.38	5.28	10.98
2.32	45.91	5.36	6.30
			9.14
1.30	20.05	3.10	20.33

2.71	52.00	7.71	4.94
1.14	18.71	3.00	6.56
2.11	39.33	6.89	5.25
1.80	34.90	4.90	5.15

ANALYTICAL PROCEDURES

Petrography

Polished thin section samples were used for petrographic analyses in a light microscope (Olympus B60XM). The identification and characterization (shape, size, fractures, inclusions, etc.) of heavy minerals and matrix of the clastic rocks were done using a scanning and backscattered electron microscope using energy dispersive spectrometry (SEM-BSE-EDS). A Zeiss Supra 35 VP equipped with EDAX EDS system with Genesis software and Polaron PP2000 cryo unit (Universitetet i Stavanger) was used. The SEM-BSE-EDS system was set at 15 keV, a working distance of 20 mm and a live time of 60 s per spot

Geochemistry

Powders were prepared by milling to a very fine mesh. Pressed powder pellets (for selected trace elements) containing 8.0 g of sample powder mixed with 4 g of binder, were placed in an aluminium cup and pressed at a pressure of 20 tons. Glass beads (for major elements) were prepared by fusing sample powder with a flux containing 50 % LiM (lithium metaborate) and 50 % lithium tetraborate with $LiNO_3$ as oxidant. XRF precision and accuracy were controlled by international and internal rock standards and below 5 % (1s) for measured elements. Geochemical analyses were performed by ACTLABS (Ontario, Canada). Sample powders were dissolved in lithium metaborate flux and the resultant bead rapidly digested in dilute nitric acid. INAA precision and accuracy based on replicate analysis of international rock standards are 2-5 % (1s) for most elements and ± 10 % for U, Sr, Nd, and Ni. For further information please see www.acmelabs.com.

Isotope geochemistry

C-O isotope measurements

A Dremel minidrill was used to obtain powders of the samples where care was taken to avoid obviously recrystallised parts of the rock. Carbon and oxygen isotope analysis was undertaken at the Scottish Universities Environmental Research Centre using an automated triple-collector gas source mass spectrometer (Analytical Precision AP2003) linked to an automated gas preparation device. In the latter, c. 1 mg of the powdered sample is reacted with 103% phosphoric acid to produce carbon dioxide which is then purified before analysis. Precision and accuracy were monitored by reference to long-term analysis of laboratory and international standards. Precision is better than 0.2‰ at 1 for carbon and oxygen. Data are reported as ‰ values relative to V-PDB.

U-Pb dating of detrital Zircons

Samples were crushed and zircons separated using standard techniques (Rogers water table, heavy-liquid separation and Frantz magnetic separation). Representative zircons were pipetted in alcohol onto a grain mount under a fibre optic illuminated binocular microscope.

Analyses were carried out at the NERC Isotope Geosciences Laboratory (NIGL), UK on a Nu Plasma MC-ICP-MS system coupled to a New Wave Research 193nm Nd:YAG LA system. A static laser spot size of 25 microns diameter was used to ablate discrete zones within zircons. The total acquisition cycle took about 45 seconds per ablation, which equates to approximately 15-18 μm depth ablation pits. Half mass and defocused baselines were carried out at the start of each group of ca 5 to 8 analyses. ^{205}Tl and ^{235}U were measured on Faraday cups to determine a Pb-U instrument mass bias of 1.006 ±0.26% (2σ). ^{202}Hg was measured simultaneously and used to correct for the ^{204}Hg isobaric interference on ^{204}Pb assuming a ^{204}Hg/^{202}Hg natural isotopic composition of 0.229883 corrected for mass bias. Due to the fact that in general zircon analyses did not give ^{204}Pb cps significantly in excess of baseline values, the U-Pb analyses presented are non-common lead corrected. As a precaution, the small number of analyses (ca 5% of total) showing a common lead intensity >400 cps were rejected. Analyses where ^{238}U beam intensity was <4mV were also rejected (ca. 1% of total). Three separate zircon standards were used; 91500 (U-Pb TIMS age 1065 ± 0.4 Ma, Wiedenbeck et al. 1995), Plesoviçe (U-Pb TIMS age 338 ± 1 Ma, Aftalion *et al.* 1989) and GJ-1 (U-Pb TIMS age 599.8 ± 4.55 Ma, Jackson *et al.* 2004). 91500 was used as a primary standard to calculate a fractionation factor for each analytical session. Plesoviçe and GJ-1 were used as secondary standards, as a general control on the precision and accuracy of analyses throughout each analytical session. U/Pb ages for these secondary standards for sessions 1 (HOL) and 2 (NUM) gave 339.1 ± 2.0 Ma (n=21), 337.9 ±3.5 Ma (n=14) (Plesoviçe) and 605.0 ±2.8 Ma (n=21), 599.9 ±4.8 Ma (n=14) (GJ-1) respectively. For each analytical session the overall reproducibility of the 91500 primary standard $^{206}Pb/^{238}U$ and $^{207}Pb/^{206}Pb$ were ca. 2% (2σ) and ca 1% (2σ) respectively.